Politechnika Wrocławska

Wydział Mechaniczno-Energetyczny
kierunek studiów: **mechanika i budowa maszyn**
specjalność: **refrigeration and cryogenics**

Praca dyplomowa
stopnia magisterskiego

Investigations on superconducting magnetic shields based on YBCO and BSCCO

Łukasz Tomków

słowa kluczowe:
.....
.....
.....

Promotor:	.....	.....	.....
	imię i nazwisko	ocena	podpis
Recenzent:	.....	.....	.....
	imię i nazwisko	ocena	podpis

Wrocław 2013

PODZIĘKOWANIA

W trakcie pisania tej pracy spotkałem się z wielką życzliwością osób pośrednio i bezpośrednio zaangażowanych w jej tworzenie. W szczególny sposób chciałbym podziękować mojemu promotorowi, Panu Profesorowi Marianowi Ciszkowi za wielki wysiłek jaki włożył w to, by mi pomóc oraz za inspirację do ciężkiej pracy.

Dziękuję dyrekcji Instytutu Niskich Temperatur i Badań Strukturalnych PAN we Wrocławiu za możliwość przeprowadzenia części pomiarów w laboratoriach Instytutu oraz zapewnienie niezbędnych materiałów.

Pragnę też podziękować Panu Profesorowi Maciejowi Chorowskiemu za wsparcie finansowe badań, w szczególności umożliwienie zakupu koniecznych do ich przeprowadzenia nadprzewodników.

Bardzo dziękuję też Panu Doktorowi Henrykowi Malinowskiemu za wprowadzenie mnie w tematykę ekranowania magnetycznego nadprzewodnikami oraz wspólną pracę w Zjednoczonym Instytucie Badań Jądrowych w Dubnej.

Podziękowania należą się też wszystkim nauczycielom akademickim Politechniki Wrocławskiej, którzy prowadzili mnie przez 5 lat studiów.

STRESZCZENIE

Praca podejmuje zagadnienie ekranowania pola magnetycznego z wykorzystaniem osłon wykonanych z nadprzewodników wysokotemperaturowych. We wstępie teoretycznym przedstawione zostały fizyczne właściwości nadprzewodników, historia badań nad nimi oraz obecne i przyszłe zastosowania. Scharakteryzowano podział na nadprzewodniki I i II rodzaju oraz oceniono ich przydatność dla celów ekranowania magnetycznego. Opisano sposób produkcji i strukturę nadprzewodników wysokotemperaturowych (HTS) wykorzystanych w części eksperymentalnej - YBCO i BSCCO. Przeprowadzono przegląd literaturowy by ocenić obecny stan wiedzy na temat wykorzystania nadprzewodnikowych ekranów magnetycznych.

Scharakteryzowano modele stanu krytycznego Kima i Beana oraz porównano ich przydatność dla modelowania pola magnetycznego ekranowanego przez cylindryczny nadprzewodnik. Model Kima, biorący pod uwagę wiecej zjawisk zachodzących w nadprzewodniku II rodzaj, został wybrany dla celów porównania z wynikami eksperymentalnymi przeprowadzonymi w stałym polu magnetycznym. Wykorzystano go również do modelowania zachowania komercyjnego cylindra wykonanego z BSCCO w przemiennym polu magnetycznym.

Zastosowanie ekranu wykonanego z nadprzewodzącej taśmy z YBCO spowodowało konieczność zastosowania dodatkowego modelu. Oczekiwano, że ze względu na obecność złącza będącego w stanie normalnym stałe pole magnetyczne będzie zdolne penetrować taki ekran. Pojawienie się efektu sprzężenia elektromagnetycznego przy pewnej częstotliwości granicznej powinno doprowadzić do pojawienia się dodatkowego efektu ekranującego. Stworzono model, na podstawie którego obliczono przewidywaną wartość graniczną częstotliwości.

Zbudowano układ eksperymentalny w celu weryfikacji modeli. Większość jego elementów stworzono specjalnie na potrzeby realizacji niniejszej pracy. W warunkach normalnych zbadano zachowanie nawiniętego magnesu i przyrządów pomiarowych. Dla badania wielkości stałego pola wykorzystano hallotron, zaś dla pola przemiennego - niewielką cewkę pomiarową o znanej geometrii. Pomiary w temperaturze 77K obejmowały badanie zachowania cylindra z BSCCO oraz podwójnego ekranu w polu zmiennym i stałym. Badanie ekranu wykonanego z taśmy przeprowadzono tylko w polu przemiennym.

Wyniki eksperymentalne pozytywnie zweryfikowały zastosowanie modelu Kima oraz wykazały, że w istocie wpływ ekranu z taśmy na stopień ekranowania jest niezauważalny w stałym polu magnetycznym. W polu zmiennym natomiast dodatkowy efekt ekranowania okazał się widoczny i zależny od częstotliwości pola magnetycznego. Przeprowadzono analizę uzyskanych rezultatów celem odnalezienia częstotliwości granicznej przy której pojawia się ekranowanie. Jej szacunkowa wartość to 8,3 Hz, blisko uzyskanej z obliczeń wielkości 9,3 Hz. Pomiary wykazały też obecność innych efektów - między innymi zamarzania pola magnetycznego w nadprzewodniku oraz związanej z tym histerezy pola magnetycznego.

Główne cele pracy zostały zrealizowane. Modele teoretyczne zostały pomyślnie zweryfikowane. Rozpoznano interesujący efekt, który może znaleźć praktyczne zastosowanie w postaci prostych i tanich ekranów z taśm. Można wykorzystać je dla zwiększenia efektywności ekranowania za pomocą konwencjonalnych ekranów monolitycznych. Przeprowadzone zostaną dalsze badania w celu ulepszenia modelu dla ekranu wykonanego z taśmy nadprzewodzącej oraz dalszego rozpoznania ich właściwości.

SUMMARY

The concern of this thesis is the issue of magnetic screening with the shields made of high temperature superconductors. Theoretical introduction shows the properties of superconductors, history of their research and their applications, both present and future. Division on type I and type II superconductors has been characterised and each type has been assessed for the purpose of magnetic shielding. Manufacturing process and structure of YBCO and BSCCO, superconductors which have been used in experimental part, was characterised. Literature review was performed to investigate state of the art on this issue.

Bean and Kim critical state models have been characterised and their usability for the purpose of anticipating the behaviour of magnetic field inside a superconducting tubular sample was assessed. Kim model was chosen for comparison, as it considers more of the physical phenomena which occur within the superconductor. It was applied for the modeling of the hollow cylinder and double shield in direct current magnetic field. It was also used to model the behaviour of solid cylinder in alternating current magnetic field.

The application of tape-screen posed the need to apply another model. It was expected that due to the presence of solder in normal state magnetic field will be able to propagate into the shielded cavity. The appearance of electromagnetic coupling effect in some threshold frequency was expected to cause the shielding effect. The model was created which was used to anticipate the value of threshold frequency.

Measurment stand was assembled to verify models. Most of its elements were produced for the purpose of thesis. Some measurments were performed in normal state to check the behaviour of magnet and sensors. For the measurments of DC magnetic fields Hall probe was used and for alternating current fields - small measuring coil. The measurments in the temperature of 77K included the investigation of solid BSCCO cylinder and double shield setting behaviour in direct and alternating current field. The research on tape screen were performed in AC magnetic field only.

Experimental results led to positive verification of Kim model and have shown that in direct current there is indeed no effect from the application of tape-screen. In alternating field the effect became visible. It turned out the it is dependent on frequency. Analysis was performed to find the value of threshold frequency. Its estimated value was 8,3 Hz, close to the value of 9,3 Hz obtained during calculations. Measurments revealed also some other effects - hysteresis of magnetic field and its freezing in the superconductor, among others.

All objectives of thesis have been completed. Interesting effect has been recognised, which might find a practical application. Simple and cheap magnetic screens made of superconducting tape may be applied to increase the efficiency of soild magnetic screens. Further research will be performed in order to increase the quality of model for tape-screens and investigate their properties.

Contents

1 INTRODUCTION

The issue of magnetic shielding is important in several branches of science, medicine and industry. The development of the sophisticated detection and measurment techniques requires a careful control of magnetic environment. Superconductors, due to their unique magnetic properties, may serve this purpose well. The application of high temperature superconductors (HTS) appears to be the best choice due to higher operation temperatures than in case of conventionally used superconducting materials and therefore lower exploitation costs.

The aim of this thesis is to investigate the attenuation of magnetic field due to the application of superconducting magnetic shields. The measurments have been performed to research the behaviour of field shielded with two types of shields made of high temperature superconductors. Specimens investigated were solid shield made of BSCCO and tape-screen made of YBCO tape. Interactions between these superconducting shields screening single cavity have been investigated as well. Literature review have shown that no such measurments were done before. Mathematical model of magnetic shields system was created. Experimental results have been compared with those obtained from calculations.

Thesis is organised into chapters containing theoretical introduction, description of mathematical model, experimental part and discussion. Conclusive remarks are provided as well. Attachments contain the technical documentation of test stand elements and researched specimens. Measurment results and their interpretation and analysis have been shown in proper sections. Contents of each chapter have been summarised below.

Theoretical introduction contains general introduction to history and applications of superconductivity. This is followed be section concerning magnetic shielding. There the informations about current status of this technology and research on it may be found. Next section is devoted to comparison of type I and type II superconductors. In this section main differences are listed and general information about behaviour of both types is provided. Further section contains the detailed description of type II superconductors magnetic behaviour. The final section of this chapter describes the properties of YBCO and BSCCO, the materials used in the experimental part of thesis.

Mathematical model part consists of the description of models applied for the prediction of magnetic shield behaviour in alternating and direct current fields. In order to model the behaviour of solid shield subjected to DC and AC field Bean model and Kim model have been considered. Double shield setting in DC field is also expected to obey these models. Both are described and compared in proper section. Modeling of double shield setting bases on the concept of electromagnetic coupling. Assumptions for this model and calculations are shown.

Experimental part of thesis contains the description of test stand and raw results of measurments. Test stand description consists of pictures and comment on each part of equipment used for measurments. The process of sensors preparation as well as its results are shown there. Measuring circuits schemes have been provided in this part, along with the description of superconducting specimens used. Results are shown from each measurment, both in AC and DC mode and in double, solid and tape-screen shield configuration. The description of measuring process accompanies each graph.

Discussion part consists of the analysis of the results obtained during the experimental parts and model calculations. All modes of operation are compared and connections between them are shown. Several phenomena affecting experimental values have been recognised. Shielding factors are calculated for different settings. Models are assessed by comparison of their results with values obtained during measurments. Finally, the applications of different shield settings are proposed.

Conclusions contain shortened description of obtained results and their consequences. Main points of discussion part are presented and their significance is shown. Fulfilling of the aims of thesis is assessed. Plans for future research are stated, as well as their expected outcome. Possible practical applications of thesis results are proposed. Further usage of test stand is suggested. Several final commentaries are added.

The choice of topic was affected by the author's training period in Joint Institute for Nuclear Research in Dubna. In Veksler and Baldin Laboratory of High Energy Physics research is conducted on the application of superconductors, and especially superconducting magnetic shields for newly build particle accelerator NICA. The application of superconducting magnetic shields offer fascinating possibilities in the control of magnetic field propagation and shaping. The usage of superconductors is going to become more common, therefore research in this area will become more and more important.

2 THEORETICAL BACKGROUND

2.1 GENERAL INFORMATIONS

Two distinct properties of any superconductor are zero electrical resistance and expulsion of magnetic from the inside - they become perfect diamagnets. A superconductor exists in such state below certain parameters known as critical parameters. These are temperature, magnetic field and electric current density. This section contains summary of superconductivity research as well as basic description of the most important properties of superconductors. General remarks concerning current and future applications are also included.

2.1.1 History of superconductivity

History of superconductivity started on 8th April 1911. On this day sudden drop of resistance of mercury has been observed in Heike Kamerlingh Onnes' cryogenic laboratory in Leiden. Prior to this date it was expected that resistance of any metal would gradually drop down to certain minimum value, then rise to infinity. The explanation was anticipated freezing of electron gas. However, no minimum resistance was observed in temperatures of liquid hydrogen. This lead scientists to expand the temperatures of investigation to liquid helium. The new theory was formed, which assumed zero resistance in perfectly pure metals close to absolute zero [1]. Measurments of electrical resistance of different temperatures in helium temperatures became part of Leiden laboratory regular program.

The observation of sudden resistance drop in 4,19K was completely unexpected. Initially it was considered an error and assigned to a short-circuit. After several changes of test stand it was found that reversed transition (sudden reappearance of electric resistance) happens when temperature rises above certain threshold. At this moment no theory was able to explain this phenomenon. Ohm's law was applicable only above transition temperature. Onnes quickly found that impurities did not suppres superconductivity. He also revealed that certain value of electrical current causes the material to leave superconducting state. Later in the same laboratory tin and lead were found to become superconducting below their transition temperatures. This opened the way to produce first superconducting coils. In 1916 Francis Briggs Silsbee concluded that the value of critical current was related to critical magnetic field.

In 1933 second major property of superconductors has been discovered. Walther Meissner and Robert Ochsenfeld have found that materials in superconducting state become perfect

diamagnets [2]. They have observed the expulsion of magnetic field from the bulk of superconductor when it was cooled below critical temperature in a weak magnetic field. This property is a proof that superconductors are more than perfect conductors. In the next year Fritz and Heinz London created model for explanation of this phenomena, later known as Meissner-Ochsenfeld effect or just Meissner effect. This relatively simple model, named two fluids model, not only explained the effect but also predicted existence of penetration depth λ. This is characteristic distance in which magnetic field can enter superconductor. In this region screening currents are induced which cause magnetic field attenuation. Induction decreases exponentially, according to equation 1[3].

$$\mathbf{B} = \mathbf{B}_0 e^{-x/\lambda} \tag{1}$$

There $\mathbf{B}$ is a local magnetic induction, $\mathbf{B}_0$ is an external induction and x is a distance from superconductor surface. Londons' equations will be analysed in further section.

New theory to explain superconductivity has been developed by Lev Landau and Vitali Ginzburg in 1950. It is known as phenomenological or macroscopic theory. This is more general than former London theory and takes into consideration variable density of superconducting electrons [2]. Theory is based on Landau's works on second order phase transitions. It introduces order parameter, which may be interpreted as the density of superconducting electrons at a certain point. GL theory predicts many properties of superconductors, such as coherence length (the largest length in which changes of order parameter will be observed in case of disturbance). Finally, it anticipated existence of two types of superconductors, which will be explained further.

In 1957 John Bardeen, Leon Cooper and Robert Schrieffer presented microscopic theory of superconductivity (BCS theory). This theory was based on analysis of interaction between conducting electrons and crystallic lattice vibration [2]. In low temperatures the electrons which normally repel by means of Coulomb forces may attract each other. In this case Cooper pair is formed. Attraction is realised by deformation of lattice - moving electron causes local increase of positive ions density close to its track. This increaseof positive charge density attracts another electron with opposite momentum. Below critical temperature this attraction becomes sufficiently strong to form a pair of electrons with opposite spins and momenta. Since such pair cannot be dispersed on lattice deformation as normal electron, the movement of Cooper pairs is lossless. BCS theory explains well the behaviour of classical superconductors. Nevertheless, there is still no comprehensive theory for high temperature superconductors.

Very important step in development of superconductors was taken in 1986. Georg Bednorz and Karl Alex Müller, researchers working in IBM Rüschlikon laboratory, discovered superconductivity in ceramic materials containing copper oxides. Transition temperature of *LaBuCuO* was found to be 30K. Large number of laboratories started to develop ceramic superconductors. In next year YBCO ceramics was discovered. Its transition temperature is 92K. This was the first superconductor with critical temperature higher than this of liquid nitrogen.

Next years brought new discoveries - bismuth containing superconductor with critical temperature of 110K have been found, as well as thallium superconductors (critical temperature 125K). To date the superconductor with highest transition temperature is discovered in 1995 $HgBa_2Ca_2Cu_3O_{8+\delta}$ with the transition temperature of 135K. [4] Superconductors with high critical temperatures are often complex and contain expensive rare earth elements. MgB_2 is the example of cheap superconductor, which may be widely applied. Its transition temperature is 39K.

2.1.2 Basic properties

As mentioned, three critical parameters (temperature T_c, magnetic field H_c and electric current density J_c) govern the state of superconductor. These values are interdependent. One may draw a three dimensional diagram showing superconducting region in coordinate system formed by these properties (figure 1). This diagram is valid for perfect type I superconductors. In type II superconductors additional critical fields exist, which are detailly described in further section.

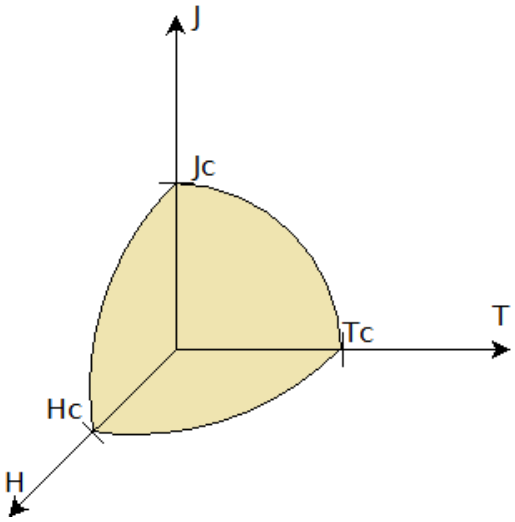

Figure 1: Three critical parameters

In a perfect superconductor dependence of critical magnetic field is close to parabolic and is described by equation 2 [2].

$$H_c = H_0 \left[1 - (T/T_c)^2\right] \tag{2}$$

Here H_c is the critical value of magnetic field in temperature T, H_0 is a critical value of magnetic field in absolute zero and T_c is critical temperature with neither electric current nor magnetic field in a superconductor. In type I superconductors critical current is directly related to critical magnetic field. This is a current which generates critical magnetic field on the surface of superconductor. Magnetic behaviour of type II superconductors is more complex and will be explained in proper section. Distinction should be made betweeen intergranular and intragranular critical current. The first flows between grains of material, while the second inside them. Intragranular critical current is much higher than intergranular.

2.1.3 Present applications

Presently the most applied superconducting material is niobium titanium alloy (NbTi) [5]. This is low temperature superconductor with transition temperature of 9,2K. This alloy is relatively easy to form and over time became the main material for superconducting magnets. Such magnets use the ability of superconductors to carry large currents for production of very strong magnetic fields. The largest area of commercial applications of these strong fields is medicine, especially imaging devices.

Most of modern magnetic resonance imaging (MRI) and nuclear magnetic resonance (NMR) devices use circular and semi-circular superconducting magnets to produce the fields required for high resolution imaging. Another group of applications consists of high energy physics machines, especially accelerators. There magnets serve to control the movement of particle beam.

Strong magnetic fields are used there to bend the track of beam and to focus it. Particle accelerators use also superconducting RF cavities for the purpose of actual acceleration of particles. The most spectacular example of superconducting accelerator is LHC in CERN. Another scientific application of superconducting magnets are plasma confinement systems in fusion reactors. Extremely hot plasma is there kept within strong magnetic field to protect the rest of reactor and enable fusion reaction. ITER is the major currently realised project.

Major industrial application is currently magnetic separation of kaolin clay and other magnetic materials. Due to high magnetic fields achievable, superconducting magnets are capable of removing impurities from water or other media. The other include minor applications of superconducting magnetic energy storage (SMES). The capacity that they are capable of achieving continuously increases. They are used to increase the quality of power delivered by an electric system. They are used as an emergency storage in case of power outage. Power system also benefit from the application of superconductors in power electronics. Superconducting devices are capable of carrying and switching large currents more efficiently than the devices based on normal materials.

There are also some smaller applications of superconductors, most notable of which is magnetoencephalography (MEG). This is the method of brain activity mapping. It is done by measuring very small magnetic fields produced by intracellular electric currents generated by dendrites. This measurments are realised by the array of SQUIDs - superconducting quantum interference devices, capable of recording these subtle magnetic fields. SQUIDs are based on Josephson effect realised in Josephson junctions. High temperature superconductors usage is far less extensive. Currently their main mass application are electronic filters. Such devices are used in wireless base stations. According to [5] 10000 such devices were installed in 2009.

2.1.4 Future applications

It is anticipated that future will bring plenty of new applications for high temperature superconductors. The first large field of new applications is electric power. Current transmission infrastructure causes large losses and its transmission capabilities might soon become insufficient. Also it is not elastic enough to fully accomodate electric energy supplied by unconventional sources of energy. Superconducting wires are capable to carry even 100 times larger electric current than copper wire with the same dimension [5]. Transmission is lossless, however the cable has to be cooled. Currently several large projects are realised, most notable of which are Tres Amigas in USA (interconnection of three independent power grids) and AmpaCity in Germany (replacement of existing conventional power cable with superconducting one in the urban environment of Essen). Another application of superconductors in energy industry are fault current limiters. These are devices which protect electric systems from large currents produced by short-circuits. Superconducting element placed in such limiter changes its state to normal when current exceeds certain threshold thus stopping electricity supply to the protected system.

There are also plans to produce superconducting transformers for power lines and wind turbines. Application of superconducting transformers in power grid would save space and decrease environmental footprint. Electrical losses would be avoided and there would be no production of waste heat. Such devices might also operate in overload, which would help accomodate peaks and increase system elasticity. For applications in wind turbines the major advantage is the lower weight (one third as [5] reports) of superconducting winding when compared with the application of conventional copper wires. Such decrease allows to increase a turbine power rating while keeping the same height. Another issue strongly connected with a new energy economy is electric energy storage. Volatility of both supply and demand causes

need to maintain additional generation capacity in case of sudden misalignement of production and needs. This might be decreased by application of large SMES devices. Such device may quickly react to changes in power system and immediately provide needed power.

The future of transport industry will also see increase in superconductors applications. The role of superconducting drives in marine applications would similar to these in future wind turbines - to save space and decrease weight. Spared place and lifting capacity would be utilised in more economical way. Military ships would also use compact HTS wiring for the purpose of degaussing. Land transport already benefits from the usage of superconducting magnets. They are used in magnetic levitation trains to lift and to propel a vehicle. It is important to notice that the magnets are used only to obtain high magnetic field and Meissner effect does not find use in current systems. Further research might change this, as well as introduce HTS as a material for the magnets. Future may bring large development to this mode of transportation.

Medicine is expected to further benefit from superconductivity development. Number of MRI devices will continue to grow. Their quality will also increase with the construction of better superconducting magnets, which will provide better homogeneity of field and larger power. Another development to MRI is ULF-MRI. This stands for ultra low field magnetic resonance imaging. In this technique weak field are applied and precise detection system consisting of SQUIDs is used. Magnetic field shielding is required to obtain proper results for all the techniques utilising SQUIDs [6]. It is expected that ULF-MRI and MEG would be combined into a single diagnostic system to save money and increase results quality. Precision of SQUIDs finds use also in magnetocardiography, precise system to diagnose heart diseases.

Usage of superconducting electronics is anticipated to become much wider than today. Application of such elements will lead to decreased size and better economy through elimination of analog pre-processing subsystems [5]. Josephson junction applied in future devices will bring closer the creation of quantum computer. In rapid single flux quantum (RSFQ) devices silicon is replaced with niobium. The drawback is the need to cool such devices to 4K for niobium to become superconducting. Usage of such elements allows for greater frequencies with reduced heat generation. Radar technologies also greatly benefits from application of superconducting sensors. They have found use especially in radioastronomy. Their field of application is expected to grow further, particularly into defense applications.

Bright perspectives open up before the superconductivity. Its history started unexpectedly and since then steady growth has been observed. Current developments in materials brings hope to increased usage of superconductors. New superconductor, such as exotic superconductors are being researched. It is also important to study all properties of superconductors in order to find new uses and improve existing. As shown above magnetic shielding is often in the background of most of the detection and computing technologies. It provides environment which is needed for these technologies to operate. Its importance will be further explained in the following section.

2.2 MAGNETIC SHIELDING

This section contains informations on the concept of magnetic shielding. At first general informations are provided along with the description of currently used methods, which use ferromagnetic materials. Nextly properties and advantages of superconductors application are shown. Examples of contemporary and future applications are shown. Finally literature review is conducted to show the status of research and rationale for investigations done in this thesis.

2.2.1 Definition and current solutions

Magnetic shielding is a set of techniques used in order to decrease magnetic field in certain area. It might be applied in two directions. Firstly the field might be shielded in order to reduce or eliminate radiation of electromagnetic energy from electronic devices. Magnetic field is confined in shielded zone. This might be done to decrease electromagnetic noise, obey the regulations or hide the device in case of military appliances. In such case so called emission problem is prevented [7]. Field may also be shielded in other direction. Sometimes it is desirable for equipment to operate in magnetic vacuum or uniform field. This the case especially for precise detectors such as already described SQUIDs. This is known as immunity problem. Shielding of external field against entering into the shielded region is the main concern of this thesis.

The main parameter describing magnetic shield is shielding factor SF. It is expressed in dB and in general it is calculated according to equation 3 [7].

$$SF = 20 \cdot log\left(\frac{H_a}{H_i}\right) \tag{3}$$

Here H_a is an applied magnetic field and H_i is an internal shielded field. Shielding factor depends on geometric and material properties of a screen and the frequency of excitation field. That results in differences between shielding low and high frequency fields, which effected in development of several traditional shielding methods using ferromagnetic materials. The principles behind these methods have been described below.

DC magnetic field is shielded by the deviation of flux lines. This method takes advantage of lower reluctance of ferromagnetic material than surrounding air. Because of this lines of magnetic field tend to pass through the shield rather than region surrounded by the latter. That leads to large decrease of field behind the screen. This effect strongly depends on a shield geometry. In case of infinitely long tubular shield in uniform parallel magnetic field reduction depends on magnetic permeability of shield material and ratio between its internal and external diameter. The more permeable and thicker shield is used the better shielding is obtained. Shielding factor in such case is estimated according to formula 5 , which is derived from more general equation 4 [7]. Here μ_r is relative magnetic permeability, a_1 and a_2 are internal and external diameters respectively.

$$SF_{DCtube} = 20 \cdot log\left(\frac{(\mu_r+1)^2 a_2^2 - (\mu_r-1)^2 a_1^2}{4a_2^2\mu_r}\right) \tag{4}$$

$$SF_{DCtube} \cong 20 \cdot log\left(\mu_r \frac{1-(a_1/a_2)^2}{4}\right) \tag{5}$$

Any varying magnetic field is shielded by the skin effect, which is present in every conducting material subjected to such field. This phenomenon is caused by the nonuniform distribution of time-varying currents. This is expressed as the increase of current density close to the surface of conductor and is observed especially in alternating electric current applications. Due to variability of current induced inside a conductor by magnetic flux an extra flux is formed, which opposes the primary one [9]. Generally the efficiency of the field attenuation with the skin effect is proportional to a shield thickness d. It is also inversely proportional to skin depth δ, as in formula 6 [7].

$$SF = 8,68\frac{d}{\delta} \tag{6}$$

The δ depends on the magnetic field pulsation ω, the electric conductivity σ and the magnetic permeability μ as shown in formula 7 [9].

$$\delta = \sqrt{\frac{2}{\omega\sigma\mu}} \tag{7}$$

In real shields both the skin effect and the flux deviation contribute to shielding factor. Ferromagnetic plates are better for shielding of low frequency fields than ordinary conductors such as e.g. copper. [7] reports more than 50 times better shielding efficiency of ferromagnetic plates for 100 Hz magnetic field.

There are several problems with magnetic field shielding with ferromagnetic materials. The first problem is need to use materials with high magnetic permeability. Otherwise the shields would be very thick. Generally magnetic alloys with high content of nickel are used. Such shields have to be thermally processed after manufacturing. Application of this treatment causes large increase in costs. Another problem is the saturation of magnetisation. Above certain threshold induction the shielding capabilities significantly decreases. This rises need for concentric shields with different magnetic properties. Finally there is the problem of decreasing magnetic permeability in high frequency magnetic fields [7]. Usage of superconductors as materials for magnetic shields may help to solve aforementioned problems.

2.2.2 Superconducting magnetic shielding

Analysing equation 4 one may notice that the value of shielding factor remains the same when $1/\mu_r$ is used instead of μ_r. That means that large shielding factor may be obtained using materials with very low permeability. In this case flux lines instead of being channeled through the shield are expelled from this [7]. Typical diamagnetic conductors has relative permeability very close to 1, which makes efficient shielding impossible [10]. Conventional material with the lowest permeability is bismuth. Its value is 0,999834 [10]. For this material shielding factor is negligible. This calls for the application of perfect diamagnet - superconductor.

Using such materials very high shielding factors can be achieved. Superconducting body expels magnetic field from its bulk. This state is preserved by screening currents flowing in thin penetration region close to a surface. These currents flow in manner opposing external magnetic field so the total magnetic induction (which obeys relation $\mathbf{B} = \mathbf{H} + \mathbf{M}$) is equal to 0 (formula 8).

$$\mathbf{H} = -\mathbf{M} \tag{8}$$

Here $\mathbf{M}$ is magnetisation caused by screening currents and $\mathbf{H}$ is an external magnetic field applied to superconductor. If superconductor is cooled with external field applied screening currents sustain this state. Hence magnetic field is present even when external field is no longer applied [2]. If there is no external field during cooling there will be also no field generated by screening currents. The explanation of this behaviour comes from Ohm's law and Maxwell equations. When superconductor is cooled magnetic induction remains constant and is the same as in the moment when the transition occurred. Since there is no resistance, no electric field is generated, according to formula 9.

$$\mathbf{E} = \rho\mathbf{J} \tag{9}$$

This is the form of the Ohm's law, $\mathbf{E}$ is here electric field, ρ specific resistance and $\mathbf{J}$ is electric current density. Using Maxwell's equation the following result is obtained (formulas 10 and 11):

$$rot\,\mathbf{E} = -\delta\mathbf{B}/\delta t \tag{10}$$

$$\delta\mathbf{B}/\delta t = 0 \tag{11}$$

This relation holds for type I superconductors and type II superconductors in the Meissner state. Bulk of such superconductor below the penetration length is always free from magnetic field [2]. This property can be used to construct "vacuum pump" for magnetic field [11]. A shield which is used for the purpose of magnetic vacuum creation should be able to being folded. Cooling is performed and after reaching superconducting state the shield is unfolded thus reducing magnetic field inside. Similar shield should place inside the first and process should be repeated until desired field will be obtained. [11] reports achievement of field as low as 10^{-12}T.

External magnetic field is completely shielded in type I superconductors. They cannot be used as shield material since their critical magnetic field values are too low (e.g. critical value for aluminium is only 0,02 T). II type superconductors have higher values - critical magnetic field of YBCO is approximately 120 T [2]. In case of such materials shielding will not be full above certain value of field due to the transition to mixed state. Some field lines will be able to enter shielded region passing through superconductor. This property of type II superconductors will be explained in detail further.

Current applications of superconducting magnetic shields include mostly scientific and medical devices. They are used when high magnetic vacuum is needed for the calibration of SQUIDs [12]. Small shields are used in electron microscopy. Manufacturing process of electron lenses requires highly controlled magnetic conditions, which might be achieved using superconducting shields [13]. Larger shields are used mostly in scientific equipment requiring homogenous magnetic field. It is planned to use superconducting magnetic shield to increase the field homogeneity of electron cooling system for currently constructed accelerator NICA in JINR, Dubna [14]. Shields are used also in electrical devices, such as cryogenic current comparators [15]. Proposed superconducting fault current limiters of induction type also utilise shielding properties of superconductors [16].

The major problem connected with usage of superconducting shields is need to cool them below transition temperature. For conventional superconductors it would require application of sophisticated cooling techniques using liquid helium. In case of high temperature superconductors cooling with liquid nitrogen is sufficient. The trade-off in application of superconducting magnetic shields is between cooling needs and the cost of material and auxiliary equipment. Currently objects made of high temperature superconductors are very expensive, especially ones with complex geometry. On the other hand low temperature superconductors are relatively cheap and easy to shape. Maintaining their temperature is much harder, which limits mass applications.

2.2.3 Present status of research on superconducting magnetic shields

Meissner and Ochsenfeld were the first to observe field expulsion from superconductor and its zero permeability in 1933 [17]. Further research on this topic were conducted by Mendelssohn and Daunt in 1930s (for example [18]), who confirmed strong diamagnetic properties of superconductors. However the shielding capabilities was small due to the limited values of critical magnetic field for known superconductors. In early 1960s the discovery of Nb_3Sn superconducting properties in large magnetic fields sparkled an interest in magnetic properties of hard

superconductors [19]. Shielding was initially proposed by Cioffi for the purpose of the superconducting connections magnetic shielding [20]. Further investigations were performed by Hildebrandt, Warlquist and Elleman who proposed the application of superconducting shields to obtain uniform magnetic field [21].

Next decade brought deeper understanding of shielding properties [22] as well as new applications [13]. Similar development was observed in early 1980s [23]. At this time a lot of knowledge was found about the behaviour of type II superconductors. Besides this the next large incentive to develop superconducting magnetic shields came with the discovery of high temperature superconductors in 1986 [24]. The research were made to determine the basic shielding properties of new superconductors both experimentally [25] and theoretically [26]. After year 2000 the need for efficient shielding greatly increased due to the growth of number of devices using SQUIDs and expansion of scientific equipment. The possibilities of high temperature superconductors also rised due to progress in material science. Papers published on this topic can be divided into two major groups - ones concerning geometries and these focusing on applications. Among longer texts [7] is the most comprehensive source of informations on high temperature superconductor shielding, altough its experimental part focuses only on one material.

Geometries which are considered in recent papers contain tubular and planar screens. Tubular screens may be used as open or closed. Open type superconducting magnetic shields are generally used to obtain uniform magnetic field within some region. Superconducting element may be in such case placed in different configurations and does not have to completely surround shielded region. Closed screens are supposed to completely block the field. Seki et al. describes the application of superconducting rings at the end to improve shielding properties of a cylinder made of flexible magnetic material [27]. Another interesting solution was proposed Bertora, Molinari and Viale [28]. They propose to create self-shielding magnet for MRI, which would simultaneously produce magnetic field and, due to shielding effect, protect from disturbances. [29] provides outlook of experimental setup similar to used for the purpose of this thesis along with interesting theoretical considerations. There are also proposals of more exotic geometries, such as zigzag proposed in [30].

Recently large interest has been put in the application of coaxial hybrid systems. Many authors propose the application of superconducting screens in cooperation with ferromagnetic cylinders. Mori, Minemoto and Itoh have found the shielding efficiency to greatly improve when applying conventional and superconducting screens together [31]. Later it was proposed to increase the number of ferromagnetic screens and several effects have been recognised [32],[33]. The research on this topic are still ongoing. Numerical model has been created to study properties of such systems [34]. The most recent papers contain efficiency study [35] and theoretical considerations [36].

Recently many authors proposed new applications for superconducting magnetic shields. Cryogenic current comparators for the new FAIR facility which will be located in GSI in Darmstadt require highly attenuated magnetic field for the purpose of precise measurments. This is achieved by the usage of meander shaped shield [37]. Another scientific application is already mentioned stochastic cooling system for the accelerator NICA [14]. Applications for the shielding of SQUIDs are thoroughly investigated in many facilities [12], [38]. An interesting proposal is found in [39]. Author proposes there the application of superconducting magnetic shield for the purpose of shield screening in levitating train. It was also proposed to use superconducting magnetic shields to protect astronauts from harmful cosmic radiation during interplanetary voyages [40]. Large scale applications of second generation superconductor were also considered [41].

To the author's best knowledge no data concerning the application of hybrid high temperature superconductor shields have been published. The research have been conducted on multilayer high temperature superconductor coated on a single cylinder [42]. There is also a paper published on stacked cylinders made of NbTi [43]. Major effort has been put in research of single tubular shields and superconductor/ferromagnet hybrid systems. The performance of coaxial cylinders made of different high temperature superconductors was therefore chosen to be investigated.

2.3 TYPES OF SUPERCONDUCTORS

2.3.1 Division

There are two types of superconductors, which differ in their physical properties. As mentioned, these are known as type I and type II superconductors. Type I superconductors can exist only in pure Meissner state where all magnetic field is expulsed from the inside of superconductor. Type II may exist in both Meissner and mixed state. In mixed state (which will be described detailly in the next subsection) some magnetic flux passes through the superconductor. This division is crucial for the application of both types as a material for superconducting magnetic shields.

All superconducting elements (and their lean alloys) are type I superconductors, with an exception for niobium, vanadium and technetium [2]. Londons' theory explains their behaviour [7]. This theory assumes that among total number of electrons n in a certain volume there is some number of superconducting and normal electrons (n_s and n_n respectively), as seen in formula 12.

$$n = n_s + n_n \tag{12}$$

Superconducting electrons behave abnormally, since they do not scatter on impurities and phonons. Thus they do not lose energy and no electric resistance is observed. This forms the basis for two-fluid model and Ohm's law modification. As shown in previous section combining this knowledge with Maxwell equations one may conclude that the only consequence of infinite conductivity is constant magnetic field. However experiments prove that actually magnetic field inside the superconductor is not only constant, but also equal to 0. That is how the Londons' equation was found (formula 13).

$$rot\,\mathbf{J} + \frac{\mu_0 n_s e^2}{m} = 0 \tag{13}$$

$\mathbf{J}$ is here superconducting current density, e the charge of electron and m is its mass. Using this equation it is possible to derive several properties of superconductor, such as field expulsion, penetration depth and dependence of $\mathbf{J}$ on vector potential $\mathbf{A}$. Rearrangement of this equation leads to formula 1 shown before. Equation 13 describes the behaviour of shielding currents which protect the bulk of superconductor from external magnetic field. Formula 14 replaces Ohm's law for superconductors. $\mathbf{r}$ is there position vector.

$$\mathbf{J}(\mathbf{r}) = -\frac{1}{\mu_0 \lambda^2}\mathbf{A}(\mathbf{r}) \tag{14}$$

Londons' theory fails when the number of superconducting changes. It does not consider neither external mangetic field nor electric current. To describe this Ginzburg and Landau have presented in 1952 phenomenological theory of superconductivity, which was the first step

in the recognition of type II superconductors [2]. According to Landau's theory of second order phase transition there is a certain parameter (T_c in case of superconductors) below which transition takes place. Originally this theory explained spontaneous magnetisation of bodies below Curie temperature. To model superconductivity Ginzburg and Landau decided to replace magnetisation with a certain wave function $\psi(\mathbf{r})$ known as the order parameter, which is a complex scalar (formula 15).

$$\psi(\mathbf{r}) = |\psi\mathbf{r}|\, e^{i\phi(\mathbf{r})} \tag{15}$$

The modulus $|\psi * \psi|$ of this parameter can be interpreted as superconducting electrons density at point $\mathbf{r}$. It takes nonzero values in superconducting state and is zero in normal state. Its phase ($\phi(\mathbf{r})$) is related with superconducting current. In order to find order parameter and vector potential it is needed to minimise Helmholtz free energy with respect to both these parameters. This yields two formulas (16 and 17) [2].

$$\alpha\psi + \beta|\psi|^2\psi + \frac{1}{2m}(i\hbar\nabla - 2e\mathbf{A})^2\psi = 0 \tag{16}$$

$$\mathbf{J} = rot\,\mathbf{h} = \frac{e}{m}[\psi(-i\hbar\nabla - 2e\mathbf{A})\psi + c.c.] \tag{17}$$

Here $\mathbf{h}$ is local magnetic field and $\hbar$ is the reduced Planck constant. α and β are phenomenological parameters. β is temperature independent constant and α depends on temperature as shown in formula 18. Both these parameters can be obtained using experimental data.

$$\alpha = a(T - T_c) \tag{18}$$

Using fomulas 16 and 17 one may calculate thermodynamic critical field, penetration depth and coherence length. To calculate critical field formula 19 is used.

$$\mu_0 H_c^2 = \frac{\alpha^2}{\beta} \tag{19}$$

To obtain penetration depth equation 21 is applied. This length might be in range several hundreds to several thousands Å.

$$\mu_0 rot\,\mathbf{h} = -\frac{1}{\lambda^2}\mathbf{A} \tag{20}$$

The Ginzburg - Landau coherence length is calculated basing on equation 21. This parameter defines the maximum length in which changes of the order parameter will be observable if disturbance will be introduced at any point.

$$\xi^2(T) = \frac{\hbar}{2m|\alpha|} \tag{21}$$

Based on coherence length and penetration depth Ginzburg - Landau parameter might be calculated (formula 22). This parameter is independent from temperature and is actually the only constant parameter in Ginzburg - Landau equations.

$$\kappa = \frac{\lambda}{\xi} \tag{22}$$

Ginzburg - Landau free energy depends only on this parameter, which means that phenomenologically superconductor is completely defined by κ [2]. Another important propery can be seen in formula 23.

$$H_c(T)\,\lambda(T)\,\xi(T) = const = \frac{\hbar}{2e\mu_0\sqrt{2}} = \frac{\phi_0}{2\pi\mu_0\sqrt{2}} \tag{23}$$

Based on Ginzburg - Landau parameter it is possible to distinguish between type I and type II superconductors. If a magnetic field below which superconducting transition occurs will be marked as H_{c2}, the equation 24 is obtained using formulas 21 and 23.

$$H_{c2} = \kappa\sqrt{2}H_c \tag{24}$$

By analysing this equation one may notice that there is a threshold κ value of $1/\sqrt{2}$. Below this value magnetic field below which superconductivity appears is lower than thermodynamic critical field. Magnetic flux is fully expulsed from inside a type I superconductor. Above the threshold value superconducting transition occurs in fields above thermodynamic critical field. Magnetic field is only partially expulsed and a superconductor is of type II. In other words weakest magnetic field required to create a vortex is larger than thermodynamic critical field in type I superconductors and smaller in type II superconductors.

2.3.2 Properties of type I superconductors in comparison with type II

In figure 2 the comparison between critical magnetic field of type I and type II superconductors has been shown. One may notice that there are two values of critical field for type II superconductors. In case of type I superconductor magnetic field is either partially expulsed or a superconductor is in normal state. In type II superconductor such behaviour, known as the Meissner state, is observed below the first value of critical field. When maintaining constant temperature and rising magnetic field above the first critical value the mixed state will be achieved. In this state part of the magnetic flux is let through the superconductor in the form of vortices (fluxons). Above the second critical field a transition to normal state occurs. Generally the second critical value of magnetic field is much higher than the first one.

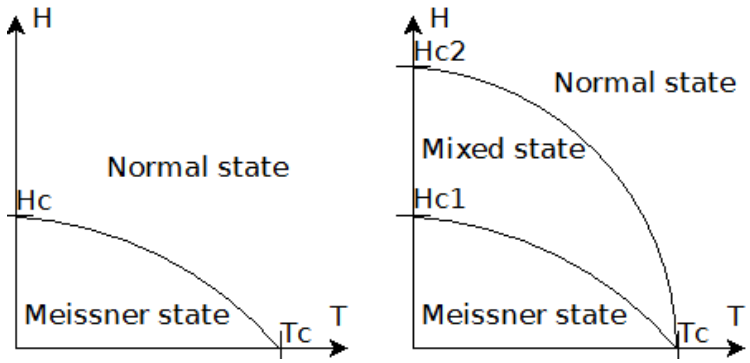

Figure 2: Critical magnetic field in type I (left) and type II (right) superconductor as the function of temperature

Figure 3 shows schematically magnetic field lines in three different states. In normal state above critical parameters magnetic flux lines pass freely through the superconductor. Skin effect and deviation of flux lines are also in power in such case. In Meissner state no magnetic flux lines enter the bulk of superconductor. Their shape is strongly affected by the presence of superconducting material. In case of mixed state deformation is smaller and some of lines are passing through the body. Due to this quench occurs in higher magnetic fields than in type I superconductors [2]. Mixed state is also known as the Shubnikov phase.

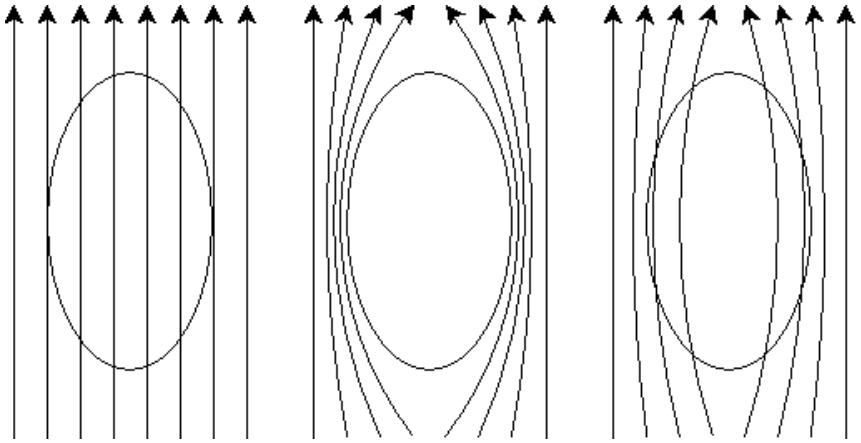

Figure 3: Magnetic field in normal (left), Meissner (middle) and mixed (right) state

Figure 4 shows the dependence of superconductor surface magnetisation versus external magnetic field. In case of type I magnetisation follows external magnetic field to fully shield it from entering the superconductor. Sharp decline in magnetisation is observed when external field exceed thermodynamic ciritical field of superconductor. In type II no such decline is observed. When the first value of magnetic field is exceeded magnetisation becomes smaller than external field. Therefore some of field is not shielded by superconducting currents and vortices are starting to form. It should be noted that not only external magnetic field may cause transition to normal or mixed states. This may be also the effect of electric current flowing through the superconductor and thus generating magnetic field (self-field effect).

2.3.3 Applicability of type I superconductors for magnetic shielding

Type I superconductors may exist only in Meissner or normal state. Figure 5 shows how average magnetic field inside infinitely long cylinder made of such superconductor changes with an applied field. The magnetic behaviour of type I superconductor is reversible, that is it does not depend on history of applied induction, but merely on its value [7]. Completely diamagnetic property below critical induction might seem attractive for the purpose of field shielding. However, it has to be noticed that cooling conditions of such superconductor significantly affects its properties.

Cooling may be performed with no external magnetic field applied. In such case zero field conditions (ZFC) are in force. It may be also done in the presence of magnetic field, which is know as field cooled conditions (FC). For the purpose of shielding infinitely long hollow tube will be considered. Knowing that field inside the cavity will be constant in time both types of cooling will be investigated. In ZFC case cylinder is cooled below its critical temperature with no external field, which is applied afterwards. Induced currents prevent induction from penetrating the superconductor and thus the hole is also protected.

In FC case external field is applied before cooling. Similarly to previous case superconducting currents block induction propagation into the superconductor. Field inside the hole also must remain constant, however. This is ensured by superconducting currents flowing on the superconductor inner surface. That means that the field inside cavity remains equal to the applied one. It is still present inside even when external field is removed. Therefore shielding with type I superconductor is possible only in ZFC case. Otherwise only the constant field is obtained, which might be of practical value in some cases. Lead cylinders were used to produce very low magnetic fields [44].

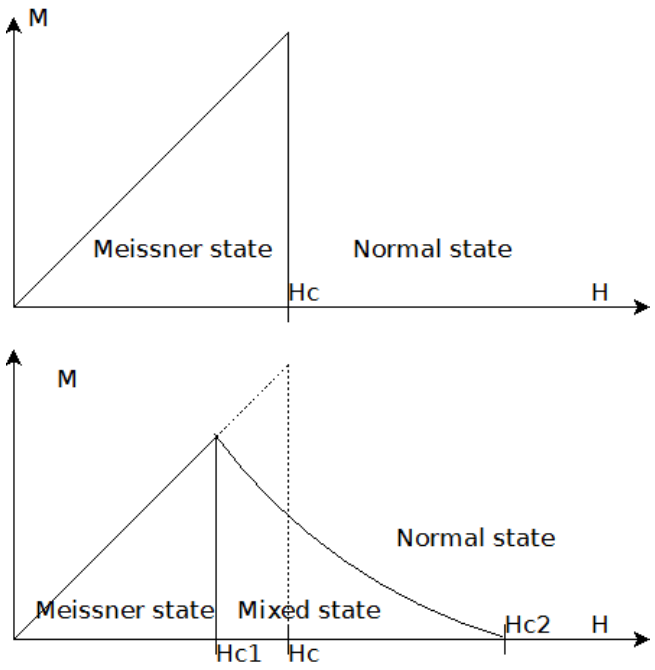

Figure 4: Magnetisation vs external magnetic for type I (top) and type II (bottom) superconductor

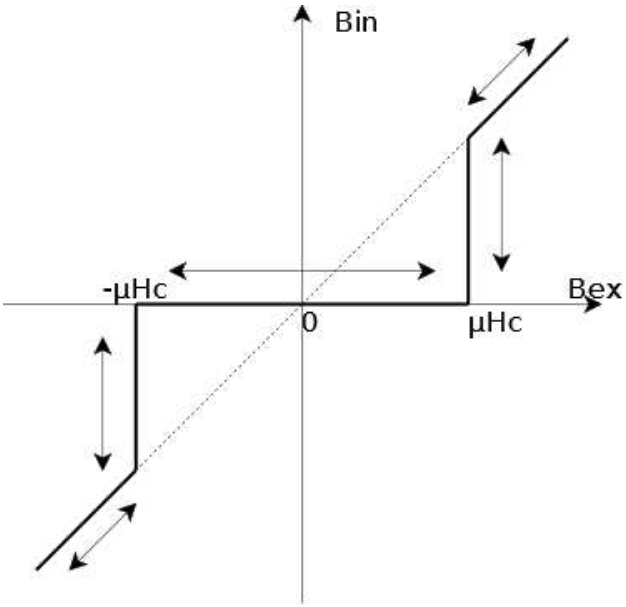

Figure 5: Internal magnetic induction versus applied external magnetic field in infinitely long cylinder made of the type I superconductor

Material	Critical temperature	Critical magnetic field	Type
-	T_c(K)	Gs	-
Ti	0,39	100	I
Zr	0,546	47	I
Pb	7,193	803	I
YBCO	93-95	$250 \cdot 10^4$	II
BSCCO	108	$200 \cdot 10^4$	II
NbTi	9,2	$15 \cdot 10^4$	II

Table 1: Properties of chosen superconductors

There are also several practical problems with the application of type I superconductors. All of them have low critical temperature. This requires cooling with liquid helium, which is rather expensive and needs considerable insulation. Additionaly the applicability is limited by their low critical field. This is enough to shield Earth's magnetic field or coming from other minor sources, but will not be sufficient for shielding of large fields. Values for critical field and temperature of several type I and type II superconductors have been gathered in table 1 [45]. Main advantage of the application of type I superconductors is the possibility of full shielding. Type II superconductors have mostly higher temperatures and critical fields, but does not offer full shielding in the whole range of magnetic fields. Their application will be discussed in the next section.

2.4 MAGNETIC BEHAVIOUR OF TYPE II SUPERCONDUCTORS

2.4.1 Vortices and lower critical field

To obtain zero magnetic field inside the superconductor some amounts of energy is needed. This is minimised in type II superconductors in mixed state by letting the magnetic field lines to pass through a superconductor in the form of vortices. Each such vortex contains single quantum of magnetic flux (fluxon). The value of flux quantum is equal to $2,0678 \cdot 10^{-15} Wb$. This value comes from formula 25. Φ_0 is there the value of flux, h is the Planck constant and e is the charge of a single electron [2].

$$\Phi_0 = {}^{h}/_{2e} \tag{25}$$

Relation between the density of vortices and magnetic induction is described by formula 26.

$$B = \blacksquare\Phi_0 \tag{26}$$

The application of this formula allows to calculate the distance between individual vortices based on the value of magnetic induction. Since the number of vortices increases with growing induction, the distances between them decreases. When the external field is close to H_{c1} the approximate distance is close to λ. If the field comes to H_{c2}, it is in the order of magnitude of vortex radius.

Figure 6 shows the structure of a single vortex. The central part of the vortex is a normal core, where no superconducting electrons are present. The radius of this core is approximately equal to the coherence length ξ. The vortex is surrounded by the superconducting current, which cause the attenuation of magnetic field $\mathbf{h}(\mathbf{r})$ according to the equation 27. $\mathbf{K}_0$ is there the Hankel function [2]. Vortex can be treated as non-dissipating superconducting current rotating around the normal core.

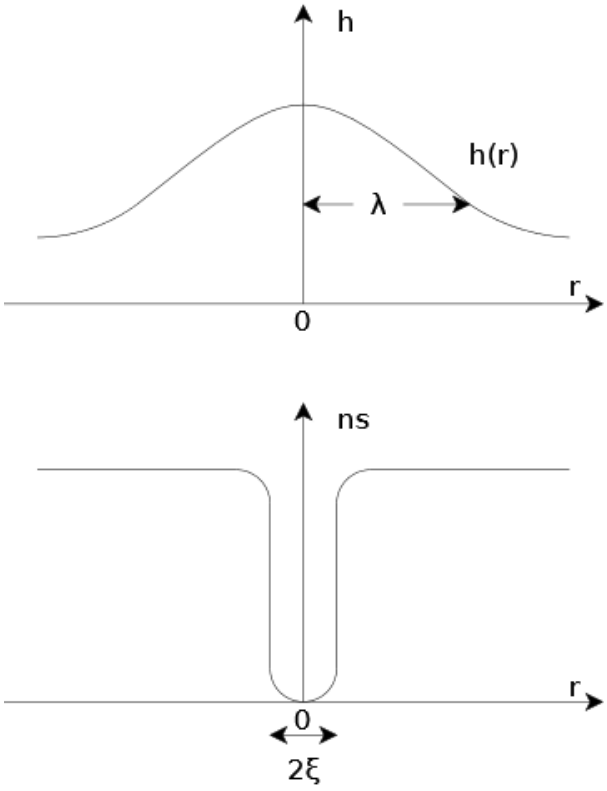

Figure 6: Structure of a single vortex

$$\mathbf{h}(\mathbf{r}) = \frac{\Phi_0}{2\pi\lambda^2\mu_0}\mathbf{K}_0\left(\frac{\mathbf{r}}{\lambda}\right) \tag{27}$$

The energy of a single vortex U_v depends on intrinsic material parameters and is given by equation 28.

$$U_v = \frac{\Phi_0^2}{4\pi\lambda^2\mu_0} ln\frac{\lambda}{\xi} \tag{28}$$

The lower critical field is a thermodynamic border above which the penetration of superconductor by vortex is energetically favorable. The change of the Gibbs energy due to the formation of ■ vortices per unit area comes from equation 29. Interactions between the vortices have not been considered due to large distances in fields close to H_{c1}.

$$\Delta G = \blacksquare U_v - BH \tag{29}$$

Combining this formula and equation 26, one obtains relation 30.

$$\Delta G = B\left(\frac{U_v}{\Phi_0} - H\right) \tag{30}$$

Since vortices enter a superconductor only when it leads to decrease in the Gibbs energy, the applied magnetic field must be higher than $\frac{U_v}{\Phi_0}$. Therefore its threshold value can be calculated with formula 31.

$$\mu_0 H_{c1} = \frac{\Phi_0}{4\pi\lambda^2} ln\frac{\lambda}{\xi} \tag{31}$$

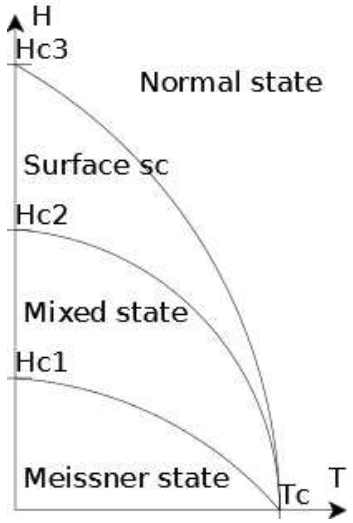

Figure 7: Critical fields in type II superconductor

Field $H_{c1}$is small when κ is large. This is the case for superconductors used in the experimental part of this thesis. Therefore only limited range of full shielding is expected. The lower H_{c1} and the upper H_{c2} critical magnetic fields are connected with thermodynamic critical field H_c by relation 32.

$$H_{c1}H_{c2} = H_c^2 ln\kappa \tag{32}$$

It means that the larger the value of upper magnetic field is, the smaller lower critical field becomes. Considerations described above are valid for infinite specimen. By adding border condition of finite length, another critical field will be observed. Ginzburg - Landau equations show that in such case superconductivity will appear below field H_{c3}. Its value is given by thequation 33.

$$H_{c3} = 1,69H_{c2} \tag{33}$$

Figure 7 shows these three fields. Between H_{c3} and H_{c2} so called surface superconductivity is observed, if the field is parallel to the specimen surface. Superconducting current is flowing in thin layer on the surface of specimen. The depth of this layer is equal to coherence length ξ. Magnetic field is not expulsed from the rest of specimen [2]. That means that no resistance will be observed, but there also will be no shielding effect.

2.4.2 Reversible type II superconductors

In a reversible type II superconductor vortices move freely within the volume of specimen. Figure 8 shows the development of internal magnetic field as the function of applied field in such superconductor. The assumption is that the superconductor is infinitely long and the field is axial. In such case external field is fully shield below H_{c1} and partially up to H_{c2}. Above this field transition to normal state occurs. Since the superconductor is reversible it does not matter if induction is rised or lowered. No hysteresis effects are observed.

Specimen lattice must be without defects to obtain the reversible superconductor. Lack of defects means that there will not be any places which would favour formation and sustainment of vortices. Such places are called pinning centres and their role will be explained along with

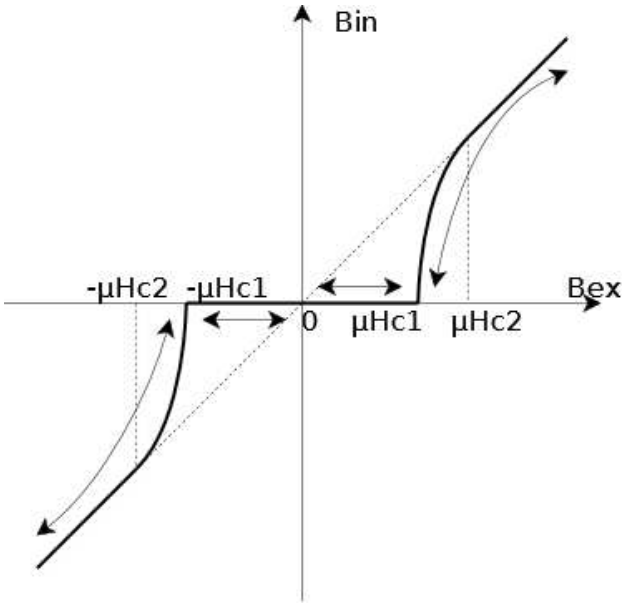

Figure 8: Internal magnetic induction versus applied external magnetic field in infinitely long cylinder made of the reversible type II superconductor

the behaviour of irreversible superconductors. Vortices interact with each other and exert repulsing force - Lorentz force $\mathbf{F}_L$. Free movement of vortices ultimately leads to the formation of triangular Abrikosov lattice (seen in figure 9). In such state equilibrium between vortices is achieved.

Lack of movement barriers causes vortices to constantly move and thus generate electric field. The energy is dissipated and transport losses are observed. Therefore reversible superconductors cannot be efficiently used for carrying currents. Shielding is also poor, due to similar reasons [7]. Below H_{c1} shielding is full, just as in case of type I superconductor. Above this field vortices pass through the superconductor. This leads to the generation of electric field within the shielded region. Since H_{c1} is often low, the practical value of reversible shields is unsatysfying.

2.4.3 Irreversible type II superconductors

The crystal lattice of an irreversible superconductor is characterized by the presence of the pinning centres. These are usually various structural defects like point defects, dislocations, grain boundaries, strange atoms, empty spaces etc. These imperfections prevent magnetic flux from movement. The sizes of the pinning centres are in order of the coherence length [7]. Due to this the distribution of vortices is not similar to the Abrikosov lattice for the reversible superconductor anymore. In 1964 Bean proposed the model to find the distribution of vortices as the function of position in strongly pinning material. This model is valid for infinitely long tube or slab made of a type II superconductor.

The basic assumption of this model is the existence of certain current J_c, which is the maximum current that can be carried by a superconductor. Electromotive force of any size causes such current to flow locally. Electromotive force is here the effect of differences in local induction $\mathbf{B}$. Under these assumption two states arise - below J_c the electric field is 0 and above this it tends to infinity. In ZFC case followed by the application of an external field these assumptions lead to situation where there is no current in regions that have not been affected by magnetic field and the current of magnitude J_c for every other region. Formula 34 coming from Ampere's

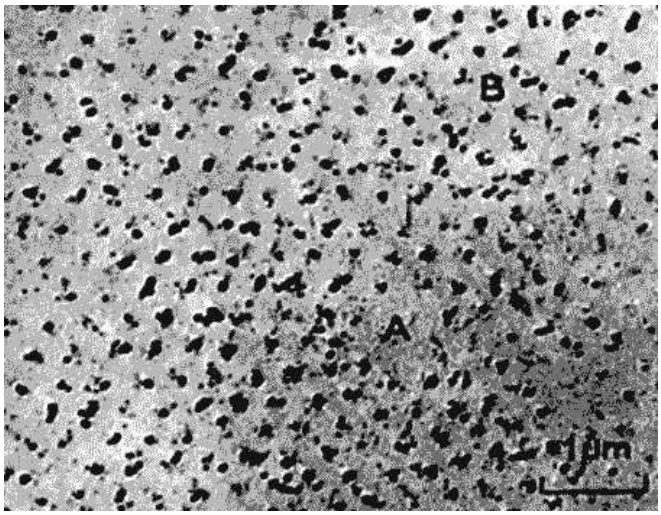

Figure 9: Abrikosov lattice for reversible type II superconductor (from [46])

law summarises these two states.

$$\nabla \times \mathbf{B} = \mu_0 J_c \; or \; 0 \tag{34}$$

Since considered tube is infinitely long, there is no demagnetising field ($\mathbf{H}_D = 0$). Bean model assumes also that lower magnetic field tends to zero, while the upper one to infinity. Surface barriers are neglected. Therefore magnetic field lines enter superconductor for any external field magnitude. If cylindrical coordinates are used, the equation 34 reduces to formula 35.

$$\frac{\delta B}{\delta r} = \mu_0 J_c \tag{35}$$

This equation allows to find the field distribution along the thickness of a superconducting tube. Since tube is infinitely long, the field inside the aperture is uniform. Due to the induction difference, there is a macroscopic current flowing, which produces Lorentz force $\mathbf{F}_L$. This would cause vortices to move, however there is also a pinning force $\mathbf{F}_P$.

The assumption of pinning conditions and maximum current leads to $\mathbf{F}_P = \mathbf{F}_L$ at any point where electric current occurs. That means that movement of vortices is limited to situations when $\mathbf{B}$ is increased above certain value and Lorentz force temporarily becomes larger than pinning forces. Then vortices, initially formed close to the surface, are pushed further into a specimen to the regions where flux is lower. After that forces become equal again and a new equilibrium state is achieved.

Figure 10 shows the distribution of field inside a superconducting tube and shielding currents for the case when $B \geq B_P$. For the certain value of magnetic field (which is usually called full penetration field H_P), it starts to penetrate into the aperture. This field can be found with formula 36, where d is the thickness of considered tube.

$$H_P = J_c d \tag{36}$$

Based on this one may calculate the penetration induction B_P ($B_P = \mu_0 J_c d$). Below this induction certain regions inside the tube are not affected by magnetic field. With the increase of external magnetic field, the field penetrates further into the superconductor. Finally, at the penetration value, magnetic flux touches the inner surface of the tube. Above this value, induction throughout all thickness of the tube increases uniformly.

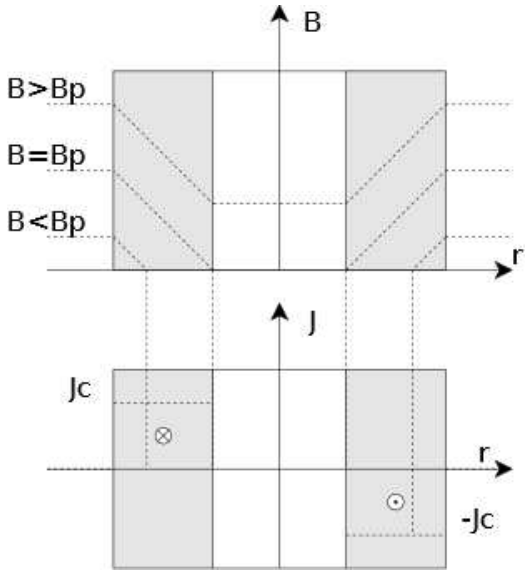

Figure 10: Induction B and superconducting current J_c in superconductor according to Bean critical state model

Irreversibility effects are observed when penetration field is exceeded. In such case shielding currents form on the inner side of tube, which sustain magnetic field even if it has been decreased below penetration value. Pinning disallows vortices to leave the tube, just as it prevents them from any movement. Examples of such effects are shown in figure 11.

Lefthand picture in figure 11 shows remnant field after the application of B such that $B < 2B_P$ and following reduction of external field. Superconducting tube starts to behave such as a permanent magnet. Picture on the right shows the state when $B \geq 2B_P$. In such case the field observed inside the cavity reaches its maximum value - $2B_P$. If the applied field was higher than this value, vortices leaked out after its removal until the value of $2B_P$ was obtained. The thicker the tube, the stronger magnetic field sustained.

Due to pinning shielding is also hysteretic. The value of field inside the tube depends not only on the applied field, but also on its history. Figure 12 shows the development of field inside the cavity due to applied external field. It is assumed that the sample was cooled in zero field conditions. Several points of interest were marked.

The region of interest for shielding applications comes between initial field of 0 and B_P. In such conditions magnetic field remains 0 inside the cavity. This shows that pinning allows to shield fields larger than H_{c1}. However, when field exceeds the value of B_P vortices start to penetrate into the cavity and remnant induction starts to appear. In such conditions shielding becomes inefficient. As it may be noticed in the figure, during the decrease, internal field obtains the value of B_P, when external field is 0. Internal field becomes 0, when external field is equal to B_P and $-B_P$ when external field is 0 during its increase. If tube was cooled in field conditions, the shielding considered as field blocking is not observed [7].

2.5 YBCO AND BSCCO AS HIGH TEMPERATURE SUPERCONDUCTORS

2.5.1 YBCO

YBCO is the name for group of superconducting ceramic materials made of yttrium (Y), barium (Ba), copper (Cu) and oxygen (O) [47]. Its chemical formula is $YBa_2Cu_3O_{7-x}$, where x

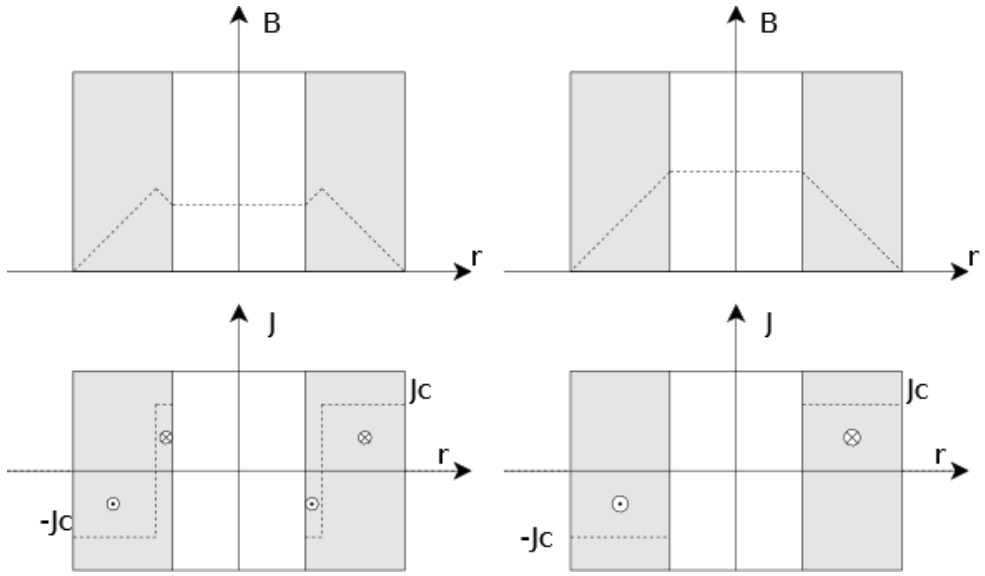

Figure 11: Irreversibility effects according to Bean model

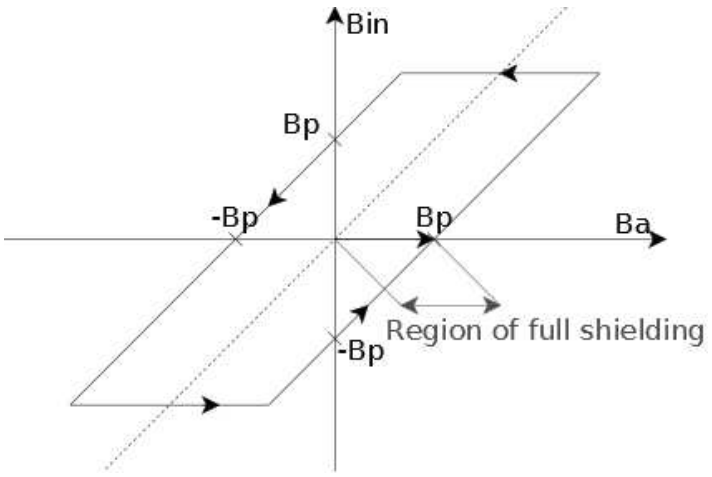

Figure 12: Characteristic points in a hysteresis curve of superconductor according to Bean model

is a parameter depending on oxygen content. It was the first material found to exhibit superconducting properties above liquid nitrogen temperature. Critical temperature of YBCO was found to be 93K at normal pressure [48]. This discovery was of great significance for the future applications of superconductors.

There are several methods of YBCO synthesis. Originally it was produced by the process of heating a mixture of metal carbonates to high temperatures (over 1000K). The chemical formula for such process is shown below (formula 37).

$$4BaCO_3 + Y_2\left(CO_3\right)_3 + 6CuCO_3 + \left(1/2 - x\right)O_2 \rightarrow 2YBa_2Cu_3O_{7-x} + 13CO_2 \tag{37}$$

This method allows to obtain relatively pure YBCO. Currently oxides and nitrates are used instead carbonates. Superconducting properties vary depending on the oxygen content. YBCO is superconducting only if x from formula 37 is in range $0 \leq x \leq 0,65$. The best properties are obtained when x is equal to 0,07 [49]. In such case critical temperature is 95K and critical field is 120T when the field is perpendicular to the superconducting plane and 250T when it is parallel.

The measurments of coherence length and penetration depth brought different results depending on a measurment method [50][51]. In case of single grain penetration depth is 120 nm in the superconducting plane and 800 nm perpendicularly. Coherence length is 2 nm in superconducting plane and 0,4 nm perpendicularly. Bulk properties depend on several other factors.

Manufacturing process strongly affects the performance of superconductor. Grains should be aligned so the superconducting planes were not separated and lay in roughly the same plane. This is done by adjusting of temperatures during sintering process. Several other methods have been applied, such as chemical vapour deposition, sol-gel [52] and aerosol [53], however sintering is still needed to obtain best superconducting properties. YBCO is often coated on the surface of flexible metal plate.

Figure 13 shows the structure of YBCO. It is a perovskite structure consisting of layers. There are two types of CuO planes - square and chain. Square planes are thought to be responsible for supercondctivity, though some superconducting currents flow also in chain planes [54]. Investigation on this matter is complex, since it is hard to isolate contribution to superconductivity coming from individual layers. YBCO crystals are ordered and clean, which eases analysis, despite variety of superconducting planes.

YBCO is used in NMR devices for probing the spatial distribution of magnetic field. High precision is obtained due to ordered nature of crystals. It is also being used in quantum physics research [55]. There are several limitation in the application of YBCO. Major problem is low critical current density in bulk superconductor due to the limiting effect of grain boundaries. However, despite technological problems and due to its high critical field it is used for the production of strong magnets. One of the shields used in the experimental part of thesis will be made of YBCO tape.

The construction of such tapes is shown in figure 14. In this example Hastelloy is used as substrate. Superconductor layer is separated from this substrate by several layers of buffer materials. Each of these layers serves different purpose. $LaMnO_3$ is used to produce lattice match. Below this layer of homo-epi MgO is placed to improve texture. Next layer is IBAD MgO followed by Y_2O_3 serving as nucleation layer. Finally there is diffusion barrier made of Al_2O_3. Above superconductor the layer made of silver is coated. Whole assembly is enclosed in copper from all directions. The tape of similar construction was used during the experimental part of thesis. Critical current density of such tape is approximately $4 \cdot 10^{9 A/m^2}$.

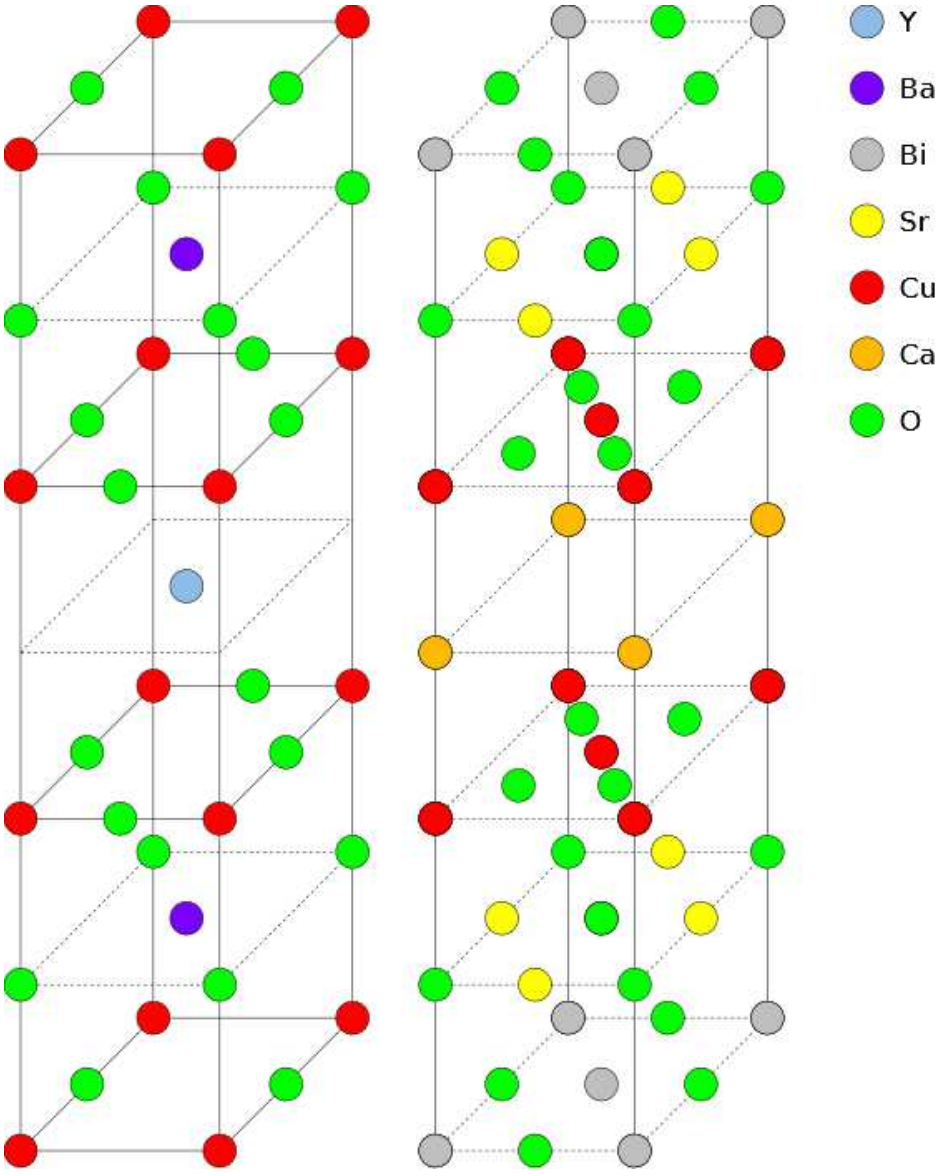

Figure 13: YBCO (left) and BSCCO (right) structure

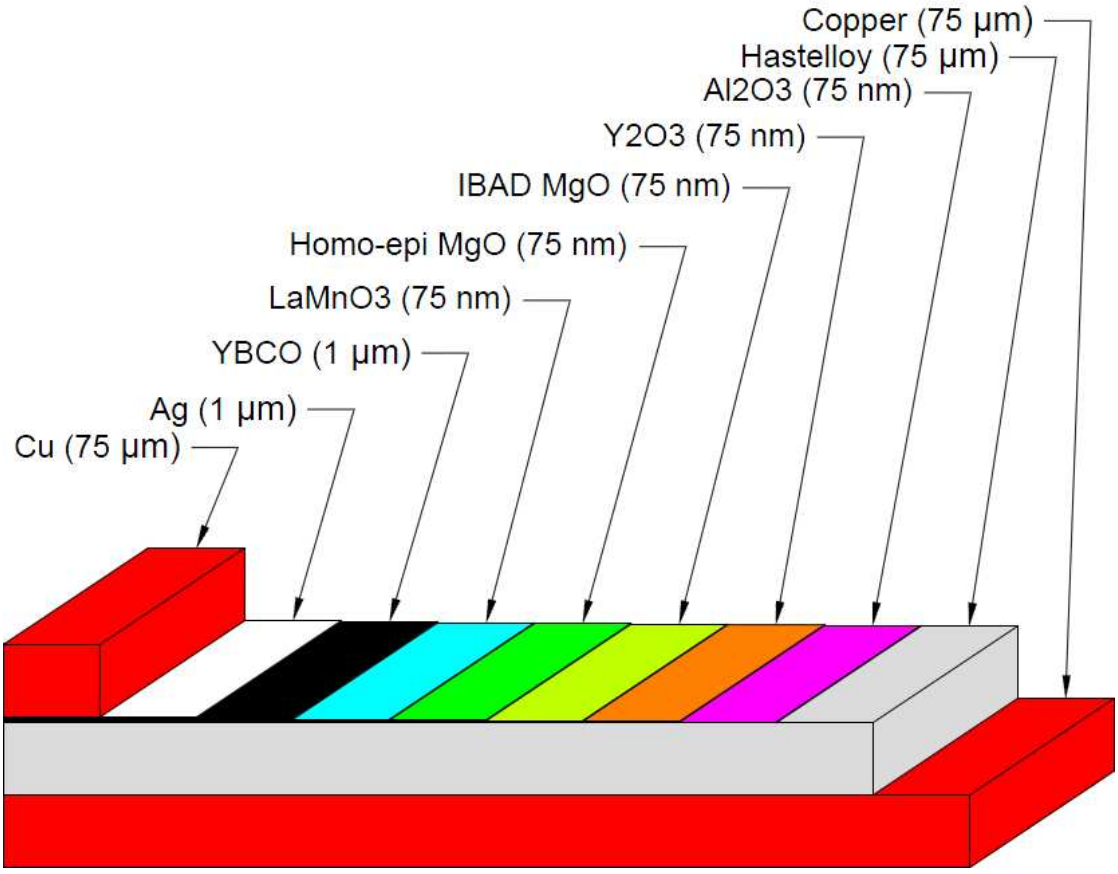

Figure 14: YBCO tape - coated superconductor

2.5.2 BSCCO

BSCCO is the group of superconductors consisting of bismuth (Bi), strontium (Sr), calcium (Ca), copper (Cu) and oxygen (O). Chemical formula of such compound is $Bi_2Sr_2Ca_{n-1}Cu_nO_{2n+4+x}$. n most commonly takes value of 2, however compounds with n of 1 and were also researched. x, similarly to YBCO denotes oxygen content. Unlike YBCO it does not contain rare earth elements. This compound was discovered in 1988 [56]. Types of BSCCO are named after the number of particular atoms and n parameter. Therefore there is Bi-2201, Bi-2212, Bi-2223 and Bi-2234.

Similarly to YBCO, BSCCO properties strongly depend on oxygen content. Optimal critical temperature is achieved when there is an excess of 0,16 holes per copper atom [57]. Overdoping and underdoping causes decreases critical temperature. Underdoping additionally leads to dramatic decrease of critical magnetic field. Optimal critical temperature for Bi-2201 is approximately 20K, for Bi-2212 it is 95K, Bi-2223 - 108K and 104K for Bi-2234. In elevated pressures these temperatures tend to increase. Upper critical magnetic field was found to be 200T in 4,2K [58]. This is limited by irreversibility field, above which vortices tend to melt and decouple. Penetration depth of Bi-2212 is 269 nm and coherence length is 1,6 nm [59].

Similarly to YBCO, grains have to be in good contact and must be aligned to obtain good superconducting properties. BSCCO is flexible and grains may be moved by means of both mechanical and thermal manipulation. Superconducting wires made of this material are generally produced by powder-in-tube technique. Precursor powders are put in silver tube, which is then repeatedly extruded to desired dimmensions. After this, everything is rolled to the form of flat type to ensure grain alignment. After powders are reacted in high temperatre and superconducting wire is formed. Typical current density achievable in such cables is in order of $5 \cdot 10^5 {}^{A}/_{cm^2}$.

Structure of BSCCO is shown in figure 13. Atoms of bismuth may be replaced with thalium or mercury, which leads to the formation of superconductor with critical temperature of 135K. The double layers of bismuth are only weakly bonded by the means of Van der Waals forces. Therefore slip may occur and structure may deform, just like in graphite. Due to this they align easily.

BSCCO finds application as material for cables due to its formability. These might be used in electrical and power industry. Such wires can form losless transmission line, what was done in Detroit Edison project[60]. Unfortunately, insulation problems compromised the success of this project. BSCCO wires may also be applied in transformers and generators as winding material. Solid Shields, which will be used in this thesis, as well as one of external shields will be made of this material.

3 MATHEMATICAL MODEL

3.1 KIM AND BEAN MODEL FOR DC SHIELDING

3.1.1 Bean model limitations

Bean model described in previous section is a good way to obtain the value of magnetic field shielded by superconductor with strong pinning when knowing the value of J_c. There are, however, several assumptions, which limits its applicability. In actual superconductors several effects are present, which are not considered by this model. In order to obtain reliable results these effects need to be included in an extended model.

Critical current density in real superconductors decreases with magnetic induction. This dependance is known as Kim law. If critical current density was considered constant, shielding capabilities of material would be vastly overestimated. Experiments found that intergranular critical current density is sensible to local induction [62]. The model was proposed to account for this effect [63]. This model is generally accepted and is in a good match with experimental results. Formula 38 describes relation between local induction and critical current density.

$$J_c(B) = \frac{J_{c0}}{1 + \frac{B}{B_1}} \tag{38}$$

J_{c0} represents critical current density when there is no magnetic field and B_1 is a material parameter.

Another limitiation of the Bean model is connected with the assumption that the only forces acting on vortices are Lorentz and pinning force. From this assumption comes an information that only the currents of value J_c flow inside a superconductor. In real superconductor current density can take whole range of values. Continuing assumption that only Lorentz force depins vortices, J_c becomes limiting current for vortices to be pinned, which means that $\mathbf{F}_P = \mathbf{F}_L$. Vortices, however, may be depinned due to variety of other reasons, especially thermal excitation.

Several different regimes of vortices movement may occur depending on relation between thermal and Lorentz forces. If temperature is equal to 0K no thermal excitation is observed. In such situation when $J < J_c$ vortices does not move, when current is larger than J_c a superconductor enters the flux-flow regime. Movement of vortices causes appearance of electric field, which is given by equation 39.

$$E_v = v \times B \tag{39}$$

Each moving vortex is a subject to viscous drag, as shown in equation 40 [7].

$$\mathbf{E} = \rho_{FF}\mathbf{J} \tag{40}$$

Flux resistivity factor is obtained with formula 41 [64].

$$\rho_{FF}(B,T) \cong \frac{\rho_n B}{B_{c2}(T)} \tag{41}$$

When $T > 0K$ thermal energy appears, capable of depinning vortices. Due to small pinning energies and relatively high temperatures involved, this method of vortex depinning becomes dominant, when high temperature superconductors are applied. If superconductor is operated close to T_c, depinning currents are very small. In such regime resistivity $\rho = {}^{dE}/_{dJ}$ is linear and is known as thermally assisted flux flow. The most often met situation is when temperature is lower than T_c. Such regime is known as flux creep and relation between E and J becomes strongly nonlinear ($E \propto J^n$ with $n \gg 1$).

Flux creep theory was initially created by Anderson to explain logarythmic decay of superconducting currents in low temperature superconductors [65]. Vortices depinned due to thermal excitation are moved by Lorentz force. Due to this the spatial variation of induction is decreased. According to $\nabla\mathbf{B} = \mu_0\mathbf{J}$ this causes the decay of superconducting currents. Unlike in Bean model, in Anderson theory only quasi-equilibrium states are possible. Experimental and theoretical considerations lead to formula 42, which describes electric field dependence on current flowing through superconductor.

$$E = E_c \left(\frac{J}{J_c}\right)^a \tag{42}$$

a is here U_0/kT, where k is the Boltzmann constant and U_0 is the barrier height of the pinning potential when there is no driving force. $E_c = Bv_0$, with v_0 being the velocity of flux lines when there is no barrier. J_c is unavailable and, according to experiments, is defined by voltage criterion as the critical current density leading to the electric field value of 1 $\mu V/cm$. When a is close to 1, specimen is either in normal state or in thermally assisted flux flow regime. When $kT \ll U_0$, flux creep is observed. Due to large powers involved (in the range of 20 for HTS), energy dissipation is small when $J < J_c$ and greatly increases in other cases. This makes J_c border between low and high losses regimes. Formula 42 allows to derive conclusions concerning alternating fields. If the frequency is multiplied by the factor of c, current density and magnetic induction are rescaled by $c^{1/a-1}$. In Bean model ($a \to \infty$) no frequency effects are observed.

The final equation for Kim model which has been used comes from [7] (equation 43).

$$B_{in} = \begin{cases} -B_1 + \sqrt{(B_1 + B_{ex})^2 - 2\mu_0 B_1 J_c d} & if\ B_{ex} \geq B_{lim} \\ 0 & if\ B_{ex} < B_{lim} \end{cases} \tag{43}$$

B_{lim} is here threshold value of external induction above which transition to mixed state occurs. It is calculated according to the formula 44.

$$B_{lim} = -B_1 + \sqrt{B_1^2 + 2\mu_0 B_1 J_c d} \tag{44}$$

Bean model cannot take into consideration geometric limitations. Therefore demagnetising effects cannot be modeled with this, since they do not exist in infinitely long tubes subjected to uniform field. Another limitation is the fact that model is unable to calculate component of **J** parallel to **B**. It is limited to situations when a current is perpendicular to an induction. Elements with axial geometry subjected to mostly uniform parallel fields will be considered in systems researched in this thesis.

It is expected that no difference will be observed in direct current field shielding when additional shield made of YBCO tape will be applied. This is due to the fact that it is not monolithic - magnetic field is free to leak inside the outer shield through non-superconducting parts of the screen. These are gaps between rings and solders. Detailed description of second shield construction is provided in further section. Only the solid inner shield will be affecting propagation of magnetic field. Thus unchanged Kim model will be used for modelling of both solid and double shield systems.

3.1.2 Simple Bean model

The outlook of basic curve obtained using simple Bean model is shown in figure 15. The units are arbitrary and the figure shows qualitative dependance of the field inside shielded cavity and applied external field. One can easily spot several important characteristic features of hysteresis curve. The curve starts in the middle of graph, when both external and internal fields are 0. Then the external field is increased. Internal field remains 0 until external field reaches the value of B_P (see figure 10). Then the internal field starts to increase so that $B_{in} = B_{ex} - \mu_0 J_c d$, where d is the thickness of tube. Thus the length of full shielding region is equal to B_p.

After external field is started to be decreased, internal field remains equal to the maximum field obtained during increase. It remains as such until $B_{in_{max}} - B_{ex} \geq 2B_P$. When this condition is not met anymore, internal field starts to decrease and obtains the value of B_p when the external field is 0. Internal field becomes 0 again when external field is equal to $-B_p$. Reverse situation takes place at the bottom of the hysteresis curve. When field is increased again, this is not

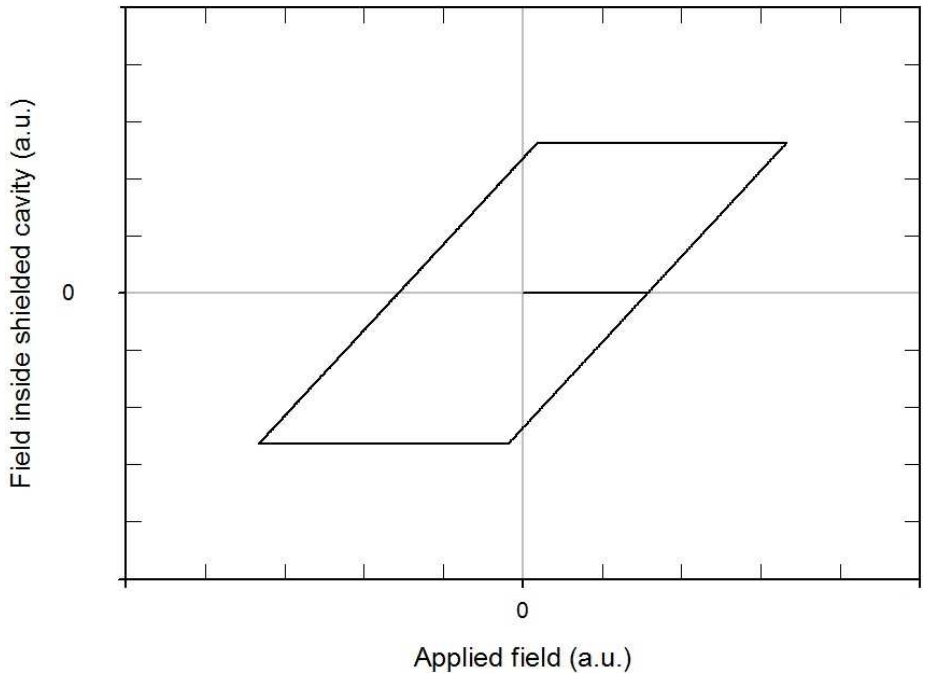

Figure 15: Basic curve obtained with simple Bean model

reflected inside shielded cavity until it will be larger by $2B_p$ than minimum internal field. Then it starts to rise again, obtains the value of $-B_p$ when external field is 0. The loop is closed when internal field becomes 0 with the external field of value B_p.

Two main factors affects the shape of hysteresis curve. The effect of changing J_c (which may be interpreted as the change of material) is shown in figure 17. The curve from figure 15 is compared there with curves obtained when the critical current is two (red - B) and five (blue - C) times smaller. It was assumed that the range of external field values is the same. It is clearly visible that the region of full shielding is reduced with the decrease of J_c. Hysteresis curves with lower J_c appear to be longer, they are also thinner. Plateaus at both ends of curves change their length accordingly, so that it remains equal to $2B_p$, which changes proportionally to J_c. The values at characteristic points hold aforementioned correlations for each of the curves. Slope remains the same for any of the respective curves.

Figure 17 depicts the effect of tube thickness on the shape of hysteresis curve. Black curve (A) comes from the figure 15. The red curve (B) shows situation when the thicknes was decreased 3 times. Blue curve (C) was obtained when tube thickness was increased 2 times. The results are similar to these obtained before and are such due to the fact that the shape of hysteresis curve in a simple Bean model depends solely on the value of B_p, which is directly proportional to thickness and critical current (equation 36). The interesting observation at this sketch is that in case of blue curve the internal field actually is not B_p when external field is 0. This is caused by too small range of hysteresis curve formation. The external field never exceeds $2B_p$ and is unable to form a remnant field of sufficient strength.

Shielding factor was calculated using the formula 3. Small value of internal magnetic induction has been added in full shielding region to make the calculations possible and account for measurment uncertainties. The results have been shown in figure 18. The black curve (A) corresponds with the one from figure 15. Results coming from the red curve in figure 16 (double decrease in critical current) have been marked in red as well (B). Similarly, results based on blue curve from figure 17 (double increase of tube thickness) were drawn also in blue (C). Shielding factor is a subject to dramatic variations as the changes in magnetic field progress.

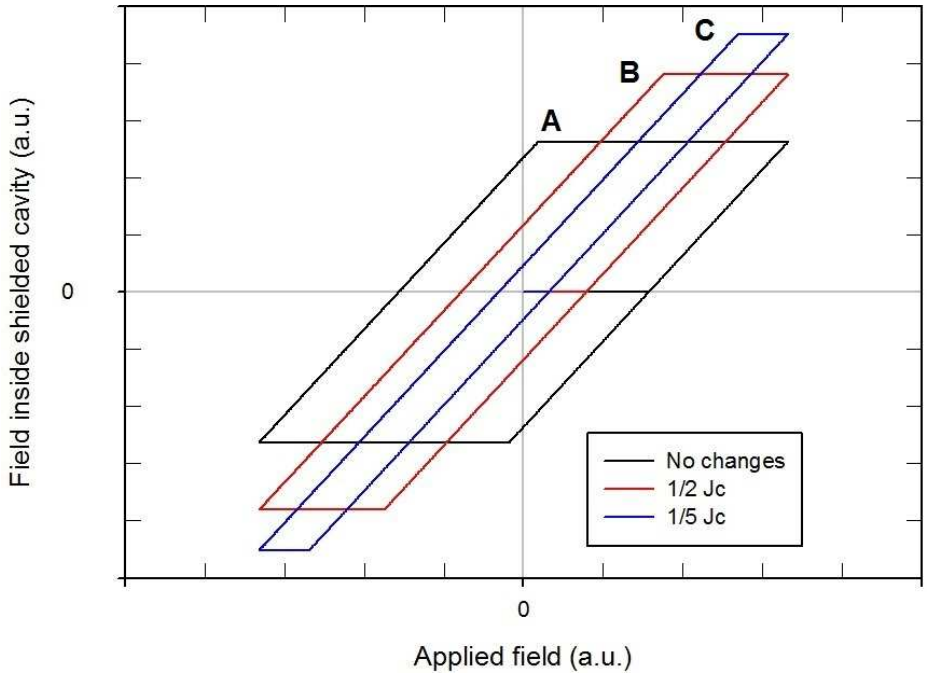

Figure 16: Effects of changing J_c according to simple Bean model

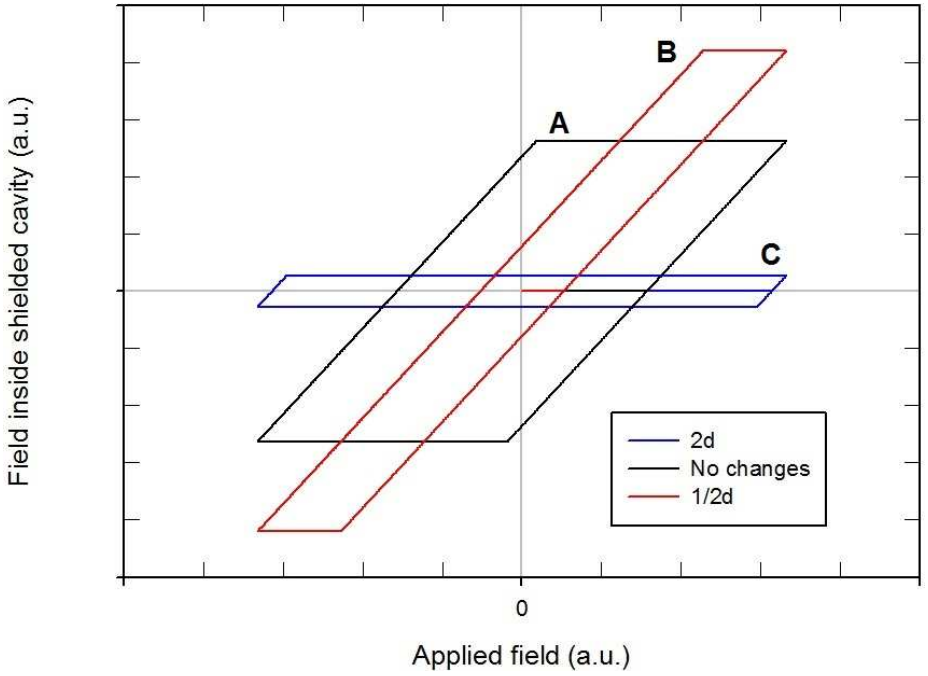

Figure 17: Effects of changing tube thickness according to simple Bean model

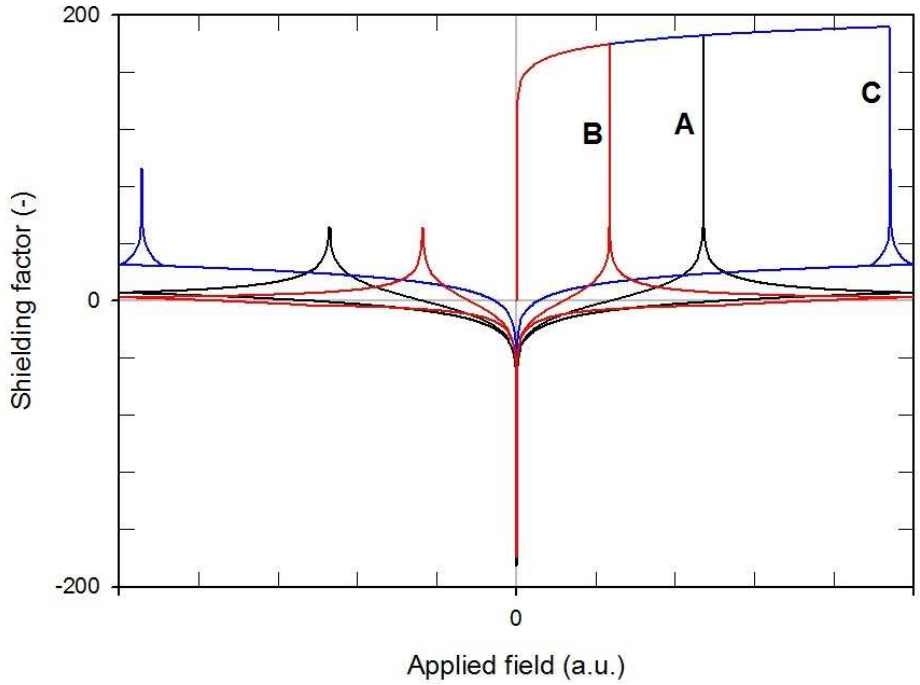

Figure 18: Shielding factor according to simple Bean model

When external field is 0, shielding factor is also 0, due to adapted convention. Then it grows logarythmically until external field reaches penetration value. Then the sudden drop occurs and shielding factor starts to decrease asymptotically with the increase of external magnetic field. Then, if the field is started to be decreased, shielding factor also decreases and becomes lower than 0 when $B_{in_{max}} - B_{ex} = B_P$. That means that the remnant field is actually higher than external field. This does not happen if external field of $2B_p$ is not exceeded, as seen on blue curve. Shielding factor continues to decrease asymptotically to infinity when external magnetic field is 0.

After that shielding factor starts to increase and becomes positive again when the module of external field value becomes equal to remnant field. It continues to grow to the maximum in the point when external field is equal to $-B_p$, which is visible as a characteristic bump on the sketch. Nextly it decrease analogically as in previous case. When external field crosses 0 it starts to grow again, up to the next maximum, which closes the loop.

3.1.3 Kim model

Hysteresis curve sketched according to Kim model is shown in figure 19. The units in the sketch are relative and only qualitative dependence is shown. The diagonal line of equal field has been marked as dotted. Similarly to Bean model this hysteresis curve starts when both external and internal fields are 0. Internal field remains 0 during the internal field increase until certain transition value B_{lim}. Above this value fast increase of internal field is observed followed by asymptotic increase up to the moment when the value of internal field is equal to the applied. When external field is started to be decreased the plateau appears (not shown in figure) and the development of internal field follows the upper branch of graph. Close to the external field of 0 the rate of internal field decrease lowers significantly. Since hysteresis curve is symmetrical due to diagonal, this leads to the appearance of wider region in the middle of sketch. The magnetization difference is there the largest when compared with the applied field. When external field is started to be increased again it follows analogical path as before.

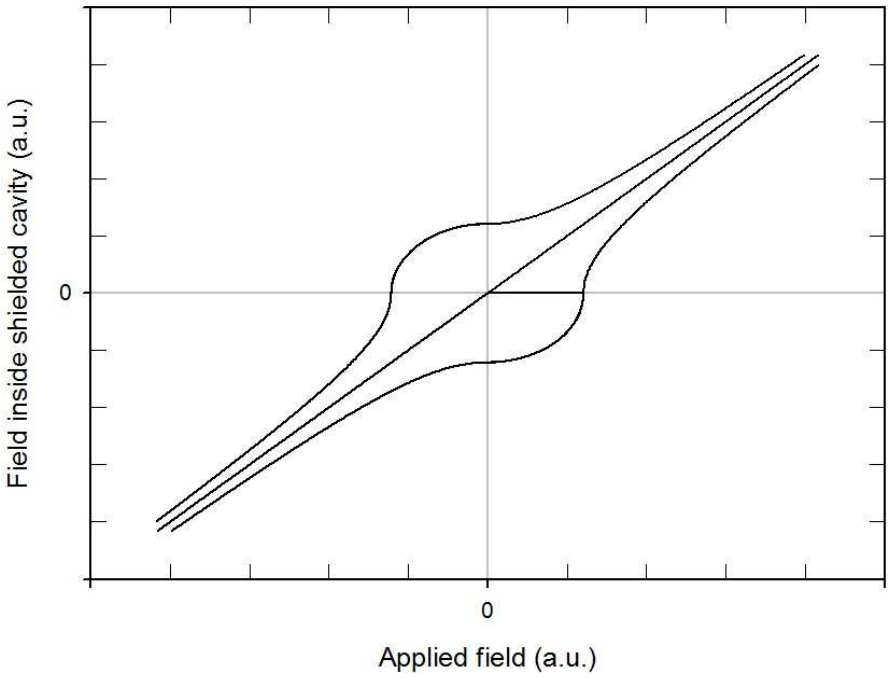

Figure 19: Hysteresis curve of superconductor according to Kim model

Effect of changing J_c on the shape of hysteresis curve is shown in figure 20. The red curve (B) represents the shape of curve when critical current is decreased twice and blue curve (C) when it increased by the same factor. Black curve (A) is the same as in figure 19. It can be noticed that the width of full shielding region depends on the value of J_c, this dependence appears to be proportional. The width of central nodosity increases with critical current along with the width of potential plateau appearing when switching the direction of field change. The lower the critical current the faster diagonal line will be achieved and the faster shielding effect will be unobservable.

Effect of changing B_1 and tube thickness are very similar to these of varying J_c. Double decrease of B_1 leads to the shape of curve which differs by less than $0,1\%$ when compared to analogical decrease in J_c. This difference is not visible at adapted scale. Analogical effect comes from varying d. The basic shape of curve is not changing and it is always symmetrical due to diagonal line. The only change in any of cases is visible as the change of width of the curve and how fast it tends to diagonal line. Increase in both d and B_1 positively affect the size of full shielding region. When adjusting model to experimental results the values of B_1 and J_c are varied to obtain the best match. Tube thickness is defined by the geometric properties of the researched shield.

Shielding factor dependence on the applied external field is shown in figure 21. It bears close resemblance to this obtained from Bean model (compare with the figure 18). In Meissner region shielding factor depends on the size of measurment uncertainties. Similarly to calculations for Bean model also here small artificial inner field has been added to make calculations possible.

Once again very high values of shielding factor are obtained in the initial region of full shielding. They increase logarythmically until the threshold value of B_{lim} is exceeded. Above this value shielding factor drops and remains close to 0. When external field is started to be decreased, shielding factor stays above 0 until the diagonal line is crossed. After that it continues to drop and decreases asymptotically to $-\infty$, when external field is 0. Then it increases, however remains below 0 until an external field is started to be increased again. Shielding factor becomes positive again, when diagonal is crossed. Then it achieves maximum when external field is equal

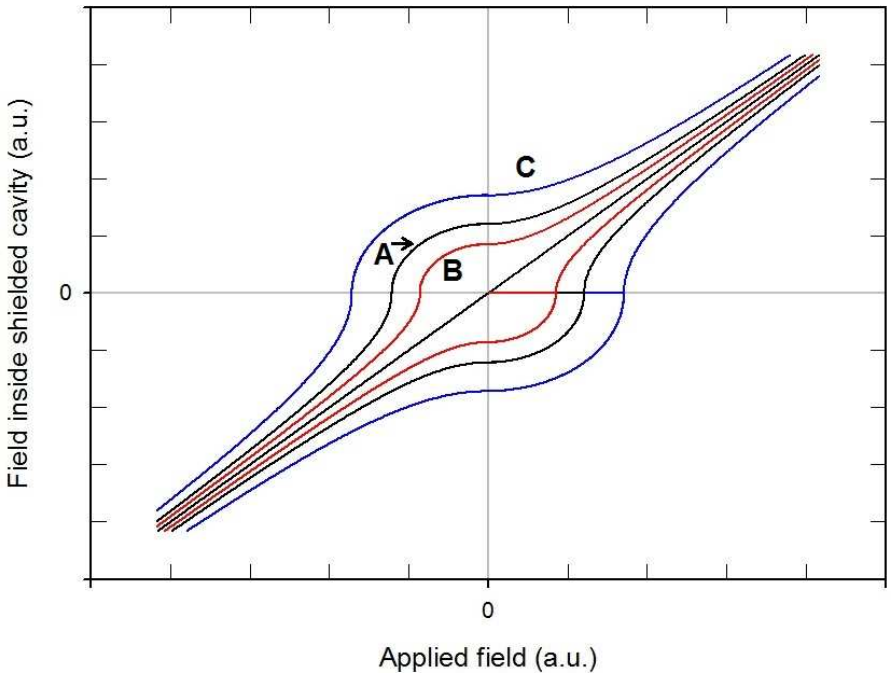

Figure 20: Effect of different values of J_c on hysteresis curve according to Kim model

to $-B_{lim}$ and quickly falls asymptotically again in 0 external field. When this field is exceeded shielding factor rises to another maximum in $-B_{lim}$, which closes the loop.

Comparison between Kim and Bean model has been shown in figure 22. J_c and B_1 have been adjusted so B_p and B_{lim} were equal, thus the width of full shielding region is the same in both models. The existance of such region is the first similarity between models. Also, the characteristic points are the same in both cases - internal field is the same when external field is 0 and internal field becomes 0 for the same value of B_p and B_{lim} respectively.

The shape of both curves differs strongly. In Bean model side curves are parallel to diagonal line, and plateaus have the same width, independent from the value of external field. In Kim model the width of hysteresis curve changes - the higher the external field the thinner the curve. Each branch of curve tends to diagonal in higher fields. When external field is in the region of B_{lim} the values of field are more extreme than in Bean model. When field is higher, they become lower. Plateaus are generally thinner. As will be shown later, Kim model is better in predicting an experimental results, than Bean model.

3.2 AC FIELD MODEL OF ELECTROMAGNETIC COUPLING

3.2.1 Model assumptions

This situation changes when it comes to the attenuation of an alternating current magnetic field. Before, superconducting currents in second shield were unable to flow due to the fact that the circuit was not closed (they were blocked by non-superconducting solder). In case of field with certain frequency an electromagnetic coupling may occur. It is capable of transfering current through solder and causes the circuit to behave as if it was closed. The strength of this phenomenon depends mostly on the frequency of field and effective electrical resistance of non-superconducting junction.

In order to estimate the size of this effect a threshold frequency has to be known. For the purpose of model single ring of magnet shield made of YBCO tape fragment soldered at both

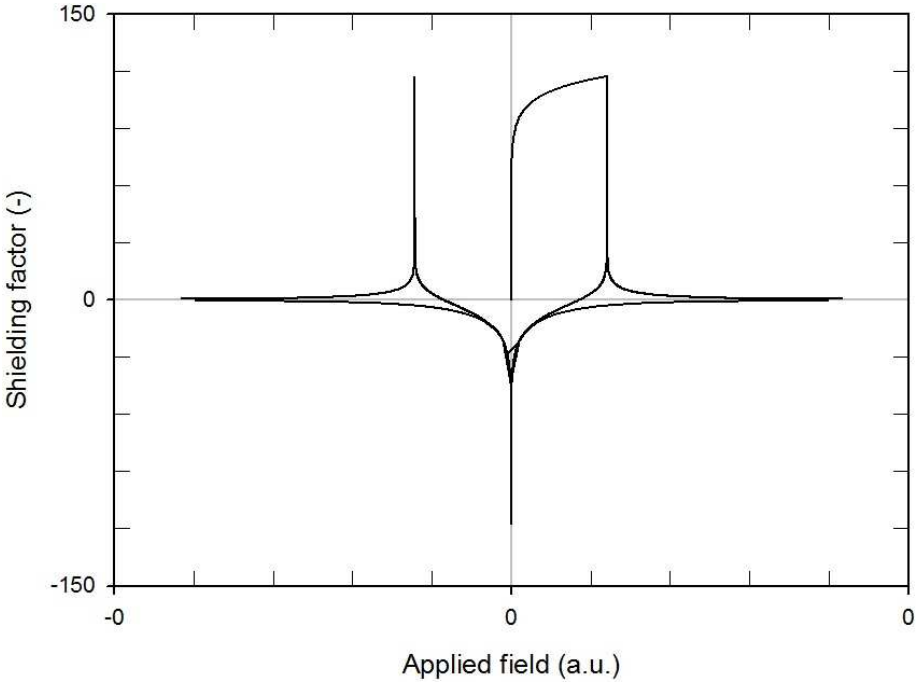

Figure 21: Shielding factor according to Kim model

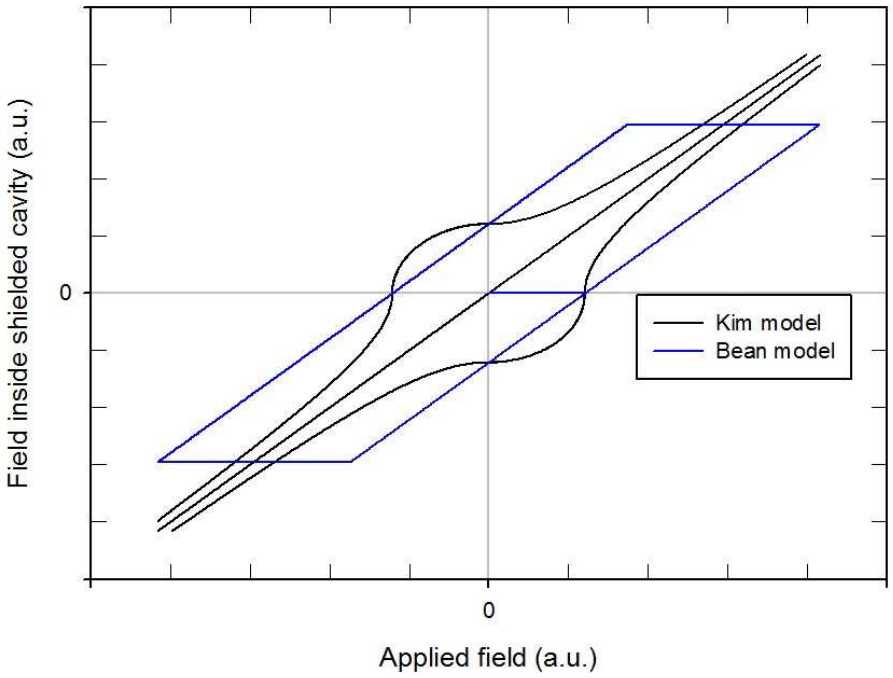

Figure 22: Comparison between Kim and Bean model

ends can be treated as RL circuit. L is there is there inductance and R is ohmic resistance. Such circuit when positioned in external alternating magnetic field can be considered as an electronic filter with inductive resistance factor of ωL and ohmic resistance factor R. When $\omega L \geq R$ inductive factor starts to close the circuit. Eddy currents forming in superconducting layer start to join through resistive junction. Magnetic field can now be shielded by these currents. Equation 45 is used to find a threshold frequency. It can be seen that the values of junction resistance and ring inductance have to be known.

$$f_{th} = \frac{R}{2\pi L} \tag{45}$$

Resistance of connector can be estimated with an assumption that major contribution to the effective resistance comes from Hastelloy which is the substrate material of tape. Its resisitivity is high when compared with other materials forming tape and solder. The resistance of copper and tin layers is small, even despite the thickness of solder. It is expected that, due to the fact that copper layer is thin, skin effect coming from this will be negligible. Based on this assumption expected effective resistance of junction can be estimated based on the knowledge of the thickness of Hastelloy layer, its resistivity and the area of junction. Equation 46 is used to calculate the resistance of junction.

$$R = \frac{\rho d}{S} \tag{46}$$

ρ is the resistivity of material, d the thickness of layer and S is the area of junction. This is the standard formula used to obtain the value of resistance of a certain object.

In order to find inductivity the ring will be considered as conducting toroid. Equation 47 is used to calculate inductivity of such toroid. r_t is there the radius of ring and r_{in} is its inner radius. μ is magnetic permeability of material. Figure 23 shows the marking of dimensions on a toroid.

$$L = \mu_0 r_t \left(ln\frac{8r_t}{r_{in}} - \frac{7}{4}\mu \right) \tag{47}$$

To find the dimensions of torus based on a ring several assumptions will be made. It is expected that the area of torus' forming circle will be equal to the cross-section area of tape S_{cs}. Therefore the equation 48 is formed.

$$r_{in} = \sqrt{\frac{4S_{cs}}{\pi}} + d \tag{48}$$

y is there the width of tape. Torus radius will be assumed to be equal to the radius of ring with the radius of forming circle added.

Knowing these values one may estimate the frequency of magnetic field at which the effects of electromagnetic coupling will appear. The final result may vary from actual due to assumptions taken. This model still needs to be refined in order to yield results closer to experimental - full knowledge on the structure of layers within the superconducting would be needed. The method of estimation of inductivity also might be distorted.

3.2.2 Model results

Based on the data from [61] the resistivity of Hastelloy was found to be equal to $1,235 \cdot 10^{-6} \Omega m$. Figure 24 shows the dimensions of single ring with solder marked. The thickness of Hastelloy layer through which coupling occurs is $50\,\mu m$. The area of junction is $24\,mm^2$. The result of

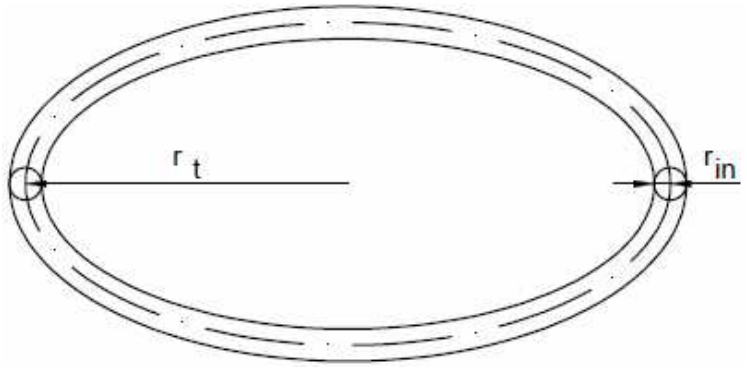

Figure 23: Dimensions of toroid

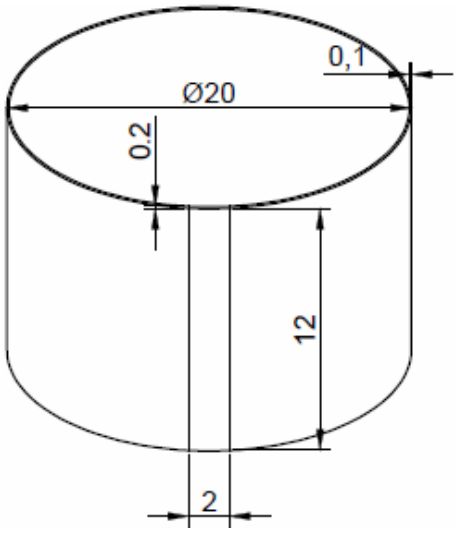

Figure 24: Dimensions of the single ring of tape-screen

adding these values to equation 46 is $2,57 \cdot 10^{-6}\Omega$. This is the expected resistivity of non-superconducting junction. This might differ slightly from an actual value due to different type of Hastelloy applied, local differences in the thickness of layer and the contribution to resistance from solder.

Toroid based on the dimensions of single ring would have an internal radius r_{in} of 0,44 mm, according to the equation 48. The radius of whole ring would be in such case 10,44 mm. Magnetic permeability of junction material will be assumed as 1. According to the equation 47 inductivity of ring is equal to 44,01 nH. Main difference between real and expected value may come from small differences in geometrical size of rings and magnetic permeability, which would be different than assumed

Based on considerations shown above the equation 45 yields the resultant threshold frequency of 9,3 Hz. Above this frequency it is expected to observe the effect of electromagnetic coupling. This value will be tested experimentally, as shown in further sections. Currently used model is unable to predict the magnitude of effect, only whether it will appear or not.

4 EXPERIMENTAL

4.1 EXPERIMENTAL SETUP

4.1.1 General outlook and auxiliary devices

General outlook of the measuring stand has been shown in figure 25. The scheme with the same markings has been attached as the attachment 8.1. The magnet (marked A in figure 25) with specimens inside is put into the cryostat (B). During operation magnet and specimens are cooled with liquid nitrogen, which fills the cryostat. Magnet is supplied with an electric current by cables (C). Hall effect sensor and measuring coil (unseen in figure 25) are placed at the end of carbon fiber tube (D). This tube axially penetrates the magnet and specimens inside it. The other end of tube is attached to slideway (E), which allows precise placement of sensors inside the specimen. Current coming from sensors is let out by the mean of very thin cables (F). The exact description of each component follows.

Cryostat consists of inner tank and styrofoam insulation. The bottom of tank was smoothed to obtain flat surface. During the measurments tank was filled with liquid nitrogen in order to maintain temperature of 77K and keep specimens in superconducting state. The insulation is supposed to reduce heat inleaks and reduce the usage of liquid nitrogen. The filling of cryostat was performed with great care, due to both safety reasons and the danger to britlle specimens. Violent boiling might cause dangerous tensions and damage them. Fortunately, such situations have been avoided during experiments. The cryostat was stationary. The drawing of cryostat has been attached as attachment 8.4.

Slideway is shown in figure 26. It was adapted from automated robotic arm by removal of electronic elements and their replacement with hand drive. Machine is capable of performing precise movements in three dimensions. It is placed on wide support (A) equipped precise screws allowing exact vertical positioning of machine. Also there is movable axis allowing whole device to perform circular motion. Above this long thread (B) is placed allowing for vertical motion. Its pitch is 3 mm. It is driven by the knob (C). Its one turn causes the movement of sensors 3 mm upwards or downwards. Horizontal arm is almost exactly the same, however it has not been used in measurments performed for this thesis Instead of an electronic grip, firm holder (D) was placed for the attachment of tube with measuring equipment.

The tube on which probes were installed and introduced into the magnet is made of carbon fiber. This material has low thermal conductivity, which leads to the decrease of the losses of liquid nitrogen used for cooling. External diameter of tube is slightly less than 10 mm. This allows the tube to fit into the BSCCO specimen and move precisely along its central axis. The tube is empty inside and the cables coming from sensor are led through this. Close to the top of the tube a hole on the side was placed to let these cables out. During measurments the top end of tube is placed in holder, as described before.

4.1.2 Probes calibration and measurment circuits

Two measuring devices used to find the value of magnetic field inside shielded region were Hall effect sensor and measuring coil. Hall probe was used when direct current fields were produced by magnet and measuring coil was applied for the measurment of alternating current fields. Both devices were put at one of the carbon fiber tube ends. This was shown in figure 27. Hall probe was marked as A and measuring coil as B. Before actual measurments were started both have been calibrated to study thier behaviour in 77K.

Hall probe bases on Hall effect. This is the change of movement of electrical charges within

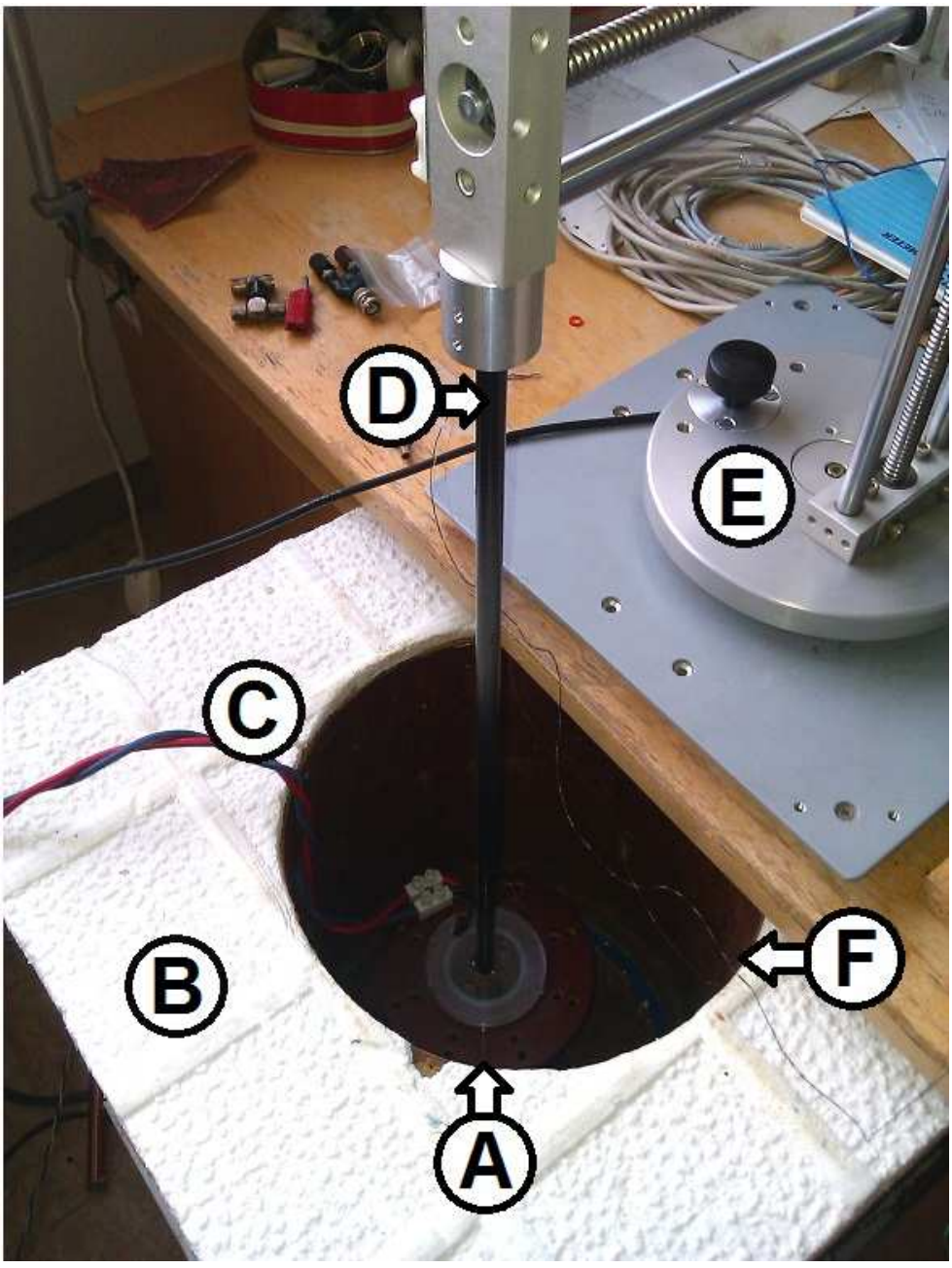

Figure 25: General outlook of test stand

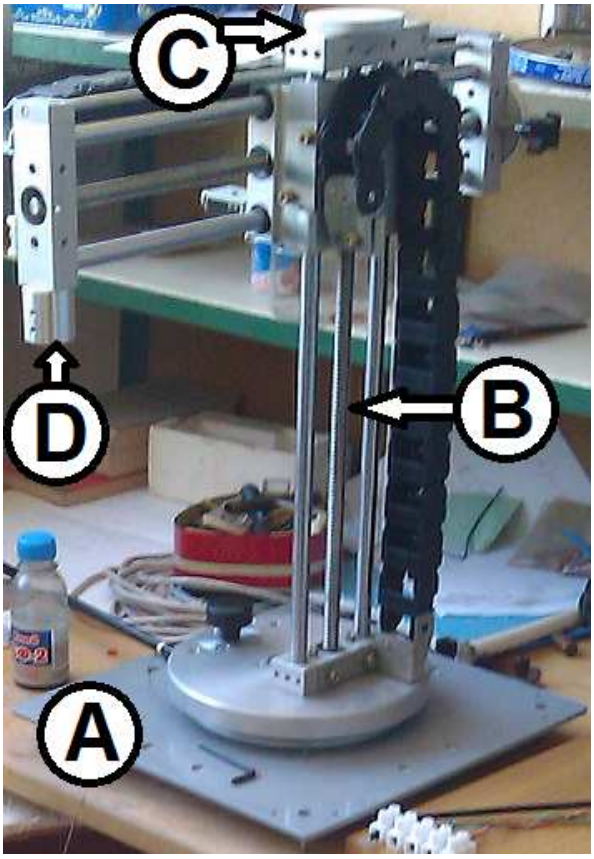

Figure 26: Slideway used for measurments

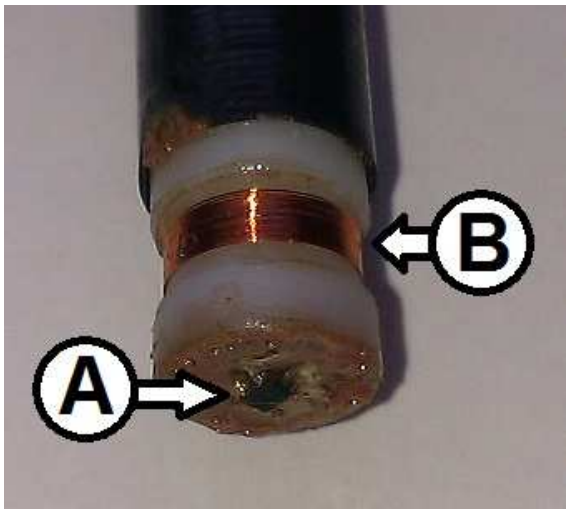

Figure 27: Close-up of the end of carbon fiber tube with sensors

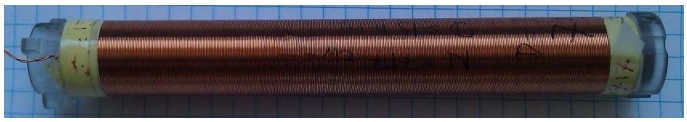

Figure 28: Calibrating coil

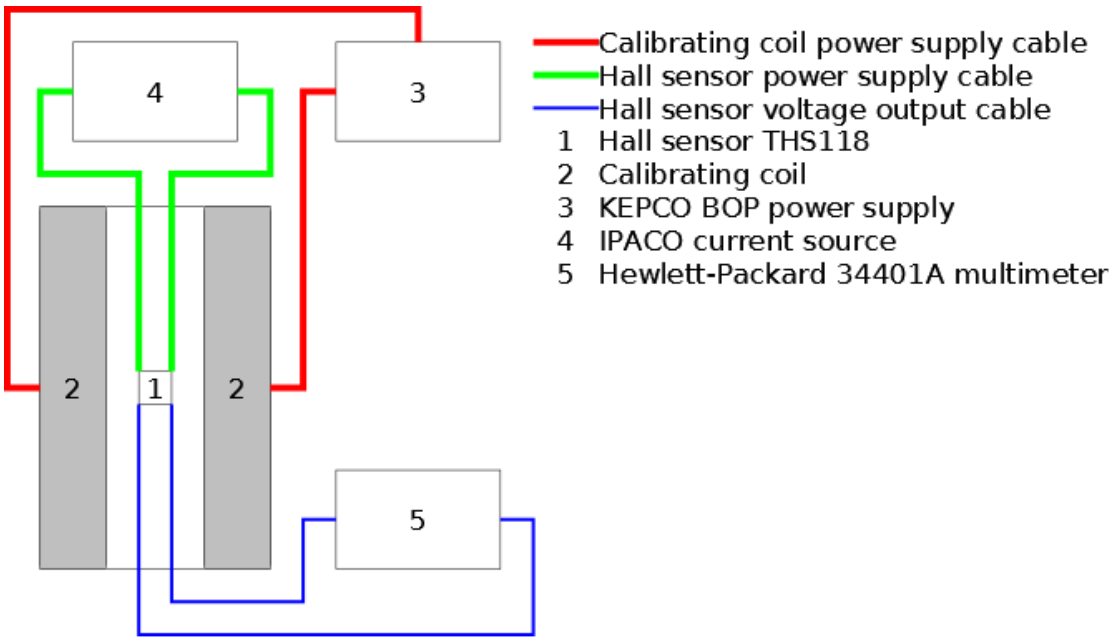

Figure 29: Calibration stand for Hall effect sensor

a semiconductor due to the presence of external magnetic field [66]. Hall effect sensor changes its electrical output proportionally to the size of magnetic field it is subjected to. Transducers are often made of semiconducting materials, such as silicon and germanium. A device has to be powered with certain small current in order to produce Hall voltage. The value of Hall voltage depends on both field direction and magnitude. Since field geometry is expected to be uniform in both calibration coil and the one used during measurments, parameter obtained during calibration will be valid in normal operation. The calibrating coil is shown in figure 28. Hall probe used in measurments was Toshiba's THS118 gallium-arsenide probe. Data sheet for this probe has been attached as attachment 8.2.

Calibration process was performed in both room temperature (approximately 20ºC) and liquid nitrogen temperature (77K). The scheme of calibration stand has been shown in figure 29. Investigated Hall sensor (1 in figure 29) has been placed inside the calibrating coil (2) of strictly defined dimensions and magnetic constant, in order to obtain precise regulation of magnetic. The number of turns was 717, its diameter - 15 mm, length - 10,5 mm. The magnetic constant of coil was equal to 7,575$^{mT}/_{A}$. The coil was powered with KEPCO BOP power supply (3) in the range of -50A and 50A. IPACO current source (4) provided 5 mA current to the Hall probe. Resulting Hall voltage was measured with Hewlett-Packard 34401A multimeter (5). Several series of measurments have been performed, but only two most representative will be shown. During one of the measurment series Hall probe was fed with the current of 10 mA - twice as large as normally. This caused some changes in probe constant, which were taken into account.

Calibration results are shown in figures 30 (measurments done in room temperature) and 31 (measurments done after immersion in liquid nitrogen). As it can be seen in both cases

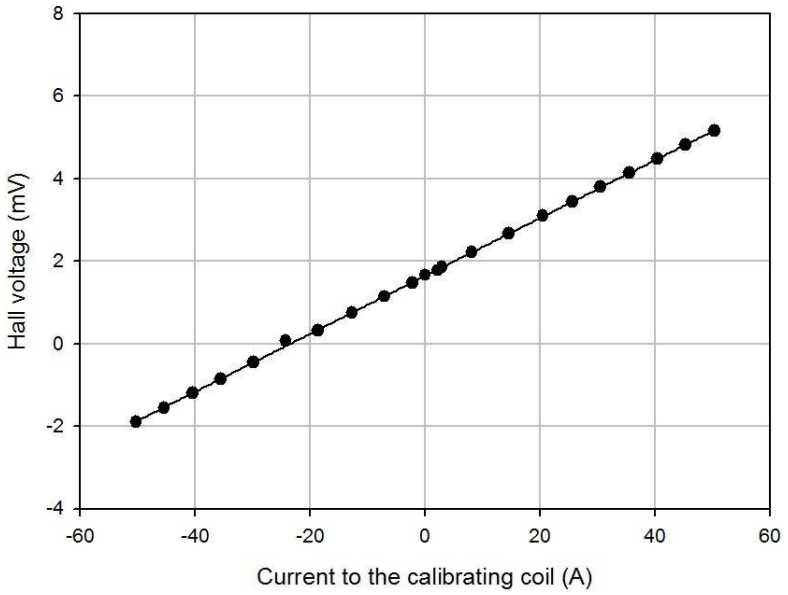

Figure 30: Calibration results in room temperature

the characteristic of probe is almost linear. In room temperature the coefficient of $0{,}0701^{mV}/_{A}$ was obtained after regression. Background voltage coming from calculations (1,64 mV) was slightly lower than obtained during measurments (1,66 mV). In case of measurments made in liquid nitrogen temperature coefficient increased to $0{,}905^{mV}/_{A}$. Calculated background voltage (2,505 mV) was slightly higher than measured (2,48). In other series of measurments the same slopes were obtained in both room and liquid nitrogen temperature respectively. There were some differences in background voltage which in effect led to the practice of measuring this value at the beginning of each day of measurments.

In order to recalculate Hall voltage obtained from measurments into the value of magnetic field one needs to know the value of the calibrating cell magnetic constant and coefficient obtained during calibration. These values are combined according to the equation 49. $\widetilde{\beta}$ is there the value of measured coefficient in $^{mV}/_{A}$, M_{cal} is magnetic constant of calibrating coil in $^{mT}/_{A}$ and β is conversion factor in $^{mV}/_{mT}$.

$$\beta = \widetilde{\beta}/M_{cal} \tag{49}$$

The values obtained for conversion factor are $0{,}924^{mV}/_{mT}$ in room temperature and $1{,}19^{mV}/_{mT}$ in liquid nitrogen temperature. Equation 50 was used for the recalculation of Hall voltage U_{hall} into measured magnetic field.

$$B = \frac{U_{hall}}{\beta} \tag{50}$$

DC mode circuit is very similar to this used for calibration of Hall probe. Its scheme is shown in figure 32. Used Hall sensor (1) is the one calibrated before, thus its power supply (4) and data reading (5) are the same as during calibration. Calibrating coil was replaced with main magnet (2) described in further section. It is powered with IPACO current source (4). The main change in comparison with calibration stand is in the application of model resistor with the resistance of $0,01\Omega$ (R). This is used for indirect measurment of current flowing through the magnet and thus output magnetic field. Instead of measuring current, voltage drop on model resistor is investigated. It is done with Keithley 196 System DMM.

Measuring coil was used for the investigation of alternating current magnetic fields. Changes in external magnetic field induce electric current in coil, which can be measured. Measuring

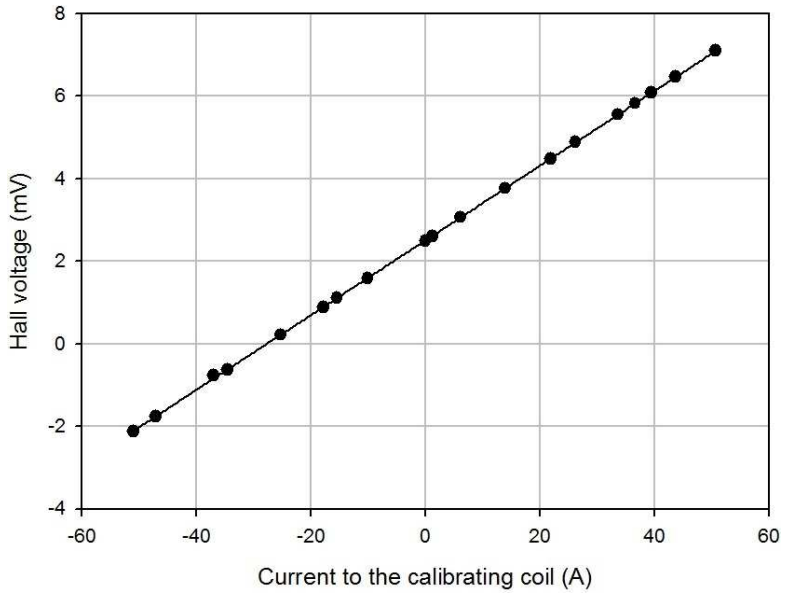

Figure 31: Calibration results in 77K

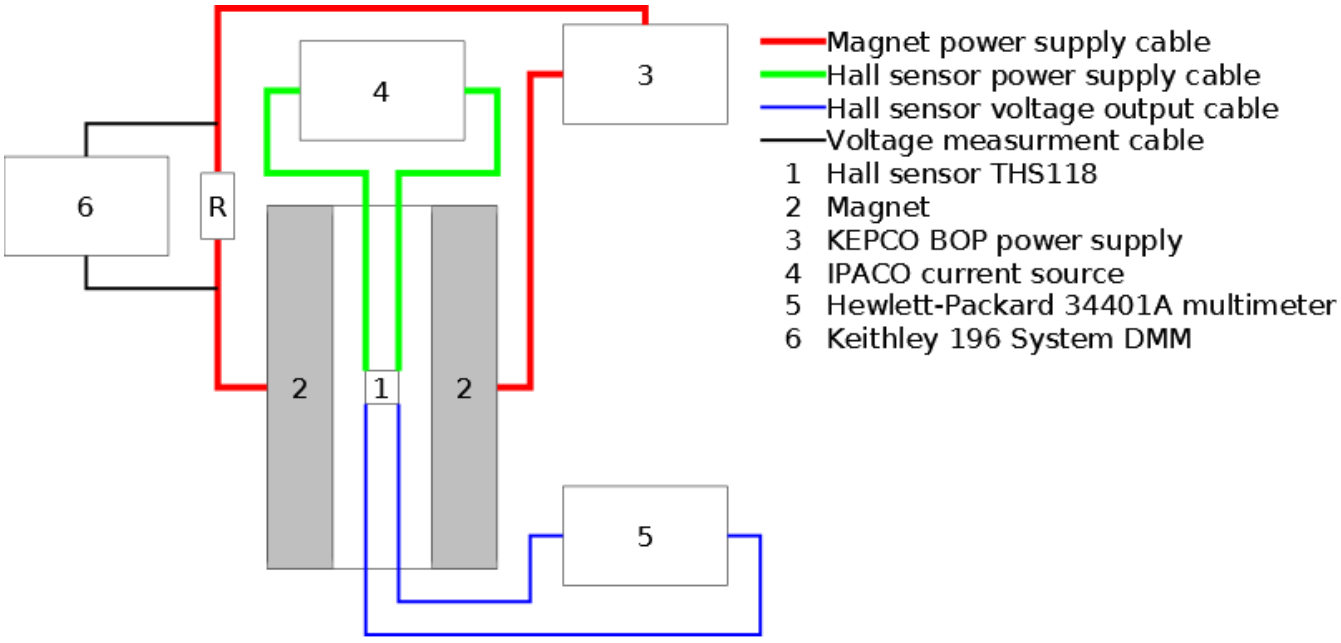

Figure 32: DC mode circuit

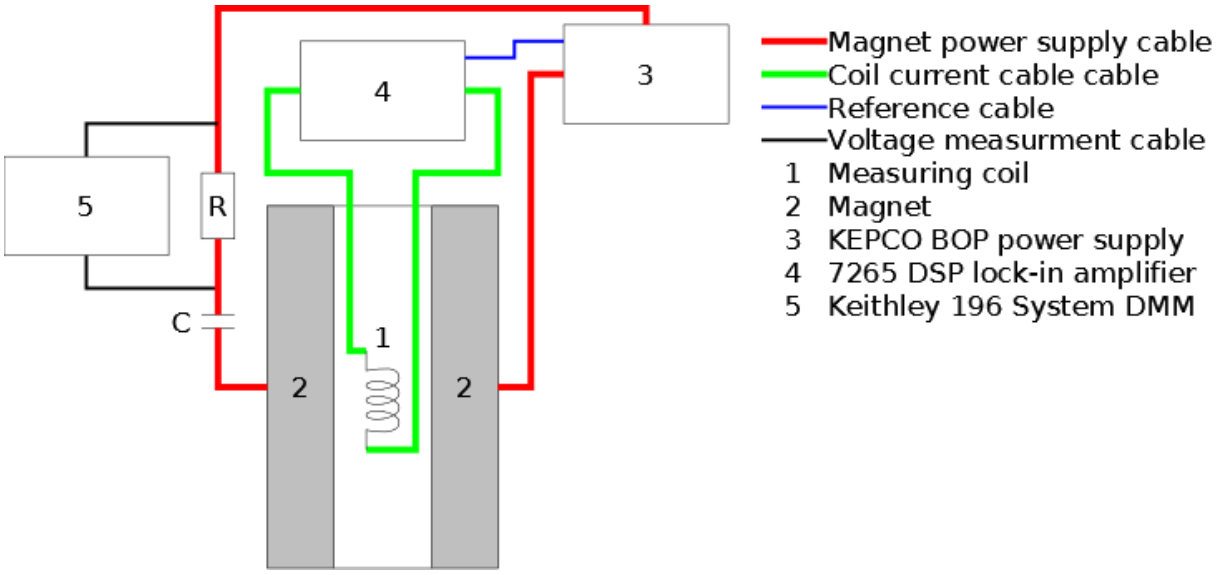

Figure 33: AC mode circuit

coil used for the purpose of this thesis can be seen in figure 27 and is marked there as B. It is made of 60 nm wire. Its internal diameter is 8 mm and the number of turns is 30. It is introduced into the magnet axis in the same manner as Hall probe, except the fact that it has to be moved by 6 mm downwards to be placed in the magnet center.

AC mode circuit was the same both for magnet calibration and measurments. It is shown in figure 33. Measuring coil (1) is placed on the axis of magnet (2). Induced current is read by 7265 DSP lock-in amplifier (4), which produces reference signal for KEPCO BOP power supply (3). This device supplied sinusoidal electric current to the magnet. In order to obtain resonance conditions the battery of condensers (C) was added. Its capacitance was varied, depending on desired frequency. Measuring system used to find current flowing through magnet consisted of Keithley 196 System DMM connected in parallel with model $0,01\Omega$ resistor (R).

Such circuit was used to find the magnetic constant of main magnet. By knowing geometric dimmensions of coil, and applied field frequency and magnitude, one can find constant conversion parameter α. It is done according to equation 51.

$$\alpha = N \cdot S \cdot 2\pi f \tag{51}$$

N is here the number of coil turns, S is the area of single turn and f is field frequency in given measurment. It should be noted that value of α changes with applied frequency. In order to calculate the area of single turn equation 52 was applied. d_{in} is there the internal diameter of coil and d_c is the thickness of wire. Thus the effective area S is obtained (formula 52).

$$S = \pi \frac{(d_{in} + d_c)^2}{4} \tag{52}$$

Since output of coil does not depend on temperature, magnet calibration was performed in normal state. It was done by positioning the measuring coil in the center of main magnet. Frequency was set to 45 Hz, therefore condensator set with the capacitance of approximately $100\mu F$ was applied, to obtain conditions close to resonance. With such frequency parameter α was equal to $0{,}43278 {}^{mV}/_{mT}$. Figure 34 shows the results of such measurments.

It can be seen that the dependence between applied current and induced voltage is linear. Now it is possible to find magnetic constant. It is done be the application of equation 53.

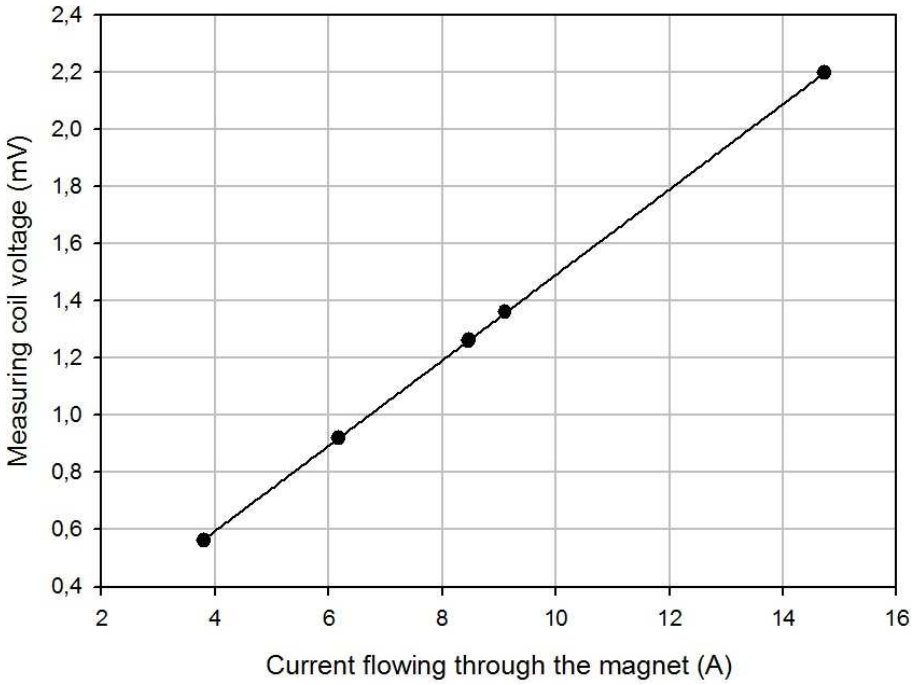

Figure 34: Magnet calibration results in AC field

$$KM = \frac{B}{I} \tag{53}$$

KM is there magnetic constant in ${}^{mT}/_{A}$, I is current flowing through the magnet in amps and B is magnetic field produced by the magnet (in case of AC current - its amplitude) in mT. B can be found from equation 54. This equation was further used in recalculation of all measurments performed in AC fields.

$$B = \frac{U_{cell}}{\alpha} \tag{54}$$

U_{cell} is there the measured voltage coming from sensing coil. According to the measurments performed, the average value of magnetic constant is $15{,}51{}^{mT}/_{A}$.

4.1.3 Magnet winding

External view of magnet used during the measurments can be seen in figure 35. Views from the top and side are shown there. The part of main winding which is uncovered by compensation winding (B) is marked with A. These are made of one piece of copper cable winded on the carcass, which parts are visible at the top and bottom. C marks power supply to the magnet. D is the bottom part of carcass which was equipped with screws (similarly to slideway), which allow adjustment of magnet position to obtain vertical setting. E marks magnet aperture inside which holders and specimens were placed during measurments.

Design of the magnet was performed with the help of homemade program “polemagn”. The data supplied were adjusted based on the size of coilformer, amount of available copper and the desire to obtain as long as possible region of homogenous field. The external diameter of coilformer was 50 mm, total length on which winding was possible was 185 mm. According to the program, the optimal number of winding layers was 19, along with 3 layers of compen-

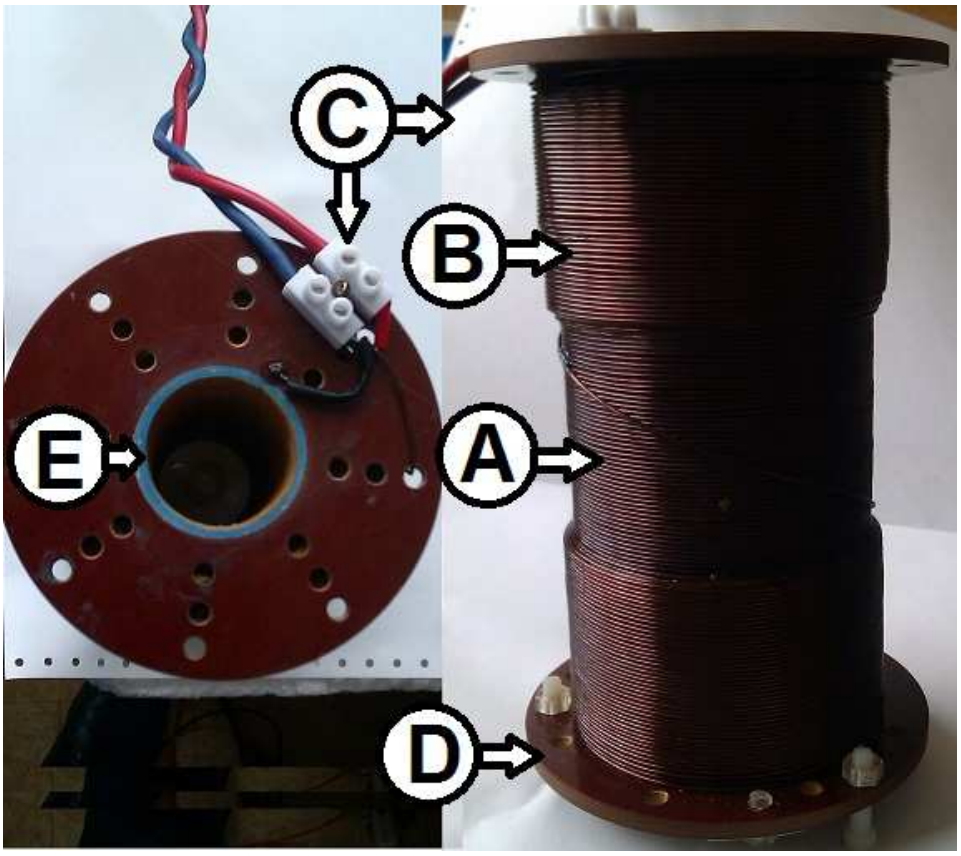

Figure 35: Magnet used for measurments

sation coils additionally winded up to 60 mm at both ends of the magnet. Magnet geometrical dimensions are shown in attachment 8.3.

Winding process was performed according to obtained design. Firstly main winding was prepared followed by compensation turns. Several imperfections occurred during production, however they were not expected to strongly affect magnet performance. Most of the imperfections were formed at the end of each layer, there copper cables had to be supported with an adhesive tape and a filler. Once the cable was broken and by-pass had to be produced. To avoid the risk of avalanche breakdown the most sensitive sites were additionally covered with thin layer of insulating material.

Holders were manufactured in fashiong allowing them to tightly fit the coilformer and allow firm grip of both superconducting specimens. They have been sized also to allow penetration by the tube with sensors attached. Length of each holder was chosen so the center of specimens was placed at the center of magnet. Figure 36 shows the upper holder with BSCCO tube mounted (A). Upper holder (B) is the same as lower expect a hole (C), which was cut to allow power cables to be connected with magnet. Holder dimmensions are shown in attachment 8.5.

Magnet testing was performed to check its behaviour and measure magnetic constant. Measurments in AC field were described before, this paragraph is devoted to measurments performed in DC fields. DC circuit used in this measurment was the same as the one in figure 32. It was done in room temperature. Results are shown in figure 37. Horizontal axis shows the current which was led through the magnet and vertical - magnetic field produced by this.

It can be noticed that results are linear, thus the magnetic constant keeps its value. In order to find its value regression was performed and the slope was found. According to this measurment, the value of $16{,}13^{mT}/_{A}$ was found. It is slightly higher than the value of $15{,}51^{mT}/_{A}$ coming from

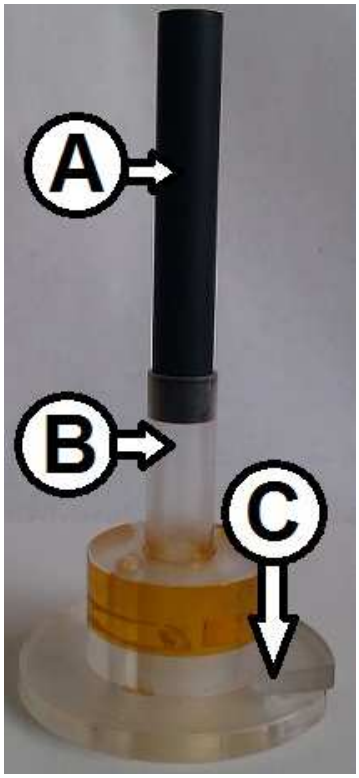

Figure 36: Sample holder and BSCCO tube

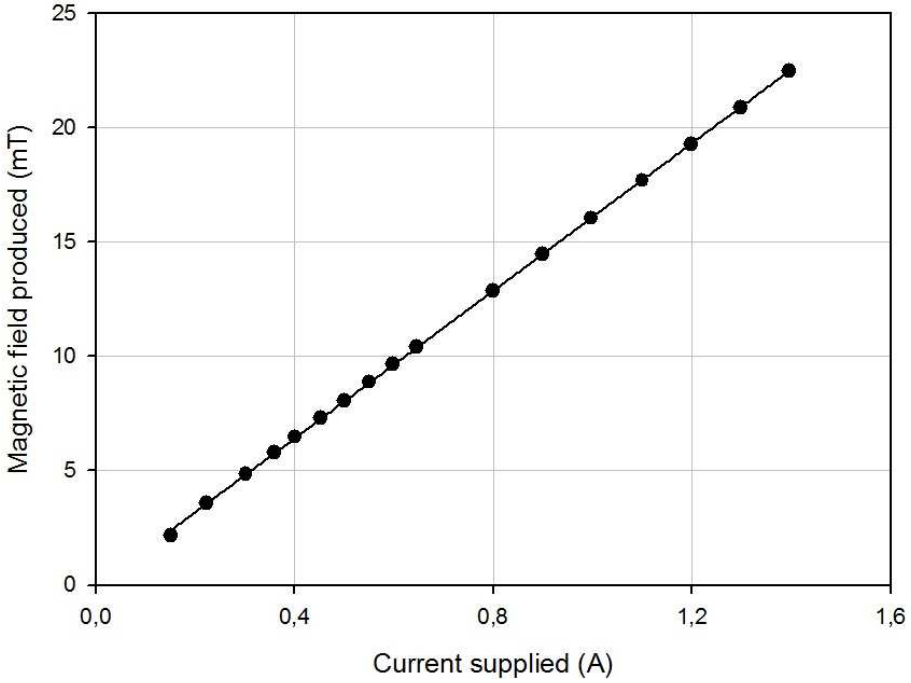

Figure 37: Magnet calibration results in DC field

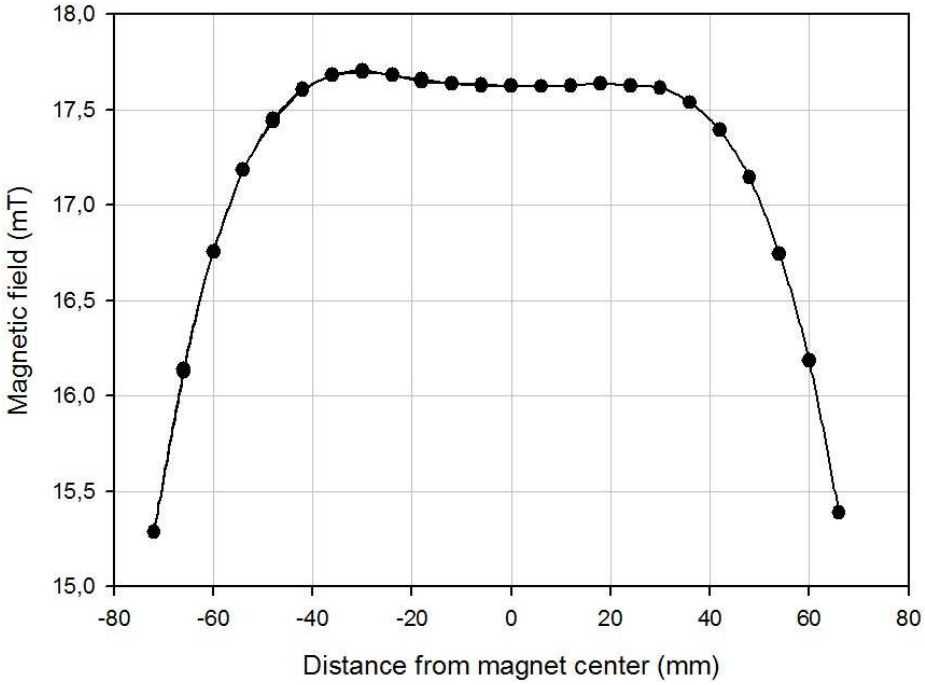

Figure 38: Magnetic field distribution in the magnet coil

AC measurments. For the purpose of further investigations the value $15{,}6^{mT}/_{A}$ for KM was adapted. Formula 55 was used to recalculate read value of voltage drop U_{mag} on model resistor with the resistance R_{mod}. This was further used in calculation of produced field for all standard measurments.

$$B_{mag} = KM \cdot \frac{U_{mag}}{R_{mod}} \tag{55}$$

Homogeneity of the magnet has been measured in room temperature and in DC conditions. It was done by passing a Hall probe upwards and downwards along the axis of the magnet. Results have been shown in figures 38 and 39. Figure 38 shows measured magnetic field along the axis of the magnet. The lower the value of length the lower the position of the probe. 0 means central position. The current which was led through magnet was 1,1A. Figure 39 shows relative magnetic field. The base value was the one obtained in the center of magnet. The results of this measurment will be used as the base for further comparisons between attenuated and expected field.

Some differences in field distribution can be noticed, especially in figure 39. This is probably due to minor errors during winding process described before. As it can be noticed in figure 39 satisfying homogeneity was obtained in the range of approximately -40 mm to 40 mm. This result is in good match with expected and allows reliable measurments of field attenuation along sufficient distance. Observed differences in the region of interest are smaller than 2%.

4.1.4 Superconducting specimens

Two superconducting shields were used during measurments. The first was a solid tube made of $Bi_{1,8}Pb_{0,26}Sr_2Ca_2Cu_3O_{10+x}$ - 2223 phase of BSCCO. It was the commercial tube offered by CAN SUPERCONDUCTORS s.r.o. as magnetic shield for shielding of fields up to approximately 5-10mT. The chosen model was CST-10/80. The manufacturer catalogue has been attached as attachment 8.6. Its length is 80 mm and internal diameter is 10 mm. This length

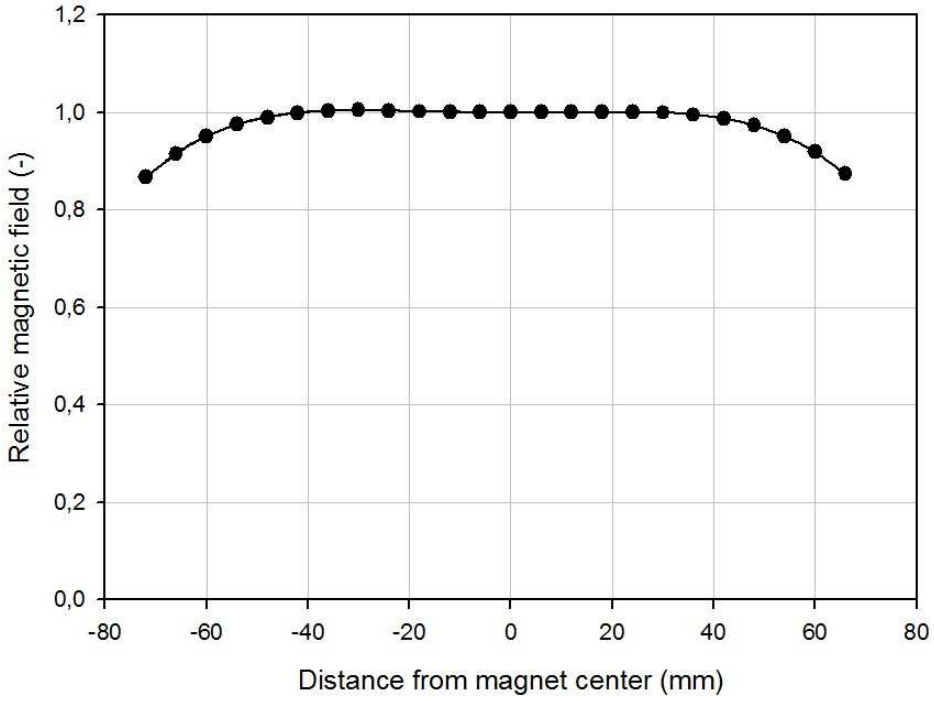

Figure 39: Relative magnetic field distribution

was expected to be sufficient to observe full field attenuation. This tube can be seen in figure 36 and is marked there as A.

Due to the fact that this tube is solid it is expected that it will provide full attenuation at some of its region and some range of external magnetic field. This specimen was present during all measurments performed in liquid nitrogen temperature (77K). Critical temperature of this tube is 108K, which means that such temperature will be sufficient to obtain superconducting state. Some deterioration of shielding performance was expected due to cyclical cooldown and heat-up connected with the brittle nature of material.

The second specimen was the shield made of YBCO tape. It was produced by attaching tape rings to the plastic tube. Such ring is shown in figure 40. Its diameter is 20 mm, while its width is the same as this of tape - 12 mm. The thickness of tape is 0,1 mm. Each ring was produced by soldering both ends of tape fragment which was cut to proper length. Overlap was approximately 2 mm. Solder was made of tin and two ends were completely separated from each other by this. Figure 24 shows these dimensions graphically. 8 rings were produced and in total they covered the length of 96 mm.

Rings have been attached to plastic tube. One at the lowest position was glued to this, while the rest remained movable. Figure 41 shows some of possible configurations. At the upper picture the configuration used during tests is shown. Lower picture presents all solders in single line. Possibilites of shield setting are unlimited. As it can be seen in figure rings touch each other to avoid gaps. Still it is expected that DC magnetic field will be able to penetrate through non-superconductiong solders and uncovered parts of the tube.

In case of solid shield measurments BSCCO tube was attached on holder as shown in figure 36. Then the holder with tube was put inside the magnet and the upper holder was put at the top of assembly. Then the position of magnet and slideway were adjusted to obtain coaxial setting of the tube with measuring coil and Hall sensor. When adjustment was finish the tube was introduced into the magnet and positioned in desired localisation inside the specimen, often its center. The position was regulated using a calliper. Similar procedure was performed when

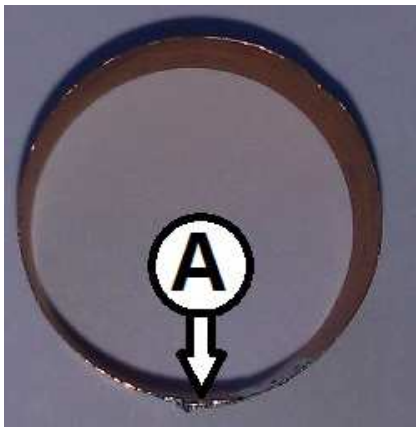

Figure 40: Single ring made of YBCO tape

Figure 41: Examples of second shield configurations

the double shield setting was used.

Assembly of specimens inside the magnet and probes positioning in the double screen mode has been drawn and attached as attachment 8.7. The magnet is marked by A. A lower holder (marked as B) is put into magnet aperture. Then the BSCCO tube (D) is located in a proper bed at the lower holder. Nextly the assembly with YBCO screens (E at the attachment 8.7) is positioned on the side surface of holder. After it is done the whole assembly is topped with an upper holder (C). Finally the tube with sensors (F) can be introduced into the magnet through a proper hole in the upper holder. The whole assembly is coaxial. In case of the tape-screen shield measurments the YBCO tube is replaced with the dummy of the same dimensions.

4.2 RESULTS

4.2.1 Direct magnetic field

The measurments performed in the DC conditions results in the production of magnetisation hysteresis loop. Several such curves for different operating conditions were obtained. The first measurment was done in order to roughly estimate the location of hysteresis curve and the region of full shielding when only BSCCO tube is used. The result of this measurment is shown in figure 42. It shows the dependence between the field inside shielded cavity and external field from magnet. The line of equal field and close-up of the region of interest have been added to help in interpretation.

As can be noticed the measurment was performed in the wide range of magnetic field, between -100 mT and 100 mT. However, significant hysteresis can be observed in the region

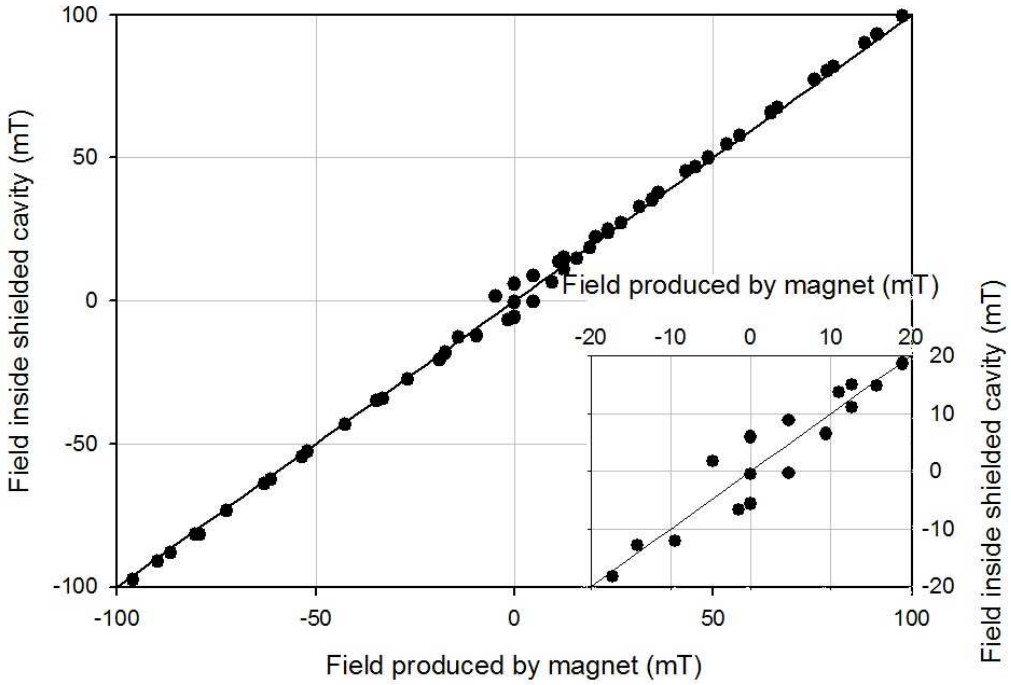

Figure 42: Localisation of hysteresis curve

between approximately -25 mT and 25 mT. The region of the full shielding is represented only by 2 measurment points. Points in higher fields lie almost exactly on the line of equal fields. Slight tilt is probably caused by uncertainities in probe calibration and magnetic constant determination.

After finding borders for the region of the full shielding a hysteresis curve for a single screen was investigated. A remnant field was washed with AC field prior to measurment and the new background field was read. It should be noted that for each such measurment background magnetic field was adjusted so the initial point of curve would lie in the center of coordinates system. The result of this measurment is shown in figure 43. This graph can be treated as the close-up version of prior measurment.

The region of the full shielding is clearly visible. Its width is approximately 7,25 mT. Several imperfections of curve can be seen, resulting probably from flux creep or flux relaxation. It can be noticed that the region of the full shielding is actually displaced. This issue will be further analysed in the discussion part of thesis, as well as the matter of its completion - additional measurment was performed to add the lacking part of the hysteresis curve. Similar measurment was performed when additional shield made of YBCO tape was installed. Its result is shown in figure 44. It has been performed in approximately the same range of external field as the prior measurment. Importantly, this was the first measurment performed after the cooldown of specimens.

Full shielding region is visible again, its width is actually smaller than in former measurment - it is approximately 6,3 mT. It is positioned in different place than in previously. In order to avoid disruptions appearing due to flux changes a longer time was allowed for relaxation before reading a measurment result. This effected in smoother curve. Plateaus at the end of curve are visible more clearly. Both measurments shown before were performed in the central part of superconducting specimen. One hysteresis curve was made when Hall probe was moved by approximately 10 mm above the center of superconducting shield. The resultant curve is shown in figure 45.

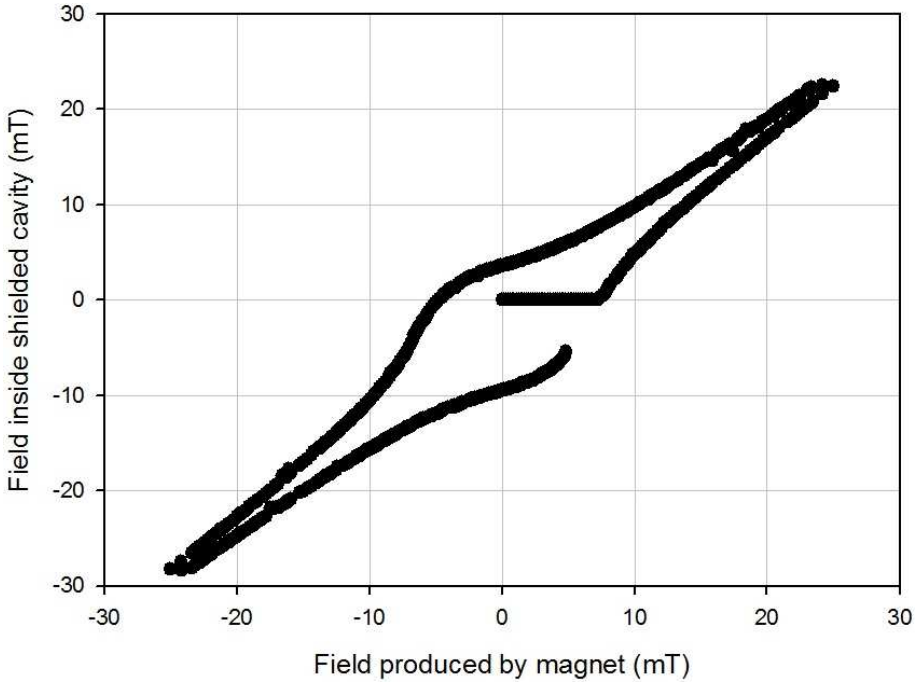

Figure 43: Hysteresis curve for a single BSCCO shield

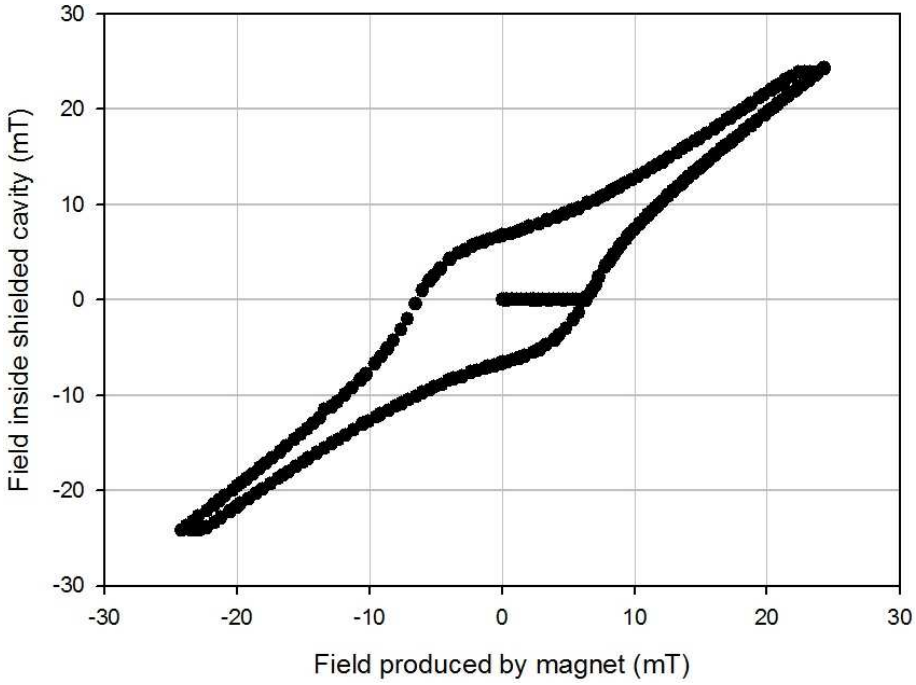

Figure 44: Hysteresis curve for the double shield

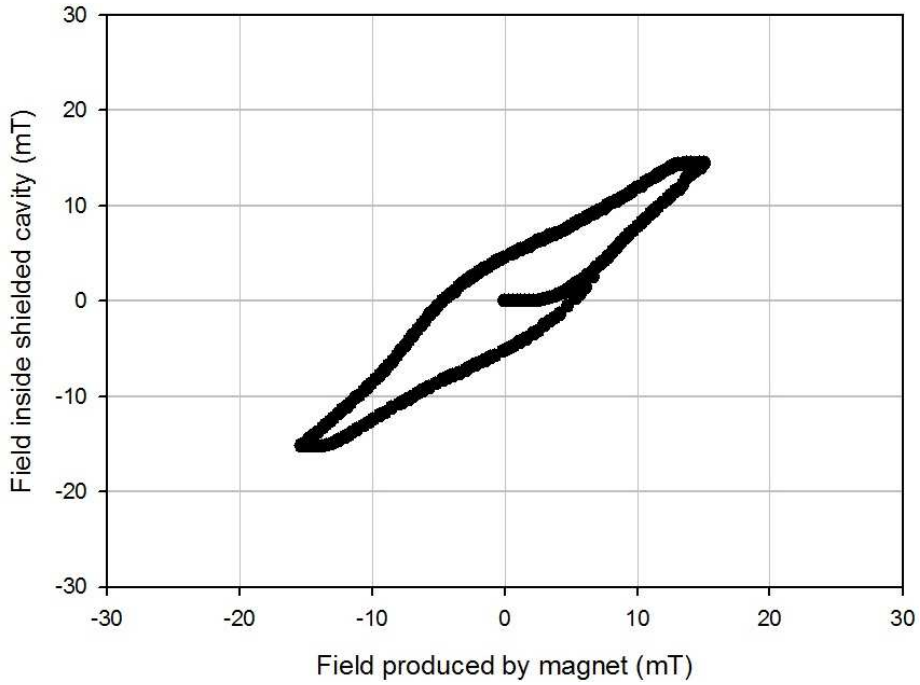

Figure 45: Hysteresis curve for double shield with Hall sensor located out of specimen center

Several differences can be spotted when comparing this curve to ones obtained previously. Full shielding region is much thinner - it is only approximately 2,5 mT. Then internal field starts to rise, however this part of curve does not belong to hysteresis loop. The shape of curve is also slightly different. It appears to be thinner in central region than previous ones. Full comparison will be performed further in this thesis. Similarly to previous curve, this one was created at the beginning of measurments day. The final hysteresis curve was created after the measurments of AC field. Two shields have been used and Hall probe is located in the center of specimen. Figure 46 shows this curve.

It should be noted the the vertical axis scale is different than for curves shown before. Initial point of the full shielding region actually lies on one of the branches of the hysteresis curve. It appears that the full shielding region is wider when compared to previous measurments - it is approximately 8,7 mT. However, it is clearly visible that this is actually the plateau of hysteresis curve. The shape of curve is generally similar to other curves measured in the shield center. The main difference is that the hysteresis loop appears to be moved towards lower values.

4.2.2 Alternating magnetic fields

Two types of AC measurments were performed - magnetic field attenuation dependence on external field magnitude with different frequencies and field distribution along the axis. Firstly measurments were performed only for BSCCO tube, in order to find the value of the full shielding region. These measurments were performed both during increase and decrease of external field amplitude to check whether the hysteretic effects would appear. Figure 47 shows the example of single series obtained for the frequency of 72,4 Hz. The equal field line has been marked as a solid line.

The region of full shielding can be observed. Its width is approximately 5,55 mT. After transition to the mixed state the fast increase of internal field occurs followed by the slow approaching of the curve to the equal field line. No hysteresis effects appeared during this measurment. All other measurments in AC mode yielded similar results. Parameter α has been

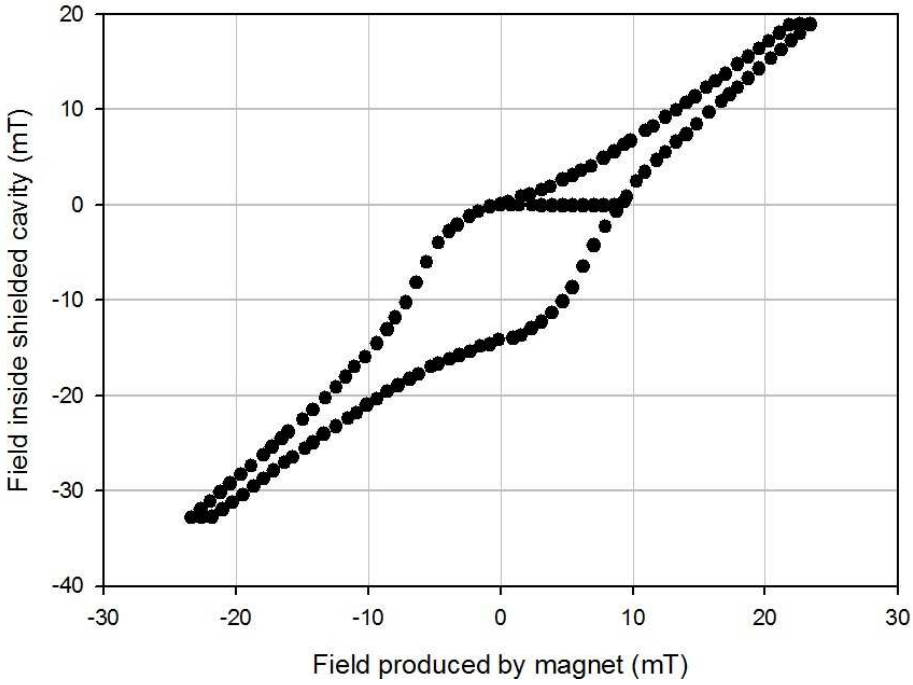

Figure 46: Hysteresis curve for the double shield with the trapped magnetic flux

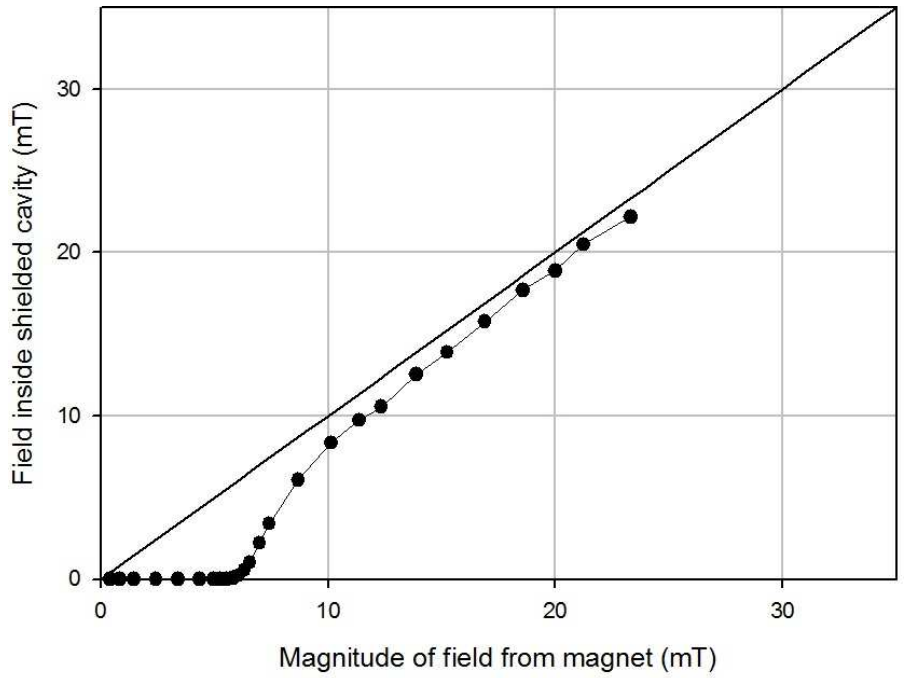

Figure 47: Measurement in the AC magnetic field of frequency 72,4 Hz for the single shield

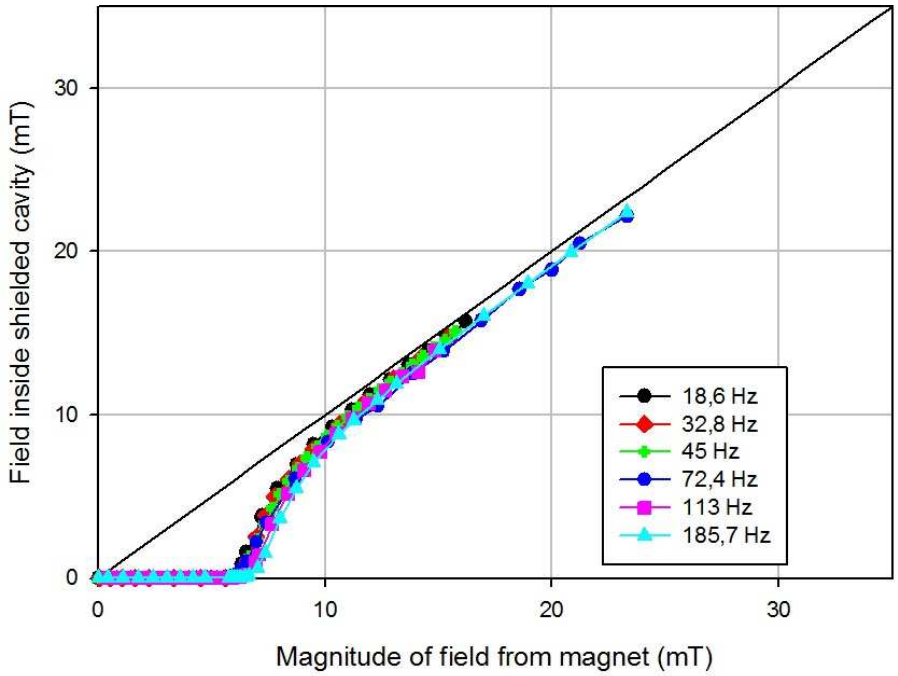

Figure 48: Measurments performed in the AC magnetic field with single shield applied

calculated according to equation 51. It was further used to obtain the value of the internal magnetic field. Based on this parameter all measurments results with the single shield applied have been gathered in a common graph shown in figure 48. The line of equal fields has been marked. Difference in the range of results comes from the fact that for lower frequencies it was difficult to obtain resonance conditions, thus available maximum current flowing through the magnet coil was lower.

Only very slight effect of frequency on shielding appears. The region of full shielding becomes wider with frequency. However, this effect is small and appears to very weakly affect mixed state region and completely disappear above approximately 15 mT of external field amplitude. The full shielding region has width of approximately 5,6 mT for the lowest measurment frequency of 18,6 Hz and 6,2 mT for the highest frequency of 185,7 Hz. Besides this effect all measurment results are generally similar and follow the path of a similar shape. For none of the measured frequencies hysteresis effects appeared.

The application of an additional screen made of YBCO tape changes the behaviour of the whole shield system. The measurments were performed using two different ranges of frequencies. During the first batch of tests, wide range of frequencies have been used i.e. from 10,2 Hz to 189,5 Hz. This was done in order to recognize the shielding effect coming from the additional YBCO tape shield. The results of measurments are shown in figure 49. The considerable influence of magnetic field frequence on shielding performance can be observed here. The full shielding region increases from 6 mT at 10,2 Hz to 26,3 mT at 189,5 Hz.

The second batch of tests used larger capacitor battery to obtain conditions close to resonance in lower frequencies. This was done in order to find the lowest frequency in which additional shielding coming from the YBCO tape-screen is observed. The graph based on these measurments is presented in figure 50. It can be seen that slight effect is visible almost immediately when frequency is rised from 3 Hz to 5,5 Hz. In higher external field some difference can be noticed even between measurments performed in magnetic fields of frequencies 3 Hz and 4 Hz. Significant increase in full shielding region can be observed, however smaller than in

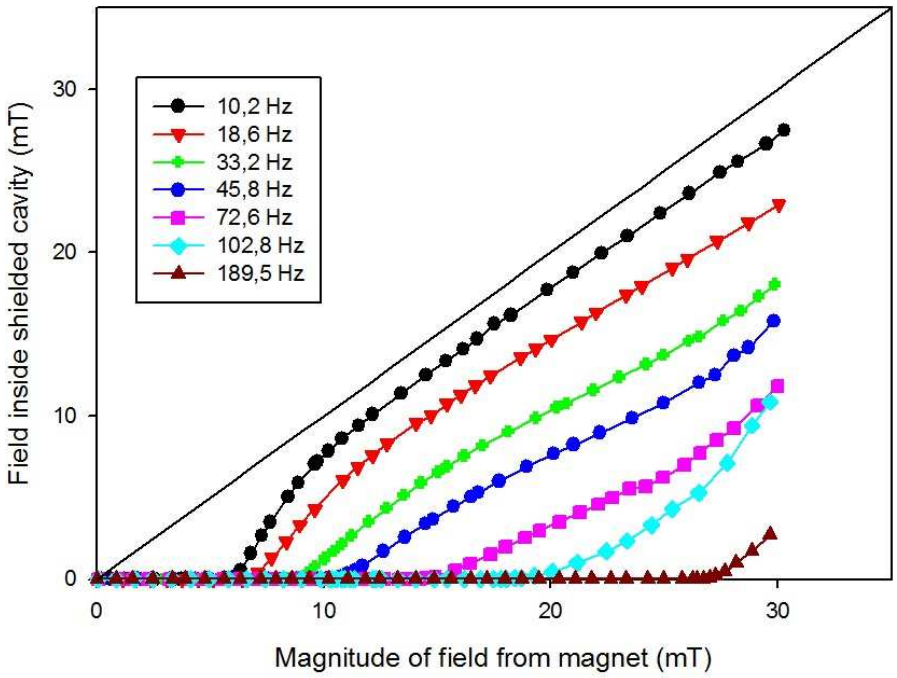

Figure 49: Wide range measurments performed in AC field with double shield applied

wide range measurments.

Similar measurment was performed when measuring cell was placed approximately 10 mm above the shield center. This measurment was performed in 5,5 Hz. Effect of changed position on the shape of curve have been shown in figure 51. As it can be noticed the most significant change occurs in the region of full shielding. It is strongly reduced and an internal magnetic field quickly starts to rise. Above certain external magnetic field it starts to follow the same path as the one observed in the center of specimen - points are positioned almost exactly the same. This is probably due to magnetic field lines bending at the open ends of the tube. This problem was investigated further by measuring the field distribution inside the specimen.

Field distribution along the vertical axis has been further investigated in several measurment runs. These measurments were performed under constant frequence and magnitude of magnetic field. Measuring coil was moved along the axis of specimen and the results were read. Figure 52 shows the distribution of the field along the axis of the single shield for two different amplitudes of magnetic field. One allows full shielding region to appear (its value is 5,27 mT) and the other causes mixed state all along the specimen (this amplitude is 8,14 mT). The frequency of magnetic field is the same for both measurments and is equal to 72,4 Hz. 0 at the lower axis marks the center of the specimen tube. It can be seen that at the ends of the tube both plots exhibit similar shape, despite the difference in their amplitude. The length of full shielding region is approximately 45 mm, it appears to be slightly shifted downwards. Except for this both graphs are regular and symmetric. It should be noted that, even though the shielding is not full, still some reduction of the internal field is observed in the center of specimen. There was additional measurment performed in lower field magnitude (2,78 mT), however flux jumps were too strong to obtain reliable measurments. The only reliable result obtained was the length of fully shielded region, which was 60 mm.

Similar measurment was performed for the double shield setting. It is shown in figure 53. The frequency of external field was 72,6 Hz to make the results comparable with former measurment. The magnitudes of magnetic field are 9,41 mT to investigate full shielding region

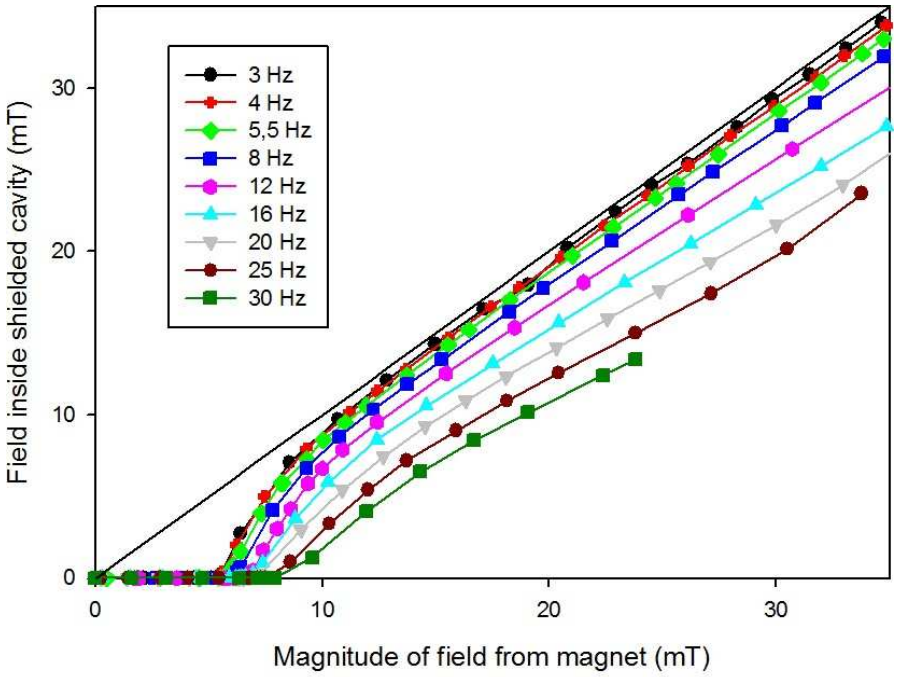

Figure 50: Low frequency measurments performed in AC field with double shield applied

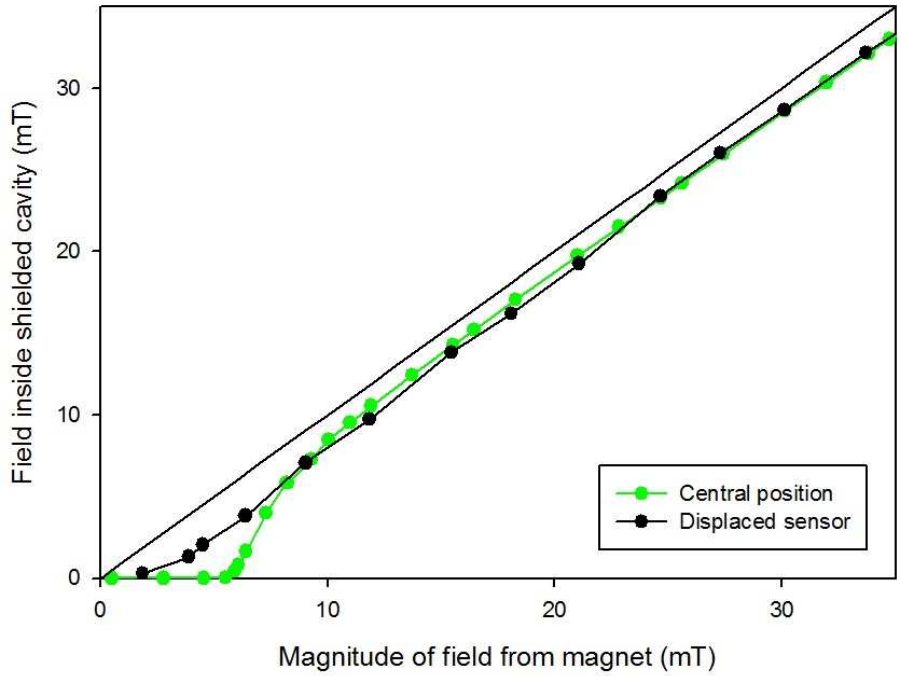

Figure 51: Effect of changed sensor position on AC measurments

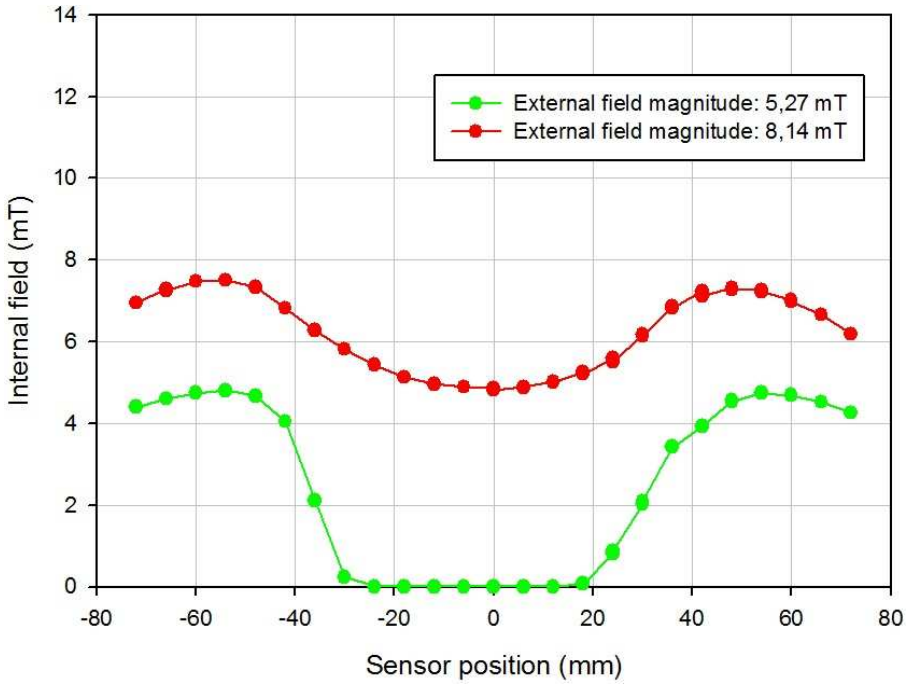

Figure 52: Distribution of magnetic field along the central axis with the single shield applied

and 17,67 mT to research the mixed state region. These values are higher than in measurment for single shield and were chosen based on the measurments of field development for this frequency (figure 49). 0 at the horizontal axis marks the center of sample shield again. It can be seen that even though much higher fields were applied than in previous measurments, field attenuation is much better. The length of full shielding region is approximately 45 mm. The very striking property of these plots is their lack of symmetry. In case of higher magnitude field, which was expected to keep internal field in the mixing region, full shielding was almost achieved approximately 12 mm below the center. Also the right part of the graphs appears to be deformed. This is due to the non-uniform shielding properties of the additional YBCO tape shield, which will be discussed later.

The final measurments were performed in the setting with only tape-screen applied. The first batch of measurments was performed in the range of frequencies between 3 Hz and 30 Hz in order to find where the effect of electromagnetic coupling appears. The results of these measurments are gathered in figure 54. During the measurments the field applied was generally ascending. It can be seen that no full shielding region appears, which is the expected behaviour of tape-screen setting. Internal field is linear in the range of measurments. The higher the frequency the lower the slope of the result curve. The effect of electromagnetic coupling starts to be significant when the frequency of external field is approximately 10 Hz. Below this frequency the internal field data closely follow the equal field line. It can be observed that the difference between external and internal magnetic field is higher when an external applied field is larger.

In order to check how the effect of electromagnetic coupling develops in higher fields the second set of measurments was performed. The measurments were performed in full resonance conditions in order to obtain as high field in the magnet as possible. Frequencies of applied fields were 9,2 Hz and 32,9 Hz. Maximum achieved fields were 64 mT for 9,2 Hz and 75 mT for 32,9 Hz. The results of these measurments are shown in figure 55 along with the equal field line. As it can be seen the results obtained for the frequency of 9,2 Hz are linear and remain close to equal field line. It is very similar to the results obtained before for lower frequencies.

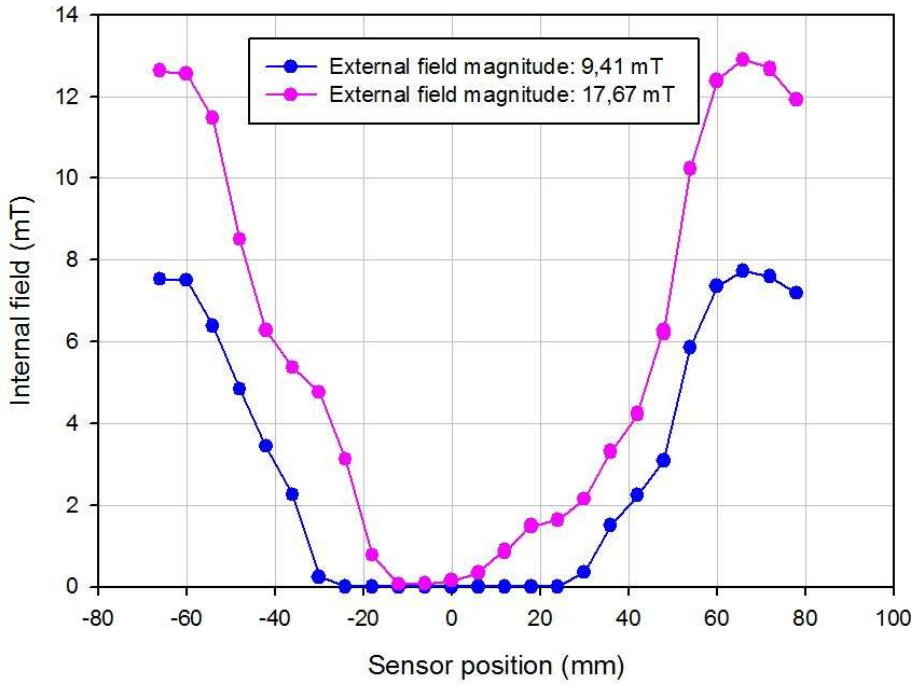

Figure 53: Distribution of magnetic field along the central axis with the double shield applied

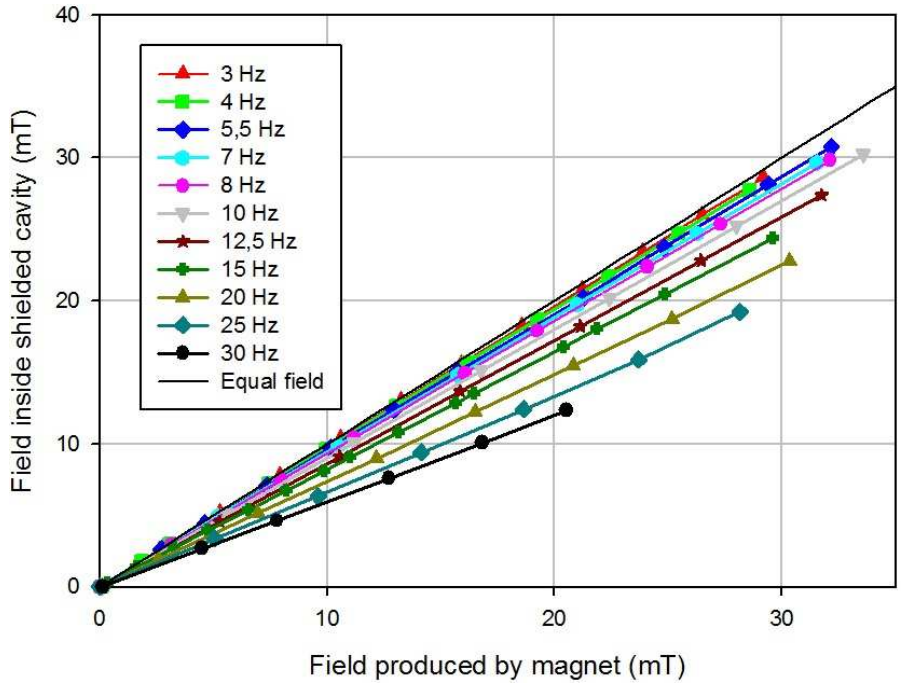

Figure 54: Measurments performed with tape-screen applied in AC field

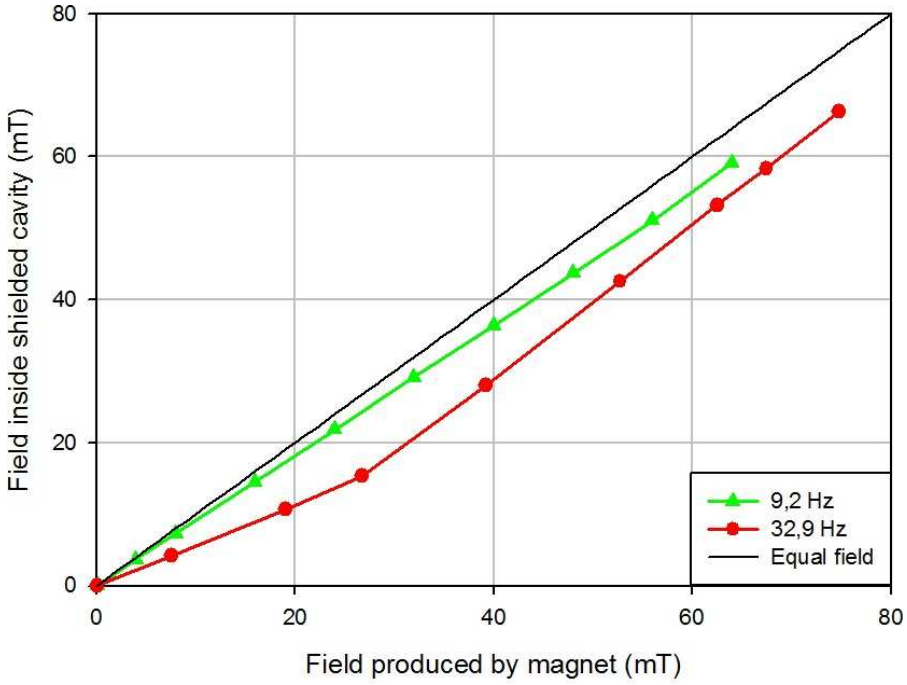

Figure 55: High field measurments performed with tape-screen in AC fields

The line obtained for the frequency of 32,9 Hz is linear up to approximately 30 mT. Above this value of external field it bends and tends to move closer to the equal field line. The interpretation of these results will be provided in the further part of this thesis.

5 DISCUSSION

5.1 COMPARISON BETWEEN MODES OF OPERATION

5.1.1 Different operation conditions in DC mode

Some frozen field was present in all of the measurments, since none of them was performed in true zero field conditions. However, at the beginning of each measurments day (right after superconducting transition of specimen) only natural background magnetic field was present. Earth's magnetic field is weak compared to fields achieved during investigations - it is approximately 25-65 μT. Such field is disregardable. The situation exacebrates when some remnant field is left after previous measurments. This is especially visible in hysteresis curves obtained during DC measurments.

Remnant field has to be countered with external field before the measurment will achieve hysteresis curve. This can be clearly seen in figure 46. The measuring points shown in this figure were read after whole day of measurments performed in double shield setting with AC field. It was expected that remnant field will be mostly washed out. However, it did not happen and some of the field was left frozen in the solid tube. The measurments started with the increase of external field. Initially the behaviour of interal appears to be the same as full shielding region. Obtained width of this apparent region was larger than obtained in prior measurments.

After the increase of external magnetic field to certain level the field change was reversed and thin plateau was observed. After that the decrease of external field was followed by the proper decrease of internal field. It crossed the initial point of measurment and then continued

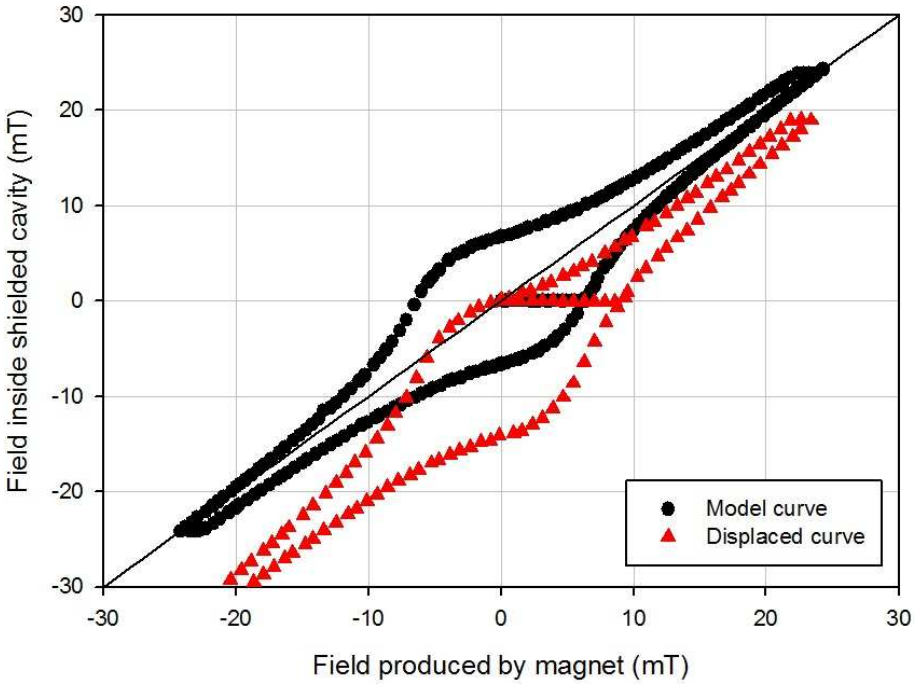

Figure 56: Comparison of displaced and normal hysteresis curve

to form normally shaped hysteresis curve. The presence of this crossing is a proof that observed region in which internal magnetic field was constant was not a full shielding region, but the plateau inside the hysteresis curve. Because of measurment method an initial background magnetic field which was read, was already affected by remnant field inside the tube.

Due to the fact that initial point is moved, whole curve is displaced. The most striking comparison comes from comparison of figures 46 and 44 which have been made for double shield setting. Similar effect, however smaller can be observed also in figure 43. Measurments which became the basis for graph shown in figure 44 were performed right after superconducting transition, therefore only natural background magnetic field is frozen. This measurment's zero point will considered as the closest to an actual zero field conditions and all other curves will be matched with this one. Comparison of two curves without adjustment is shown in figure 56.

It should be noted that the displacement of the curve comes only from the displacement of the starting point. To find match it is necessary to move displaced curve so zero point of both curves will be at the same position, preferably at the center of coordinates system. The curve should be moved only vertically - the measurment of magnetic field produced by magnet was not affected by the value of background field. As it can be also noticed the curves are slightly tilted when compared to equal field line. Correction factor will be applied in order to match the curves. Also it was done in such fashion that the line of equal field was approximately the axis of symmetry of hysteresis curve. The mechanism causing the tilt will be explained when the comparison with model will be performed. Figure 57 shows the superposition of these two curves. As it can be seen after adjustment both curves fit almost perfectly. The remnant field was approximately 6 mT - this value had to be added to obtain desired match. This is very close to the value of the full shielding region. Tilt factor was 0,9.

Moving of curves has been also applied to add the missing part of hysteresis curve for solid shield from figure 43. The additional measurment was performed the next day after base one, preceded by the measurments in AC field. The result of this operation has been shown

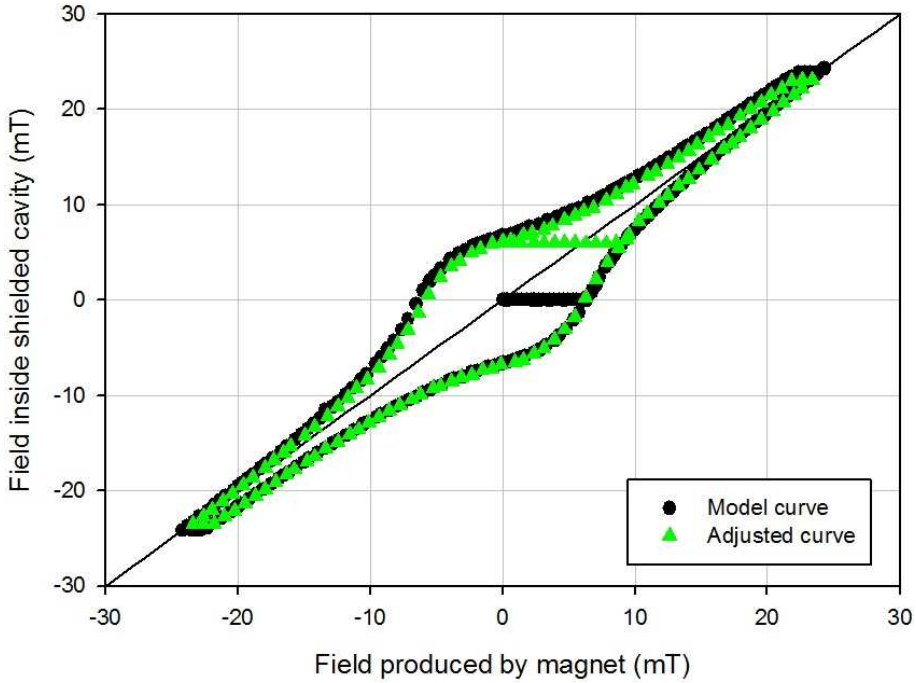

Figure 57: Comparison of adjusted and normal hysteresis curve

in figure 58. This curve after completion will be considered as one for the purpose of further investigations. The additional measurments fit well, however both base and additonal had to be adjusted. Frozen field in the case of the base curve was 2,75 mT. Tilt factor was 0,97. For additional measurments frozen field was smaller - it was 0,4 mT. Applied tilt factor was larger and amounts to 0,92.

The position of sensor also strongly affects the performance of shielding. Figure 59 shows the comparison between results from centrally positioned sensor and the one moved 10 mm above. Since both measurments were the first ones performed after superconducting transition no frozen field was added. Also tilt factors have not been applied. External magnetic field is leaking into the tubular specimen through the holes at the top and the bottom. The shape of the curve obtained with displaced sensor is changed especially in central part - the branches of curve are positioned closer to equal field line than in case of centrally positioned sensor. Effect becomes weaker at higher magnetic fields. There might be several explanations for such behaviour. It may be caused by the properties of Hall sensor - it is affected not only by the strength of field, but also by its direction. Hall sensor was calibrated in uniform parallel field. The field which leaks into the specimen is expected to change its direction. The other reason is the weaker magnetisation of superconductor - in this case part of remnant actually leaks out. By measuring the width of full shielding region one may assess the strength of internal field for which it penetrates the specimen down to the position of sensor.

Unlike in case of centrally placed sensor, when the transition to mixed region is sudden and immediately leads to hysteresis, gradual growth of external field is observed when the sensor is displaced. The field increases slowly and smoothly develops into hysteresis curve. That fact is also significant - it allows to check whether an actual transition to mixed region occured or the field leaking through apertures caused the deterioration of shielding properties. If such behaviour was observed in case of centrally placed sensor that would mean that the geometric size of specimen (in case of applied tube - its length) is to small to fully utilise benefits coming from superconducting magnetic shielding.

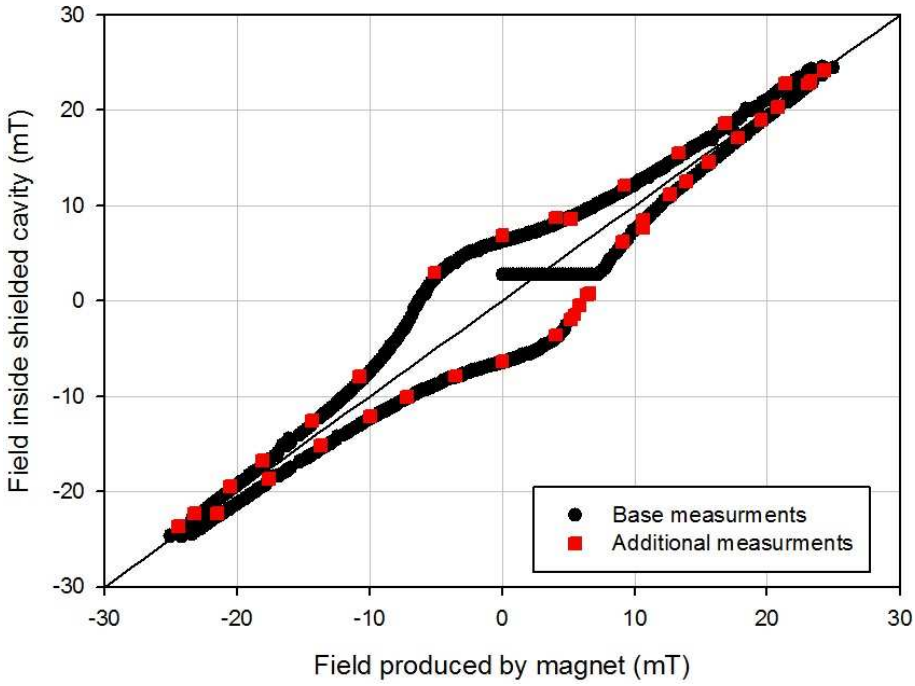

Figure 58: Completed hysteresis curve for solid shield

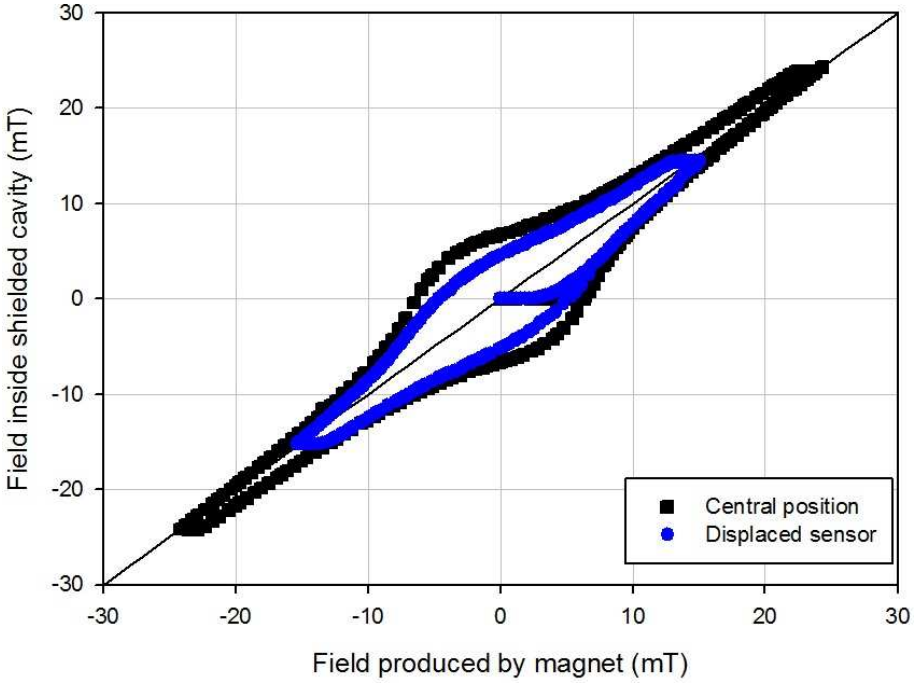

Figure 59: Comparison between results from differently placed sensors

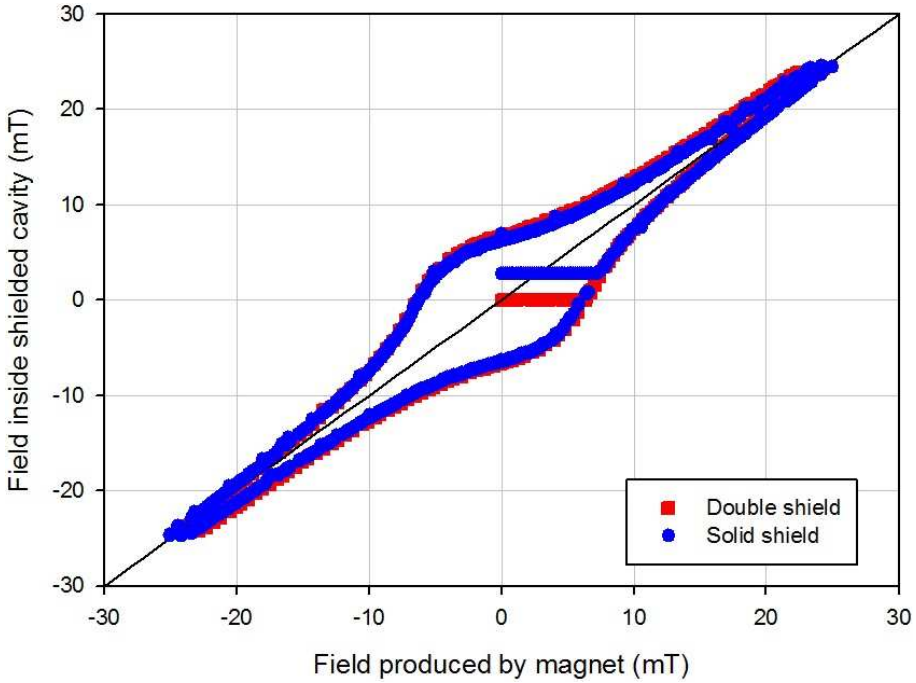

Figure 60: Comparison between hysteresis curves obtained for solid and double shield setting

Since DC measurments were performed for both solid and the double shield settings, the effect of additional shield made of YBCO tapes can be investigated. Figure 60 shows the comparison between magnetic fields inside the cavity shielded by solid and double shield, respectively. Curve shown as the one for solid shield is the same as the completed one shown in figure 58. Tilt factors and the addition of frozen field were preserved. Curve for double shield is the curve from figure 44. Neither tilt factor nor frozen field addition were performed.

As it can be seen both curves are almost exactly the same. Slight misadjustment comes from a tilt factor. The difference in the full shielding region is caused by remnant field. It can be concluded that no observable effect comes from the application of additional shield made of YBCO tape for the shielding of DC field. Probably, if the additional shield was also a solid tube, such effect would be observed. Based on the results above it was assumed that the hysteresis curve for double shield from figure 44 is the most representative. Therefore it will be used for any further comparisons and investigations including DC field shielding.

Several negative effects distorting the results were observed during measurments. They revealed as the misshape of curve and made the measurment process longer. The effect, which caused the most problem during measurments was field lines relaxation. This effect comes from the finite speed of movement of unpinned vortices [2] - it takes some time before quasi-stable formation of vortices will appear. It still randomly changes due to flux jumps, but in case of DC field this effect is limited. Some apparent errors, especially visible in the curve shown in figure 43 come from this effect. Flux jumps became significant problem during the measurments at AC field. In one case it made the assessment of field distribution impossible and in others it caused need for some extra assumptions.

Shielding factor was calculated based on the hysteresis curve from figure 44. Results are shown in figure 61. Shielding factor was calculated based on equation 3. As it can be noticed, maximum shielding factor obtained was less tahn 60 dB. The fluctuations seen in full shielding region come from the noise and frozen field. Shielding factor obtained is lower than stated in specification (>120 dB according to leaflet in attachment 8.6). This difference come probably

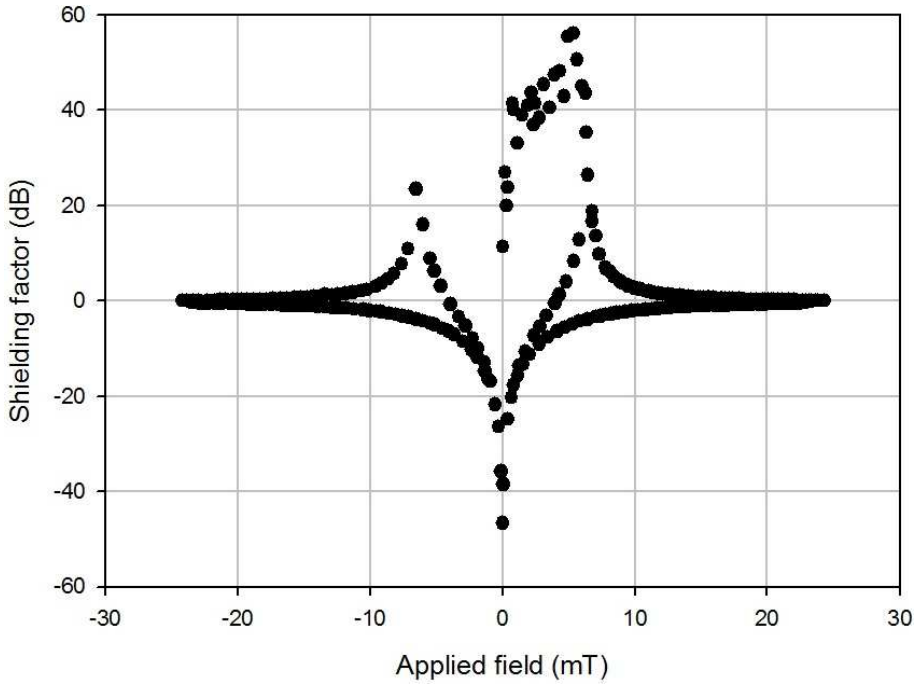

Figure 61: Shielding factor in DC mode

from the application of measuring devices which were more accurate and less sensitive to random noise. Except the full shielding region an obtained shape is symmetric. The highest value of shielding factor is obtained when internal field is close to 0 mT.

5.1.2 Solid, double and tape-screen shield in AC mode

Relationship between the transition point and frequency depends on whether the double or single shield is applied. This is shown in figure 62 comparing transition points read from measurments in the AC fields of different frequencies. Most of the results were found by averaging the values obtained during measurments. In several cases the results lacked points to ensure precise reading. Then the line was created to extrapolate the results. Logarythmic scale have been applied to highlight the region of interest where the differences start to appear.

It can be seen that in case of solid shield almost no dependence between frequency and transition field is observed. The effect is negligible when compared to double shield setting and can be accounted to reading uncertainties. Its value varies between 5,6 mT and 5,92 mT. Situation changes when tape-screen is applied as an external shield. Transition point remains relatively constant until approximately 10 Hz. In this region it varies between 5,4 mT and 5,75 mT. Above this value it starts to rise continuously with frequency. The highest obtained value was 25,8 mT in the field of frequency 189,5 Hz. This issue will be further investigated and compared with the model in the section 5.2.2.

Field distribution inside the tube have been compared with expected magnetic field produced by the magnet. Based on the relative field from the magnet obtained during magnet testing (shown in figure 39) the following figures (63- 66) have been drawn. The value of relative magnetic B_{rel} coming from the figure was multiplied by magnetic constant KM ($15{,}6^{mT}/_{A}$) and current I supplied during test, according to equation 56.

$$B_{local} = B_{rel} \cdot KM \cdot I \tag{56}$$

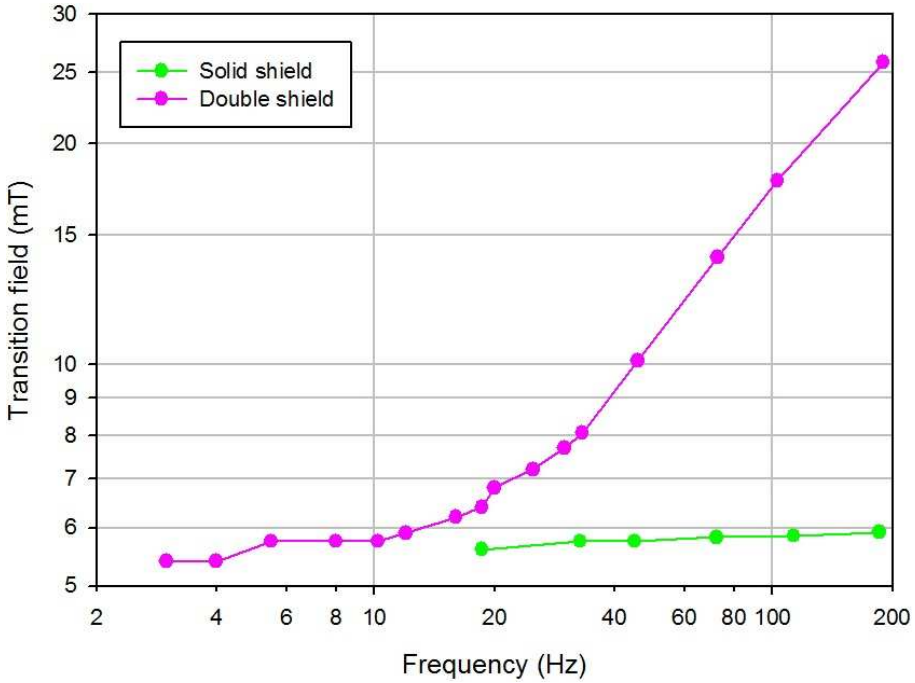

Figure 62: Dependence of transition point on frequency

The first measurment was performed in solid shield mode. The results of comparison are shown in figure 63. The current supplied through magnet was 0,338A, which yielded the field of approximately 5,27 mT at the center of magnet. Such field was insufficient to cause the transition to the mixed state and therefore the region of the full shielding was observed. The frequency of field was 72,4 Hz. The wide full shielding region can be noticed. Out of this region internal field rises steeply and, outside the tube, starts to follow the expected magnetic field.

Another measurment in solid shield mode was performed in stronger field of 8,14 mT at the magnet center. The field of such magnitude was sufficient to cause the transition to mixed region, therefore no full shielding will be observed. Result of this measurment is shown in figure 64. Frequency is equal to 72,4 Hz and is the same as in previous measurment. Some field attenuation still can be observed inside the pipe. It is symmetrical and smooth. Outside the pipe an external field is followed.

The application of second shield changed the shape of the results curve. Fields of higher magnitude were used. To produce figure 65 the field of magnitude 9,41 mT was applied. In this field specimen still remained in full shielding region. Frequency of field was 72,6 Hz, similar to previous measurments. Full shielding region appears, its length is similar to this obtained during solid shield mode measurment. Since tape-screen shield is longer than solid shield, internal field does not completely follow external field. Some unsymmetry is noticeable.

Second measurment in the double shield mode was performed for the same frequency of 72,6 Hz. Applied field amplitude was 17,67 mT at the magnet center, which was expected to be sufficient to cause the transition to the mixed state. As can be seen in figure 66 shielding is still very strong and in some parts of the shield it is close to the full shielding. Strong asymmetry may be noticed. Field attenuation appears to be stronger than in previous case in the region outside the solid shield.

Non-uniform shielding properties in distribution graph can be seen in this figure. The region with the best shielding is not positioned within the center of magnet, but moved approximately 20 mm below. There internal magnetic field is very close to 0. This non-uniformeity comes

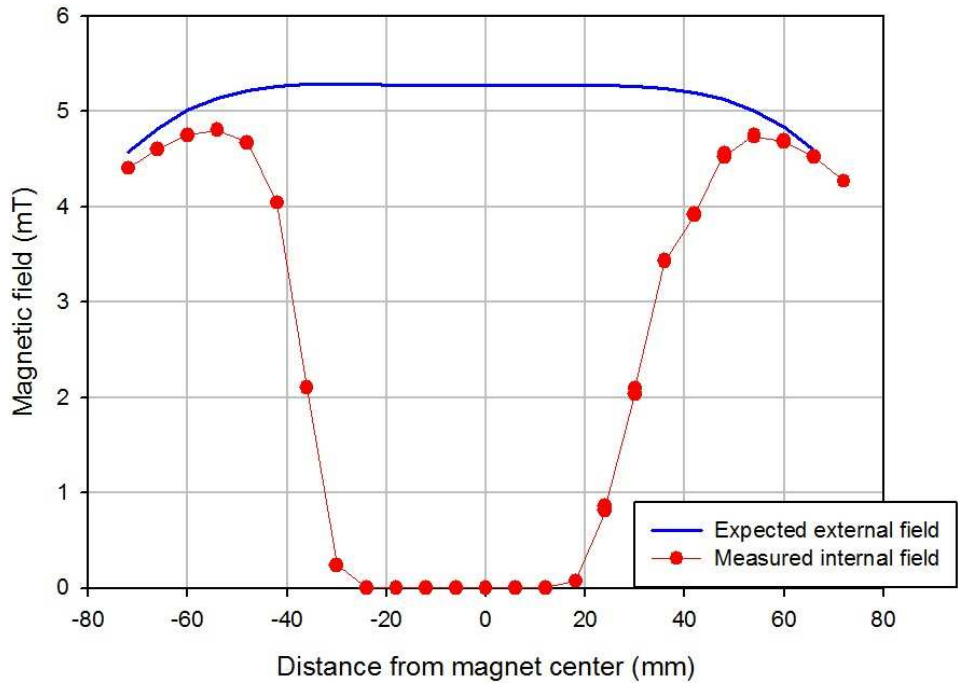

Figure 63: Full shielding in the solid shield mode compared with expected external field

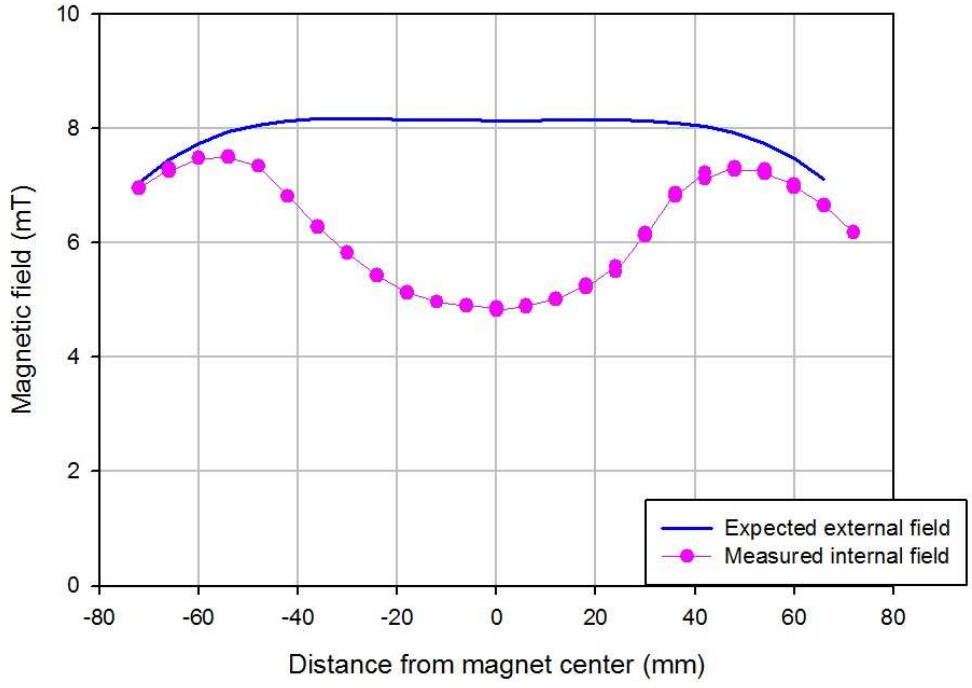

Figure 64: Shielding in the mixed state in the solid shield mode compared with expected external field

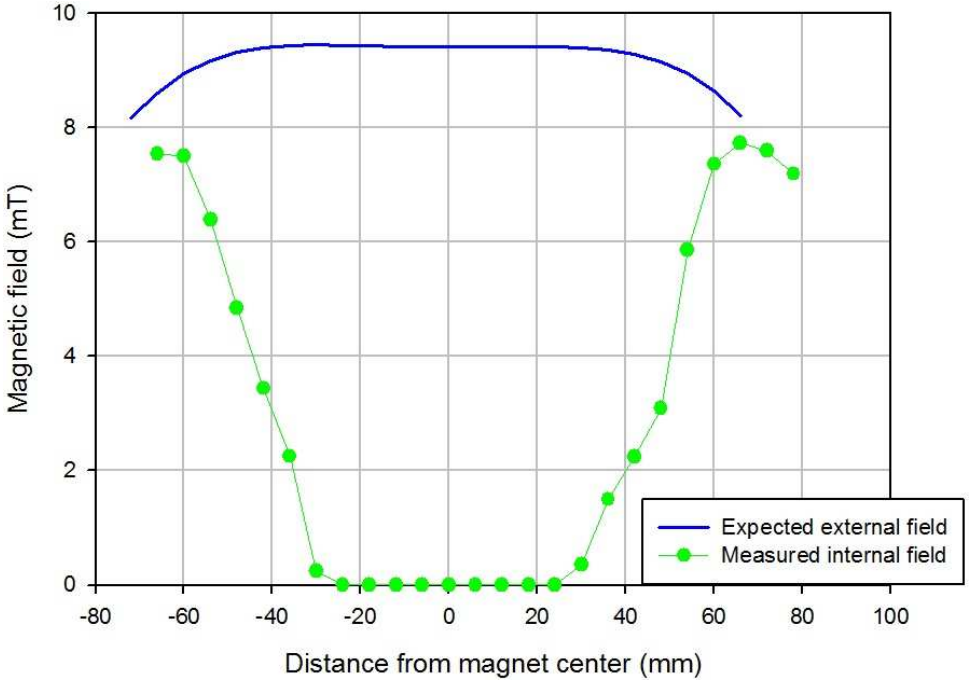

Figure 65: Full shielding in the double shield mode compared with expected external field

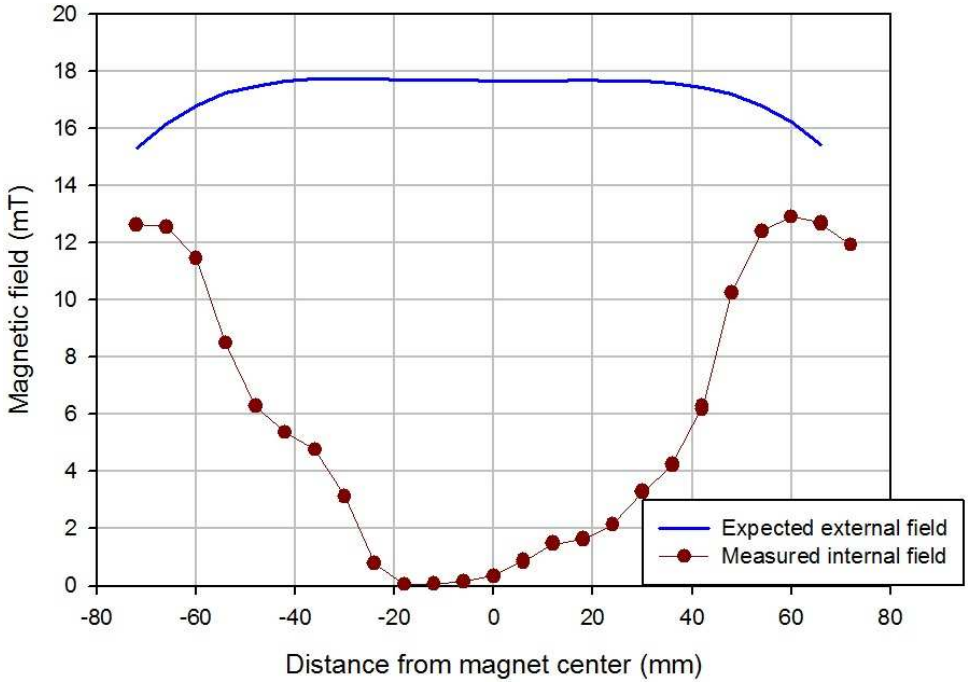

Figure 66: Shielding in the mixed state in the double shield mode compared with expected external field

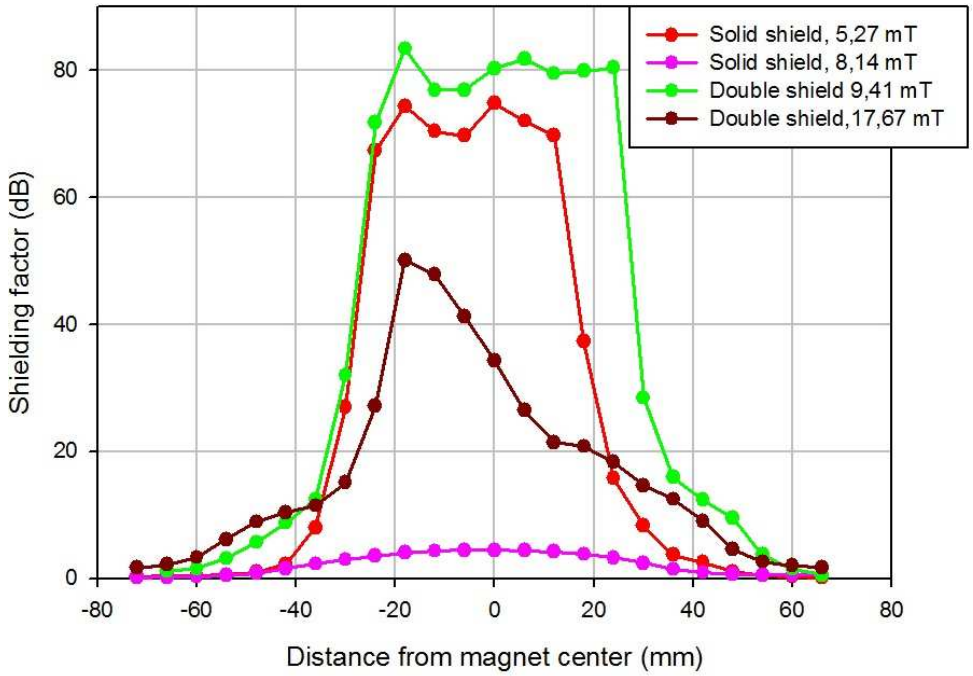

Figure 67: Shielding factor dependence on sensor position within a specimen

from different properties of rings applied for shielding and their positioning on a plastic pipe. Different properties of rings may be caused by distortions in solder, its variable thickness and shape. Some misalignements may have occured. The gap between rings might have varied.

Shielding factor has been calculated for each sensor position. The results of calculations have been gathered in figure 67. It can be seen that shielding factor is generally much higher in case of double shield. The difference is especially visible in case of comparison between mixed region shielding efficiencies. In case of full shielding the region of high shielding factor is considerably larger in double shield setting. Outside this region both curves remain similar. Interestingly, the values obtained based on noise within full shielding are also similar.

Tape-screen application also leads to some attenuation of the field. The effect does not appear in direct current field, due to the fact that magnetic field is capable of leaking through solder. In alternating field several effects appear, which decrease magnetic field within the shielded cavity. This is due to electromagnetic coupling, which allows the exchange of energy through non-superconducting junction, thus closing the circuit. This allows the formation of superconducting current around whole perimeter of shield and screening of external magnetic field.

Since the effect is smaller in the range of interest than attenuation with solid shield, shielding factor would prove insufficient in the assessment of shielding quality. Attenuation efficiency Æ have been invented in order to ease results interpretation. It is defined as the percentage of field which is attenuated by field and calculated according to equation 57.

$$Æ = \left(1 - \frac{B_{in}}{B_{out}}\right) \cdot 100\% \tag{57}$$

The results of these calculations are shown in figure 68. Attenuation efficiency is shown there for several frequencies, in the fields of different amplitude. The measurments performed in zero external magnetic field were cut due to the distortion of curves.

It can be seen that in some range of field magnitude attenuation efficiency remains approxi-

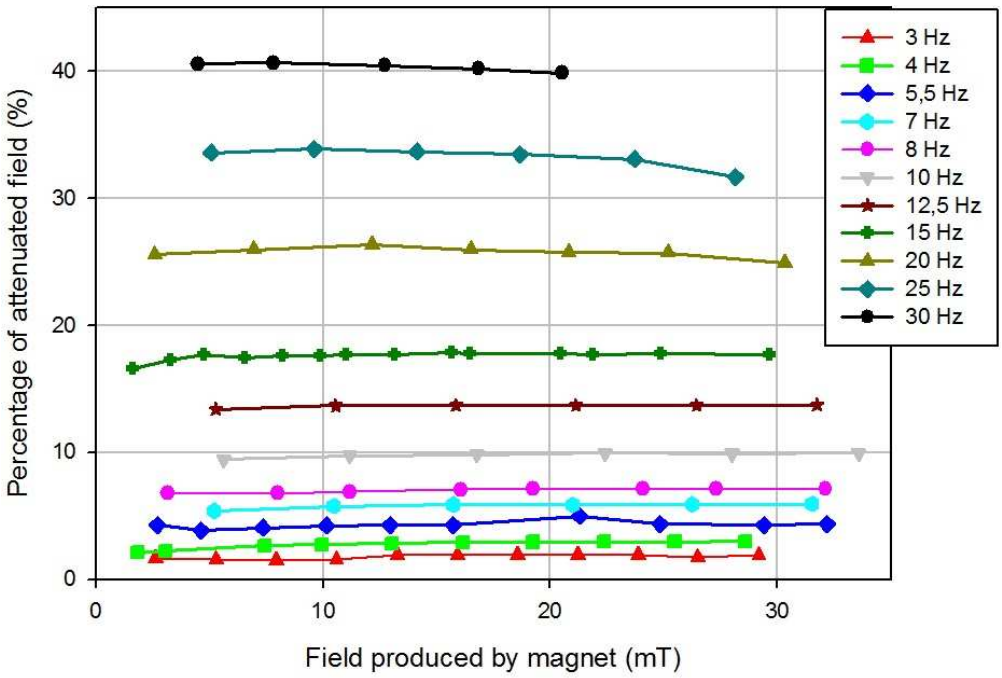

Figure 68: Attenuation efficiency dependence on frequency

mately constant for given frequency. In high frequencies some decrease can be noticed in higher fields. In some range though, this factor depends only on frequency. This the region where the effect of electromagnetic coupling will be searched in further section. Observable decrease of factor in high fields led to further investigation. Measurments were performed in resonance conditions and higher fields were obtained. Attenuation efficiency was calculated and resultant graph is shown in figure 69.

Large decrease in high field (above approximately 27 mT) can be observed for the measurments performed at 32,9 Hz. From the shape of curve it appears that the final attenuation efficiency in fields higher than 80 mT would be approximately 7%. Small decrease can be observed in the fields above 55 mT for the meausurments performed in 9,2 Hz. This decrease originates from the disappearance of superconductivity within the specimen and thus larger number of vortices which pass the bulk of superconductor. Since superconducting currents are stronger in higher frequencies, this effect appears in lower fields and is stronger.

Demagnetisation of field, which was performed by the application of AC field to magnetised specimen, also has been affected by the application of additional shield. Figure 70 shows the central region of several hysteresis curves. In order to produced this the curve obtained for zero field condition and the adjusted curve from figure 57 (both obtained in double shield setting) have been used along with the completed curve for solid shield from figure 58. Adjusted curve for double shield and the curve for solid shield were obtained after the whole day of measurments. Zero field curve was measured as the first one.

Except the region where the internal field remains constant despite the changes in internal field, curves almost overlap and may be considered the same. Within this region large differences are observable. The beginning of curve in both solid and double shield setting is situated higher than in zero field condition. This is due to the curve adjustment and marks the size of remnant field, which was present within the solid specimen at the beginning of measurments. It can be seen that in case of double shield the beginning of hysteresis curve actually lies on this, exactly the center of coordinates system. In case of solid shield this is situated between the

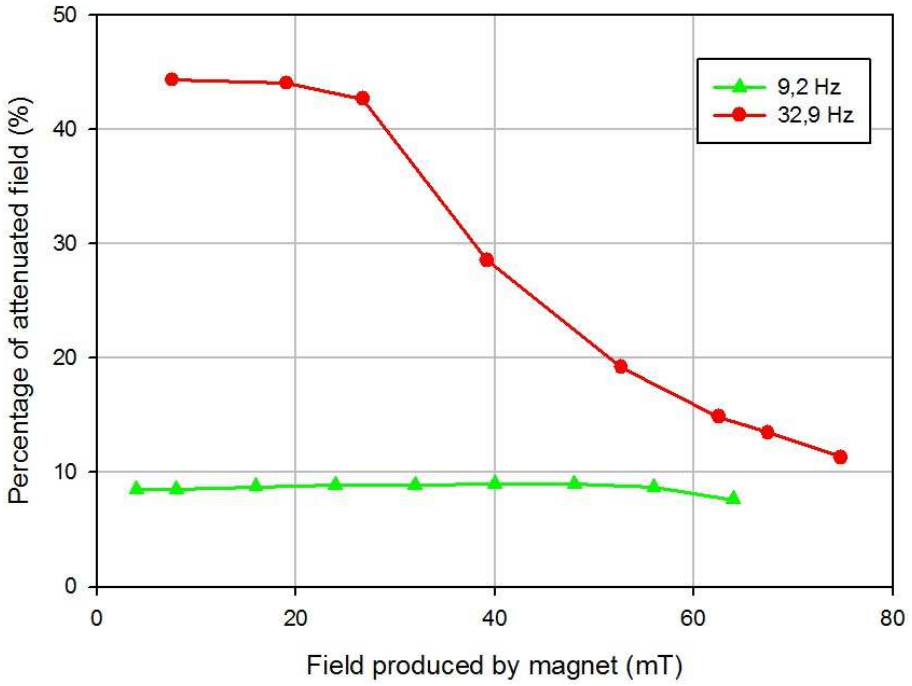

Figure 69: Attenuation factor in higher magnetic fields

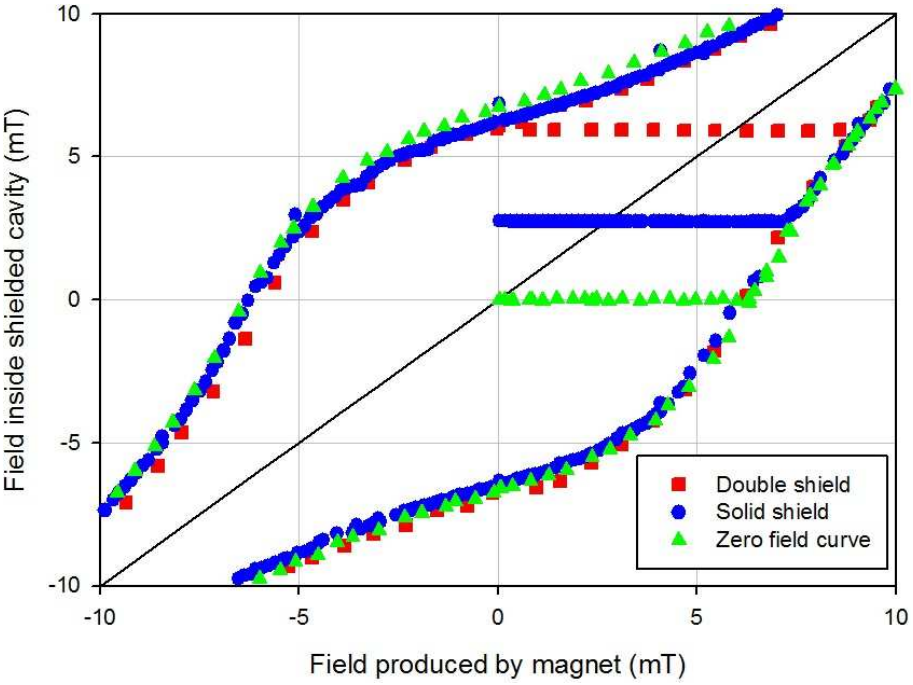

Figure 70: Field wash-out efficiency

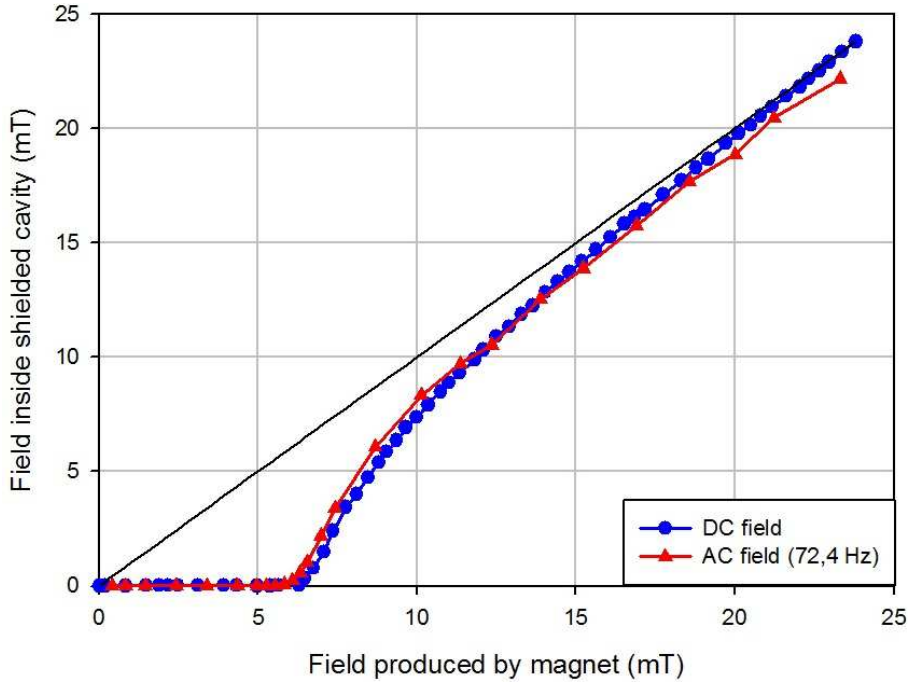

Figure 71: Comparison between first branch of hysteresis curve in DC mode and results for AC field in solid shield mode

other curves.

This difference is caused by the effect coming from the application of tape-screen. When the field was washed out in solid shield mode, it was removed only partially. However, in case of double shield setting AC field was unable to penetrate tape screen and thus the remnant field remained at the maximum possible level, as predicted qualitatively by Kim model. If specimen was infinitely long, then this value would be equal to B_{lim} for the tube of this thickness and superconducting properties. Due to demagnetising effects this is slightly lower. These results show, that the method of demagnetisation with an AC magnetic field is not always efficient way to remove a remnant field.

5.1.3 DC versus AC mode

Comparison between the first branch of the hysteresis curve and results obtained in the AC mode for the solid shield is shown in figure 71. For the purpose of this comparison the initial branch of hysteresis curve created in zero field conditions and in an increasing magnetic field was used. This is the part of curve from figure 44. The curve for AC field has been obtained from measurments in the field of frequency of 72,4 Hz in solid shield mode. Therefore no effects coming from electromagnetic coupling will be observed.

As it can be seen both curves are very similar. The region of full shielding appears to be slightly shorter in case of AC magnetic field. This difference might be caused by small residual field present in DC field measurments, which moved the beginning of curve slightly upwards, to the location where hysteresis curve is wider. Transition to a mixed state appears to be more steep in case of AC magnetic field. This difference may arise from smaller demagnetising effect in AC magnetic field. Finally, shielding efficiency in AC mode seems to be larger in higher external field than in DC mode. Internal magnetic field in AC mode appears to be almost parallel to equal field curve. This may be caused by slight distortion of the hysteresis curve. Error in the calibration of measuring coil also might have effected in such result. Therefore this

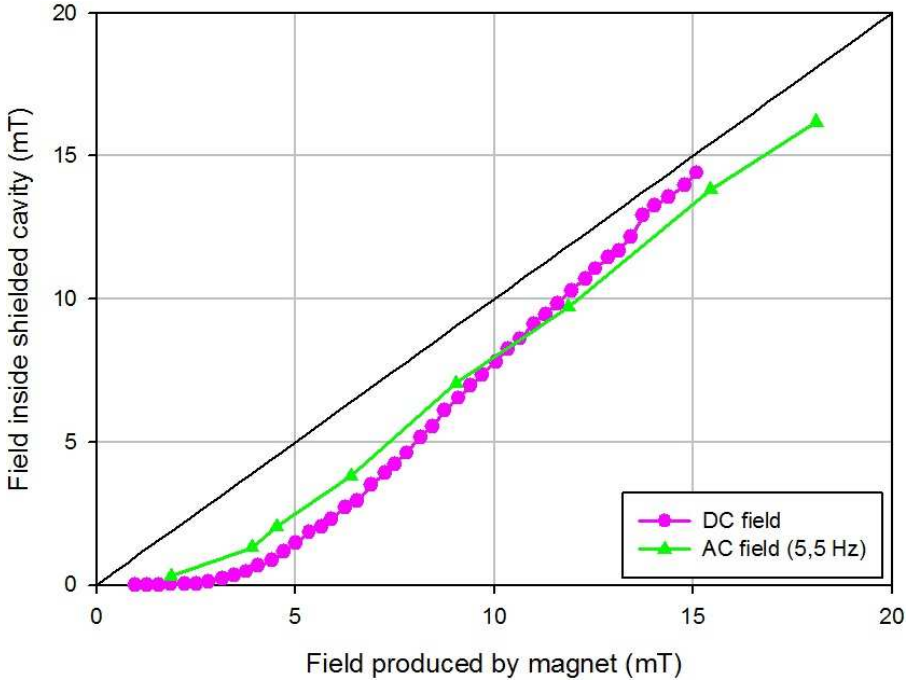

Figure 72: Comparison between the first branch of DC hysteresis curve and internal field in AC mode with the displaced sensor

difference comes probably from measurment method.

Comparison between branch and AC with displaced sensor brings some interesting results. It is shown in figure 72. Both curves were obtained at the same position of measuring cell, approximately 10 mm above the magnet center. Results for DC field were obtained as first, therefore it is assumed that the measurment was performed in zero field conditions and no initial field has to be added. The measurments were performed in double shield setting. The frequency of AC field was 5,5 Hz, which is expected to be insufficient to obtain shielding effect in tape-screen.

Curves bear more differences than in case of centrally placed sensor. As it can be seen full shielding region has not been observed in case of AC field measurments, contary to DC field. However, based on DC results, it might be expected that some region appeared below the lowest value of external magnetic field obtained in AC measurments. Until external magnetic field is above 10 mT shielding efficiency is higher in DC mode. Above this field AC field again appears to be parallel. Reasons for this effect are expected to be the same as in previous case.

Shielding factor has been calculated for all cases described above. The results of these calculations are shown in figure 73. It can be seen that in case of centrally positioned sensor, shielding factor for AC field is generally higher than for DC field. This is noticeable especially in the region of full shielding. The difference comes from measurment method - results coming from measuring cell were affected by smaller noise than these coming from Hall effect sensor. After leaving full shielding region similar steep decrease occurs in both cases.

When the sensor was displaced, the results for DC mode initially follow the curve coming from AC measurments in centrally positioned sensor. Then sharp decline occurs and shielding factor starts to smoothly decrease towards the values close to 0 dB. Measurments in AC magnetic field performed with the displaced sensor yielded the lowest shielding factor, due to the lack of full shielding region. The shape of curve is similar to this of DC field with displaced sensor. When external field is above approximately 12 mT all curves begin to overlap and shielding

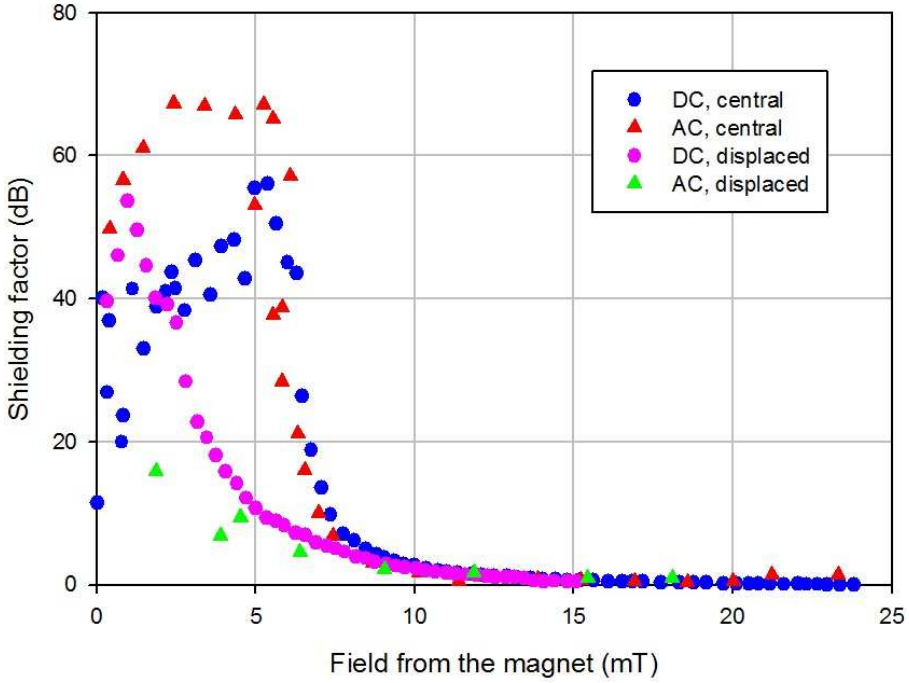

Figure 73: Comparison of shielding factors in DC and AC mode

factor decrease almost to 0 dB in the range of measurments.

5.2 COMPARISON WITH MODEL

5.2.1 Kim model and DC field results

The application of Kim model yielded several results shown in section 3.1. In order to check whether theoretical and experimental match several adjustments have to be made. The curve, which will be the base for comparison, is the one from figure 44. It was created in almost zero field conditions in double shield setting, therefore no initial field was added to the resultant curve. Tilt factor of 0,97 was applied to obtain the symmetry according to the equal field line.

The parameters in model equation (formula 43) have been set to match experimental results according to two criteria. Firstly, the thickness of superconducting tube was set to 1,5 mm in order to be the same as the one used in experiments. Secondly B_1 - the initial magnetic field and J_c - critical current density were chosen to obtain the same B_{lim} as the one coming from the experiments, according to the equation 44. The values which have been set were $1,35 \cdot 10^{-2} mT$ for the initial magnetic field and $80 {}^{MA}/_{m^2}$ for the critical current density.

Curves are in good match, almost perfect in the region of high fields. When the external field is close to full shielding region some differences are observable. The width of hysteresis curve appearing from model calculation is larger than of the one obtained during measurments. This effect comes probably from the fact that Kim model calculates the value of magnet field inside an infinite specimen. Therefore it does not take into consideration neither demagnetising effect nor the field leaking through tube's open ends. It is also supposed to model parallel field. During experiments some imperfections might have occured, which affected the shape of hysteresis curve. Another observed difference is steeper transition in the case of model results. This difference originates probably from conditions described before.

Tilt factor have been applied in order to adjust results of measurments for this comparison and several described previously. The expected results of this procedure was the symmetry

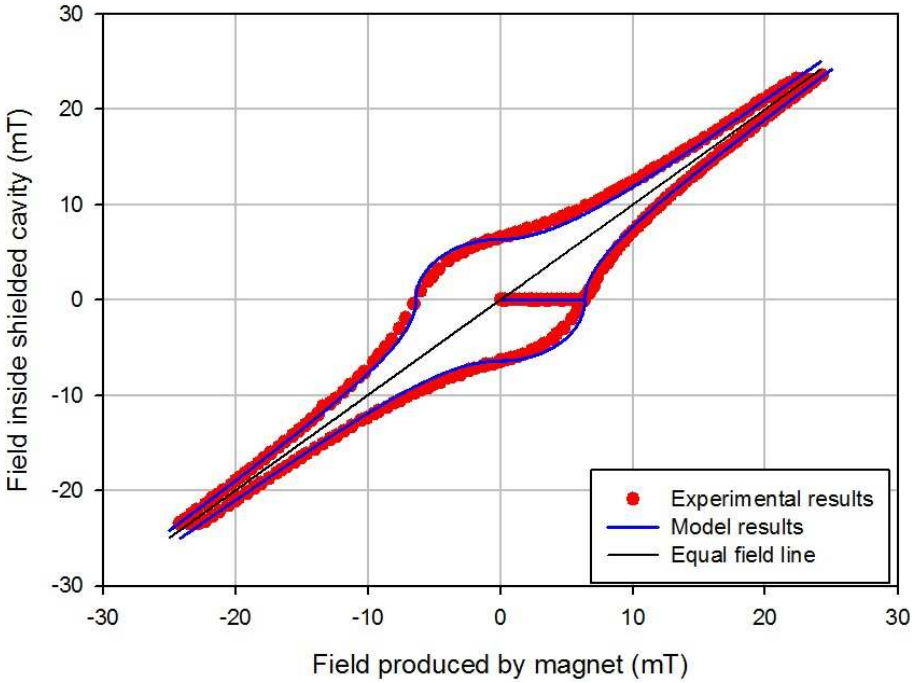

Figure 74: Comparison between model and experimental results for DC field setting

of hysteresis curve in respect to the equal field line. The reason of losing this symmetry by experimental curves was probably the deterioration of the Hall sensor. After the calibration some changes might have occured within the structure of the probe which led to the differences in the Hall current flow. This probably affected the result of measurment. The change in the Hall sensor manifested itself on the graphs of hysteresis curves as the change of their slope.

In order to prevent misleadings results a tilt factor was invented and applied. The ground for this assumption is the fact that tilt factor needed to obtain symmetry was decreasing depending on the date of measurments. The more measurments were taken, the higher Hall voltage was produced for the same field. Tilt factor for the initial measurments was almost 1, then 0,97 was applied. For the measurments taken on final day of experiments, the factor of 0,9 was needed to obtain symmetry. Instability of Hall probe was one of the major obstacles during the experiments and became especially troubling during the comparison with model.

Comparison of shielding factor predicted by model and calculated from the measurments results was also performed. It is shown in figure 75. Noise values for the calculation of model have been adjusted so the highest values in full shielding region matched. The values from experimental results come from figure 61. It can be seen that values from model and experiments are in very good match. The major differences, which are observed in full shielding region, come from the noise during measurments.

The most significant difference between both curves is the fact that in experimental results the change of shielding factor value during transition appears to be more continuous than in case of model calculations. This is due to the already mentioned lower steepness of measured transition to mixed state. The other differences observed in characteristic point come from lack of measurments taken exactly at this point due to lack of precise devices. Even though, some dependencies are well seen, such as high shielding factor obtained in the proximity of B_{lim} and $-B_{lim}$. In higher fields curves match almost perfectly.

It can be concluded that Kim model is very good tool for the prediction of superconducting magnetic shield behaviour. Calculated curves are very similar to obtained those during

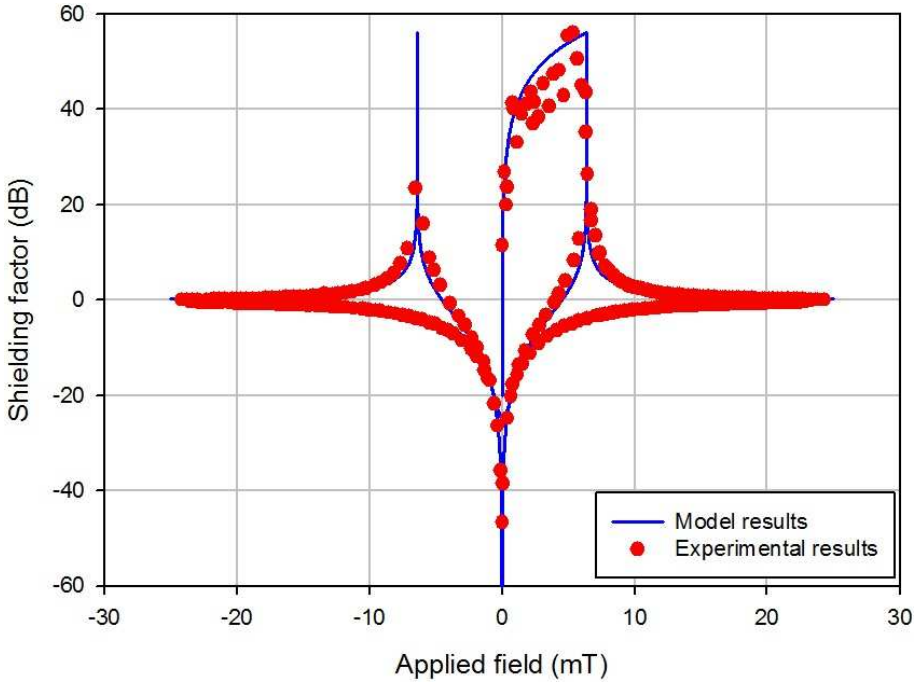

Figure 75: Comparison between shielding factor from model and experiments

from measurment data. Observable differences can be attributed to the accuracy of measurment system. The improvement of model should take into consideration geometrical parameters, especially finite size of specimens. The effect of demagnetisation and leaking field should also be considered. Even though, Kim model gives general picture and serves well for the initial estimation of internal field development.

5.2.2 The comparison of model and results of AC field shielding

The comparison between results for AC and DC modes in the solid shield setting led to the conclusion that both curves have similar shape (as seen in figure 71). Therefore Kim model might work well also for the prediction of behaviour of solid shield also in AC mode. If the frequencies of magnetic field will be insufficient for skin effect to appear, the match would be very good. The parameters for the model are the same as in the previous comparison i.e. $1,35 \cdot 10^{-2} mT$ for the initial magnetic field and $80 {}^{MA}/_{m^2}$ for the critical current density. The model results are compared with the experimental results for the solid shield setting measurments performed in the magnetic field with the frequency of 72,4 Hz.

The results of comparison have been shown in figure 76. As it can be seen the match is indeed very good, actually better than in the case of DC field. The differences are qualitatively similar, but appear to be smaller in size. Transition is less sharp in experimental results, which is ascribed to the effect of leaking field. In higher fields the match is almost perfect. Better match in case of AC field can be explained by two effects. Firstly, no tilt is observed due to the different method of measurments - measuring coil is applied instead of a Hall sensor. Secondly, demagnetising effects might be weaker in the AC field.

Threshold frequency calculated based on the model was 9,3 Hz. In order to find an actual threshold frequency based on measurments the figure 77 was created. It bases on the results shown in figures 68 and 69. The average value of attenuation efficiency was calculated for the region where it was constant for each measured frequency. The results were gathered and shown as the function of frequency of applied magnetic field.

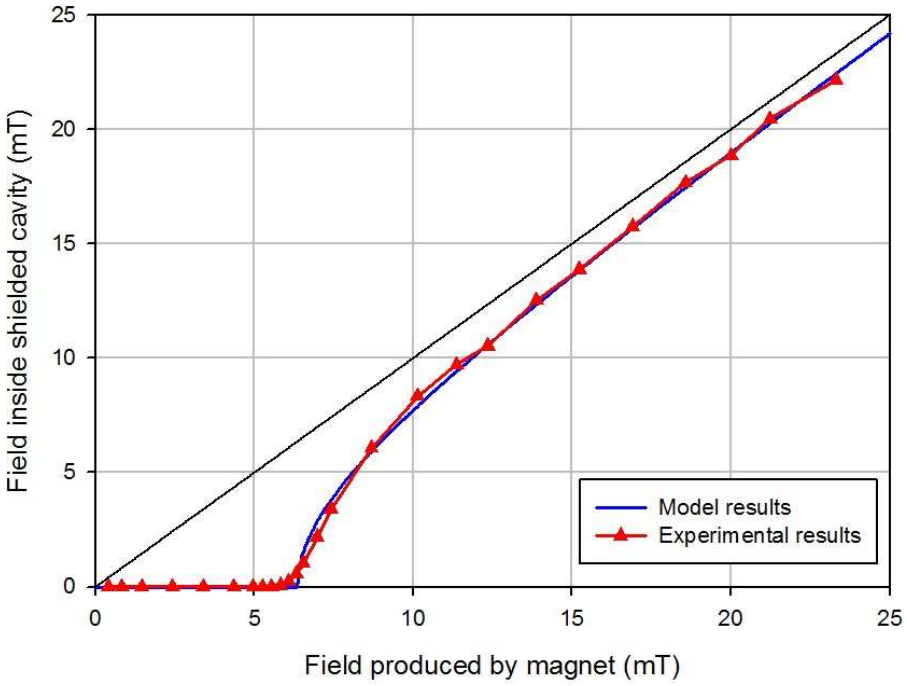

Figure 76: Comparison between results from Kim model and AC field measurments

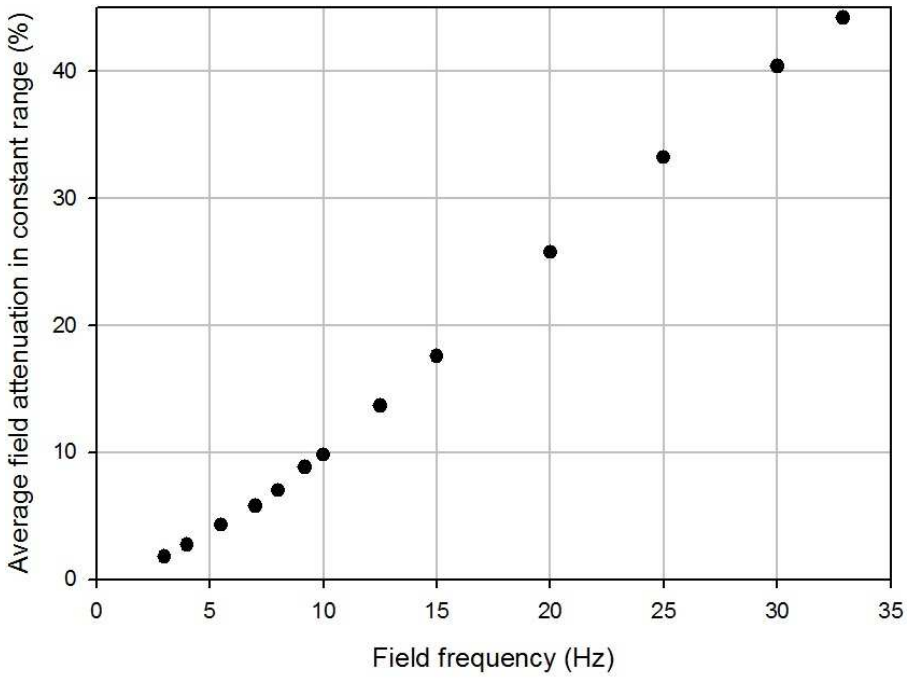

Figure 77: Average attenuation efficiency in constant region

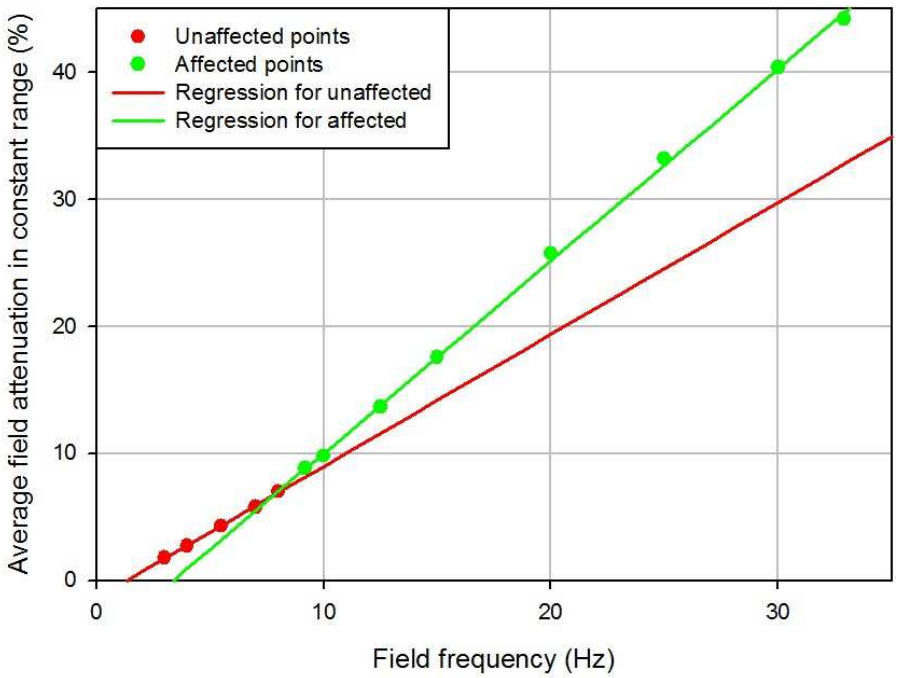

Figure 78: Division of points and the regression results

It can be seen in the figure that the results are not linear and the line bends at certain position. This position is the threshold frequency, which is the value of interest. In order to find this point the results of measurments were divided into two groups, based on the predicted value of threshold frequency coming from model and the shape of curve. The first group is expected to be unaffected by an electromagnetic coupling, and the second is expected to be affected - this is being above an actual threshold frequency. These criteria led to set the division point at approximately 9 Hz. Figure 78 shows this division. Regression was performed for each of these groups. Its results have been shown in figure 78 as well. The value of directional factor for unaffected points is approximately $1,04\%/Hz$, while for affected - $1,51\%/Hz$. It can be clearly seen that there is a large difference in the behaviour of magnetic shield when an electromagnetic coupling appeared. It can be also noticed that the magnitude of this effect rises linearly with frequency. The intersection of these curves points at the threshold frequency of 8,3 Hz, slightly lower than predicted by the model. Possible reasons for this misprediction were described before.

Another frequency effect can be also observed based on the shown results. It can come from the fact that even though superconducting currents circuit is not closed, it is still impossible for magnetic field to enter the bulk of superconductor. Therefore the leakage of field might be limited as it has to propagate by another path. The other explanation might be screening currents induced in the structure of the tape.

5.3 APPLICABILITY

There are several possible applications of magnetic shields investigated in this thesis. The answer to the question of application of superconducting magnetic depends on the magnitude of field which is expected to be shielded, the size of region and expected shielding effect. Currently used superconductors require to be cooled to low temperatures in order to keep their state. Therefore access to shielded region and its size may be limited by cryostat in which shield

would have to be kept. Also the production of large specimens made of currently used ceramic high temperature superconductors is expensive and hard.

On the other hand the application of superconductors is the simplest method to obtain the full shielding. As shown, below the transition value of external field only noise is registered, since no magnetic field was capable of penetrating superconducting tube. Therefore they may be especially useful for attenuating magnetic field around supersensitive sensors, such as SQUIDs. High precision electronic devices might also benefit from the application of superconducting shields. Such devices are often used in locations were background magnetic field is relatively low.

The application of solid tube, such as the one used during measurments allows for the full shielding of low fields. Such shield might be sufficient for blocking Earths' magnetic field and some of the fields produced by equipment. It would also stop random fluctuations which might appear during operation. In order to obtain magnetic vacuum a specimen has to be cooled in actual zero field conditions. This would include several other shields capable of changing its size in order to reduce the magnetic field in shielded aperture. Otherwise Earth's magnetic field will be trapped within the superconductor and will be still present.

Shields with initially frozen field might find some use in applications where constant magnetic field is needed. This include some scientific applications and measurments. If some external magnetic field is anticipated it is possible to produce magnetic shield with geometrical dimmensions sufficient to counter this field and ensure constant field inside shielded region. This can be done with solid specimens and Kim model would be helpful in the prediction of required thickness of such field and required frozen field.

As it was shown simple shields made of soldered fragments of superconducting tapes can be applied for the increased performance of shielding. Their application is limited to the attenuation of alternating current fields and alone are incapable of provide full shielding. However, as it was shown, in cooperation with solid shields they are capable to produce full shielding regions even 4 times wider than in case of solid shield only. Such simple shields are relatively cheap and easy to manufacture. The major problem is the fact that their performance may not be uniform.

Superconducting magnet shields can be also efficiently used for field shaping. It can be done by applying the shields of certain geometry. By proper blocking of fields and production of apertures and planes through which it may propagate virtually any shape may be achieved for a specific applications. This would require high quality specimens with precisely checked superconducting qualities. This issue was not the major concern of this thesis, however some examples of this concept can be observed on the graphs of field distribution.

Initially it was the concern that the deterioration of shields may occure due to thermal stresses caused by multiple cooldowns and heat-ups of specimens. Fortunately, no such deterioration was observed. Similar measurments performed in different test setting configurations yielded the same, repeatable results. Also no negative effect from moisture gathering between the layers of superconducting tape appeared. It is possible that some deterioration would occur in longer term, however this cannot be extrapolated from observations performed during the production of this thesis.

Several possibilities of increasing measurment quality were recognised, as well as some major problems distorting them. It would be possible to apply the sensors with lower noise observable in order to obtain the actual values of shielding factor. SQUIDs would be especially useful for this purpose. Their great sensitivity might further prove that the field attenuation is indeed full. Another problem is the fact that the specimens applied were relatively small, which might have led to the leaking of the external magnetic field into the shielded region. Flux

creep and flux relaxation became important problems during the measurments of direct current field attenuation. This may be countered by the application of materials with stronger pinning properties.

6 CONCLUSIONS

All of the thesis objectives have been completed. The properties of superconductors have been charactierised theoretically, particularly these connected with the issue of magnetic shielding. Their current applications as well as possible future usage have been stated. The importance of the issue of magnetic shielding has been enucleated. Literature review was performed and its results have been presented. History of research on superconducting magnetic shielding and its current state have been given.

Mathematical model was developed to simulate the behaviour of solid and tape-screen shields, as well as their coupled usage. In order to model the shielding in the solid shield Kim model was used. Hysteresis curves were obtained and compared with Bean model. This proved that Kim model is better in the prediction of experimental results The curves resulting from the application of Kim model has been later used for the purpose of comparison with experiments. Modeling of the tape-screen behaviour was based on the concept of electromagnetic coupling and RL filter. Formulas and methods to find threshold frequency above which the coupling appears have been shown and applied. Expected threshold frequency was 9,3 Hz.

Experimental stand was designed, build and exploited. It was proven to produce reliable results. This was entirely new stand and each element was produced especially for this stand. The magnet was wound based on the design prepared specially for the purpose of thesis. The holders were manufactured and adjusted to the size of investigated specimens. Sensors were calibrated for the application in the temperature of 77K. Also the slideway was modified to precisely position the sensor within the superconducting specimens. Measuring devices were chosen and applied in accordance with the values measured. The investigated specimens were commercial solid tube made of BSCCO and tape-screen made of soldered YBCO tapes.

Measurments were performed in several combinations of applied fields and the specimen setting used. Solid tube and double shield setting were tested in both direct and alternating fields. Tape-screen was investigated only in AC magnetic fields. The measurments performed in DC field shown that there is no effect from the application of second shield. They yielded the same hysteresis curves despite its presence. The effect became apparent in alternating current fields. Dependance on frequency was observed and further investigated. Measurments performed with tape screen alone were supposed to locate threshold frequency. Obtained results have been gathered and shown in the form of graphs.

Comparison between the results coming from Kim model have shown that this model is indeed a valid tool for the modeling of tubular superconducting magnetic shields behaviour. Very good match was observed for hysteresis curves obtained during the measurments and from the modeling. Adjustments allowed to find the properties of material used. Effects of frozen field were observed and countered by the application of correction factors. Kim model proven also to be useful in the modeling of a field shielded by solid tube in AC field. In such case the frequency dependence is weak and the results are very similar to the first branch of the hysteresis curves.

The most important findings of this thesis are the measurments performed in AC field in the double shield and tape-screen settings. It was shown that even very simple magnetic shield made of soldered tape may significantly increase the efficiency of shielding. According to the

literature review these were the first measurments of such kind. Clear effect of magnetic coupling was observed which allowed superconducting currents to exchange energy and thus stop the magnetic field from propagation. In order to check whether the RL filter model produced proper results, the threshold frequency was derived from the measurments data. It was 8,3 Hz, which is close to the value obtained in model calculations.

There are plans to continue the research started in this thesis. The phenomenon appearing from the application of tape-screen shields is interesting and requires further investigation. There is need to find the limits of this effect, both upper and lower. Tape-screen shields may find practical application as a tool to increase the performance of solid shields and produce the effect of full shielding in wider range of magnetic field magnitudes. The measurments have shown a hint that the disappearance of superconductivity at higher frequencies may decrease the applicability of simple shields. However they still might be useful because of their low price and simplicity.

The model of electromagnetic coupling needs to be refined. Its further development should include the possibility of exact prediction when this effect will appear and how strong it will be. Measurments and theoretical work will have to be applied. That means that the measurment stand used for the purpose of this thesis would find more use. It can be adapted and serve future generations of students to teach them about the phenomenon of superconducting magnet shielding.

7 REFERENCES

[1] van Delft, D.: Freezing physics. Heike Kamerlingh Onnes and the quest for cold, 2007

[2] Cyrot M., Pavuna D.: Wstep do nadprzewodnictwa, Wydawnictwo Naukowe PWN, Warszawa 1996

[3] MIT Department of Physics: Superconductivity: The Meissner Effect, Persistent Currents and the Josephson Effects, 2011

[4] Dai, P., Chakoumakos, B. C., Sun, G. F., Wong, K. W., Lu, D. F., Xin, Y.: Synthesis and neutron powder diffraction study of the superconductor HgBa2Ca2Cu3O8 by Tl substitution, Physica C: Superconductivity, Volume 243, Issues 3-4, pp. 201, 1995

[5] Coalition for the Commercial Application of Superconductors: Superconductivity. Present and Future Applications, 2009

[6] Matlashov A. N.,. Zotev V. S, Kraus R. H., Sandin H., Urbaitis A. V., Volegov P. L., Espy M. A.: SQUIDs for Magnetic Resonance Imaging at Ultra-low Magnetic Field, PIERS ONLINE, VOL. 5, NO. 5, pp. 266, 2009

[7] Denis M.: Magnetic shielding with high temperature superconductors, Universite de Liege, Ecole Royale Militaire, 2007

[8] Szubnikow L.W., Chotkiewicz B.I., Szepielew J.D, Rjabinin J.N.: Magnitnyje swojstwa swierchprowodjaszczich metallow i spawow, Zurnal eksperimentalnoj i teoreticzeskoj fiziki 7, 1937

[9] Popovic Z., Popovic B.D.: Introductory Electromagnetics, Prentice Hall, 1999

[10] Young H.D., Freedman R.A., Ford L.: Sears and Zemansky's University Physics with Modern Physics 12th edition, Addison-Wesley 2007

[11] Cabrera B., Hamilton W. O.: Electric and Magnetic Shielding with Superconductors, The Science and Technology of Superconductivity, pp. 587, 1973

[12] Claycomb J. R., Miller J. H.: Superconducting magnetic shields for SQUID applications, Rev. Sci. Instrum. 70, pp. 4562, 1999

[13] Lorant S.J. St.: Superconducting Shields for Magnetic Flux Exclusion and Field Shaping, Proc. of Int. Conf. on Magnet Technology, Upton, N. Y., Sep 19-22, pp. 227, 1972

[14] Agapov N.N., Donets D.E., Drobin V.M., Kulikov E.A., Malinowski H., Pivin R.V., Smirnov A.V., Prokofichev Yu.V., Trubnikov G.V., Dorofeev G.L.: Superconducting Shield for Solenoid of Electron Cooling System, Physics of Particles and Nuclei Letters, Vol. 9, pp. 422, 2012

[15] Giunchi1 G., Bassani E., Cavallin T., Bancone N., Pavese F.: An MgB2 superconducting shield for a cryogenic current comparator working up to 34 K, Supercond. Sci. Technol. 20, pp. L39, 2007

[16] Janowski T., Stryczewska H.D., Kozak S., Malinowski H., Wojtasiewicz G., Surdacki P., Kondratowicz-Kucewicz B., Kozak J.: Nadprzewodnikowe ograniczniki pradu, Instytut Podstaw Elektrotechniki i Elektrotechnologii Politechniki Lubelskiej, Lublin 2002

[17] Meissner W., Ochsenfeld R.: Ein neuer Effekt bei Eintritt der Supraleitfahigkeit, Die Naturwissenschaften 21, pp. 787, 1933

[18] Mendelssohn K., Daunt J.G.: Supraconductivity of Lanthanum, Nature 139, pp. 473, 1937

[19] Kunzler J.E.: Superconducting Materials and High Magnetic Fields, J. Appl. Phys. 33, pp. 1042, 1962

[20] Cioffi P.P.: Approach to the Ideal Magnetic Circuit Concept through Superconductivity, J. Appl. Phys. 33, pp. 875, 1962

[21] Hildebrandt A.F., Warlquist H., Elleman D.D.: Configurations of Superconducting Shells Required for Near Critical Uniform Magnetic Fields, J. Appl. Phys. 33, pp. 1798, 1962

[22] Hildebrandt A.F.: Shielding With Superconductors In Small Magnetic Fields, Revue De Physique Appliquee 5, pp. 49, 1970

[23] Furuya S., Tominaga A., Narahara Y.: The Wall-Thickness Dependence of Magnetic Shielding or Trapping in a Low-Field Superconductor, Pb40Sn60, Journal of Low Temperature Physics, Vol. 53, Nos. 3/4, pp. 477, 1983

[24] Bednorz J.G., Muller K.A.: Possible High Tc Superconductivity in Ba-La-Cu-O System, Z.Phys.B.-Condensed Matter 64, pp. 189, 1986

[25] Hussain A.A., Sayer M.: Simple magnetic shielding experiment on high Tc superconducting bulk ceramics and thin films, metals and alloys, Cryogenics, vol. 32, no. 1, pp. 64, 1992

[26] Brandt E., Indenbom M.: Type-II superconductor strip with current in a perpendicular magnetic field, Phys. Rev. B, vol. 48, no. 17, pp. 12893, 1993

[27] Seki Y., Suzuki D., Ogata K., Tsukada K.: Open-type hybrid magnetic shield using high-Tc superconducting wire and flexible magnetic sheets, Applied Physics Letters Volume 82, Number 6, pp. 940, 2003

[28] Bertora F., Molinari E., Viale A.: Self-shielded open superconducting magnet design, Proc. Intl. Soc. Mag. Reson. Med. 16, pp. 1148, 2008

[29] Denis S., Dusoulier L., Dirickx M., Vanderbemden Ph., Cloots R., Ausloos M., Vanderheyden B.: Magnetic shielding properties of high-temperature superconducting tubes subjected to axial fields, Supercond. Sci. Technol. 20, pp. 192, 2007

[30] Kapra A.V., Misko V.R., Peeters F.M.: Controlling magnetic flux motion by arrays of zigzag-arranged magnetic bars, Supercond. Sci. Technol. 26, pp. 1, 2013

[31] Mori K., Minemoto T., Itoh M.: Magnetic shielding of the superposition of a hybrid ferromagnetic cylinder over a BPSCCO cylinder, IEEE Transactions on Appiled Superconductivity, 1997

[32] Omura A., Oka M., Mori K., Itoh, M.: Magnetic shielding effects for the superposition of multi-layered soft-iron cylinders over a BPSCCO cylinder: Relationship between the shielding effect and the layer number of the soft-iron cylinder, AIP Conference Proceedings, Vol. 614 Issue 1, pp. 421, 2002

[33] Yasui K., Tarui Y., Itoh M.: Improvement of the Magnetic Shielding Effects by the Superposition of a Multi-Layered Ferromagnetic Cylinder over an HTS Cylinder: Relationship Between the Shielding Effects and the Layer Number of the Ferromagnetic Cylinder, Journal of Physics: Conference Series 43, pp. 1393, 2006

[34] Lousberg G.P., Fagnard J.F., Ausloos M., Vanderbemden P., Vanderheyden B.: Numerical Study of the Shielding Properties of Macroscopic Hybrid Ferromagnetic/Superconductor Hollow Cylinders, IEEE Transactions On Applied Superconductivity, Vol. 20, No. 1, pp. 33, 2010

[35] Gozzelino L., Agostino A., Gerbaldo R., Ghigo G., Laviano F.: Magnetic shielding efficiency of superconducting/ferromagnetic systems, Supercond. Sci. Technol. 25, pp. 1, 2012

[36] Yoshizaki D., Golubov A., Tanaka Y.: Theory of proximity effect in ferromagnet/superconductor heterostructures in the presence of spin dependent interfacial phase shift, Japanese journal of applied physics, 51, id. 010108, 2012

[37] Kurian F., Schwickert M., Reeg H., Kowina P., Liakin D., Huelsmann P., Geithner R., Neubert R., Vodel W.: Field Attenuation Of The Magnetic Shield For A Cryogenic Current Comparator, Proceedings of BIW2012, pp. 17, Newport News, Virginia, USA, 2012

[38] Watanabe S., Watanabe T., Ikeda T., Kase M., Katayama T.: Performance Of HTS-Magnetic Shield For Highly-Sensitive Current Monitor With HTS-SQUID, Proceedings of EPAC 2002, pp. 1992, Paris, France, 2002

[39] Takashi S.: Magnetic Shield at magnetically open site for Superconducting Magnetically Levitated Train, Papers of Technical Meeting on Application of Superconductivity, IEE Japan, pp. 23, 2005

[40] Hoffman J., Fisher P., Batishchev O.: Use of Superconducting Magnet Technology for Astronaut Radiation Protection, Final Report for NIAC Phase I Contract CP 04-01, 2005

[41] Fagnard J.F., Dirickx M., Levin G.A., Barnes P.N., Vanderheyden B., Vanderbemden P.: Use of second generation coated conductors for efficient shielding of DC magnetic fields, Journal Of Applied Physics 108, id. 013910, 2010

[42] Kvitkovic J., Pamidi S., Voccio J.: Shielding AC magnetic fields using commercial YBa2Cu3O7-coated conductor tapes, Supercond. Sci. Technol. 22, id. 125009, 2009

[43] Itoh I., Fujisawa K., Otsuka H.: NbTi/Nb/Cu Multilayer Composite Materials for Superconducting Magnet Shielding - Superconducting Performances and Microstructure of NbTi Layers, Nippon Steel Technical Report No. 85, 2002

[44] Cabrera B.: The use of superconducting shields for generating ultra-low magnetic field regions and several related experiments, Ph.D. dissertation, Standford university, 1975.

[45] Kittel, C.: Introduction to Solid State Physics, 8th Ed., 2004

[46] Essman U., Trauble H.: The direct observation of individual flux lines in type II superconductors, Physics Letters, v. 24A, pp. 526, 1967

[47] Alikhanzadeh-Arani S., Salavati-Niasari M.: Synthesis and characterization of high-temperature ceramic YBCO nanostructures prepared from a novel precursor, Journal of Nanostructures 1, pp. 63, 2012

[48] Wu M. K., Ashburn J. R., Torng C. J., Hor P. H., Meng R. L., Gao L., Huang Z. J., Wang Y. Q., Chu C. W.: Superconductivity at 93 K in a New Mixed-Phase Y-Ba-Cu-O Compound System at Ambient Pressure, Physical Review Letters 58, pp. 908, 1987

[49] Sekitania T., Miuraa N., Ikedaa S., Matsudaa Y.H., Shioharab Y.: Upper critical field for optimally-doped YBa2Cu3O7, Physica B, pp. 319, 2004

[50] Oral A., Bending S.J., Humphreys R.G, Henin M.: Microscopic measurement of penetration depth in YBa2Cu3O7 thin films by scanning Hall probe microscopy, Supercond. Sci. Technol. 10, pp. 17, 1997

[51] Gauzzi A., Johan Jonsson-Akerman B., Clerc-Dubois A., Pavuna D.: Scaling between superconducting critical temperature and structural coherence length in YBa2Cu3O6 films, Europhys. Lett. 51, pp. 667, 2000

[52] Yang-Kook S., In-Hwan O.: Preparation of Ultrafine YBa2Cu3O7-x Superconductor Powders by the Poly(vinyl alcohol)-Assisted Sol-Gel Method, Ind. Eng. Chem. Res. 35, pp. 4296, 1996

[53] Derong Z.: Yttrium Barium Copper Oxide Superconducting Powder Generation by An Aerosol Process (Ph.D. Thesis), University of Cincinnati 1991

[54] Derro D. J., Hudson E. W., Lang K. M., Pan S. H., Davis J. C., Markert J. T., de Lozanne A. L.: Nanoscale One-Dimensional Scattering Resonances in the CuO Chains of YBa2Cu3O6+x, Phys. Rev. Lett. 88, id. 097002, 2002

[55] Goswami P., Rani M., Kapoor A.: Fermi pockets and quantum oscillations in specific heat of YBCO in the presence of disorder, arXiv:1007.5041, 2010

[56] Maeda H., Tanaka Y., Fukutomi M., Asano T.: A New High-Tc Oxide Superconductor without a Rare Earth Element, Jpn. J. Appl. Phys. 27, pp. L209, 1988

[57] Presland M.R., Tallon J.L., Buckley R.G., Liub R.S., Flower N.E.: General trends in oxygen stoichiometry effects on Tc in Bi and Tl superconductors, Physica C: Superconductivity 176, pp. 95, 1991

[58] Golovashkin A. I., Ivanenko O. M., Kudasov Yu. B., Mitsen K. V., Pavlovsky A. I., Platonov V. V., Tatsenko O. M.: Low temperature direct measurements of Hc2 in HTSC using megagauss magnetic fields, Physica C: Superconductivity, pp. 1859, 1991

[59] Prozorov R., Giannetta R. W., Carrington A., Fournier P., Greene R. L., Guptasarma P., Hinks D.G., Banks A. R.: Measurements of the absolute value of the penetration depth in high-Tc superconductors using a tunnel diode resonator, arXiv, 2000

[60] Masur L., Parker D., Tanner M., Podtburg E., Buezek D., Scudiere J., Caracino P., Spreafico S., Corsaro P., Nassi M.: Long length manufacturing of high performance BSCCO-2223 tape for the Detroit Edison power cable project, IEEE Trans.Appl.Supercond. 11, pp. 3256, 2001

[61] Lu J., Choi E.S., Zhou H.D.: Physical properties of Hastelloy C-276 at cryogenic temperatures, J. Appl. Phys. 103, id. 064908, 2008

[62] Muller K. H., Matthews D., Driver R.: Critical current density of ceramic high-temperature superconductors in a low magnetic field, Physica C 191, pp. 339, 1992

[63] Kim B.Y., Hempstead C.F., Strand A.R.: Critical Persistent Currents in Hard Superconductors, Physical Review Letters 9, pp. 306, 1962

[64] Diaz A., Mechin L., Berghuis P., Evetts J.E.: Observation of viscous flux flow in YBa2Cu3O7-b low-angle grain boundaries, Phys. Rev. B vol. 58, pp. R2960, 1998

[65] Anderson P.: Theory of flux creep in hard superconductors, Phys. Rev. Lett., vol. 9, pp. 309, 1962

[66] Ramsden E.: Hall-Effect Sensor: Theory and Applications, Newnes 2006

8 ATTACHMENTS

Name	Number	Remarks
General outlook of test stand	8.1	Markings are the same as in figure 25
Data sheet for Hall effect sensor	8.2	Toshiba's gallium-arsenide sensor THS118
Dimensions of the magnet	8.3	Drawing showing geometrical dimensions of the magnet
Drawing of the cryostat	8.4	Drawing showing geometrical dimensions of the cryostat
Drawing of a holder	8.5	Drawing showing geometrical dimensions of a holder
CAN SUPERCONDUCTORS magnetic shield catalogue	8.6	Characteristic and range of magnetic shields offered by CAN SUPERCONDUCTORS
Assembly of magnet and specimens	8.7	Drawing showing holders and specimens inside the magnet

Table 2: List of attachments

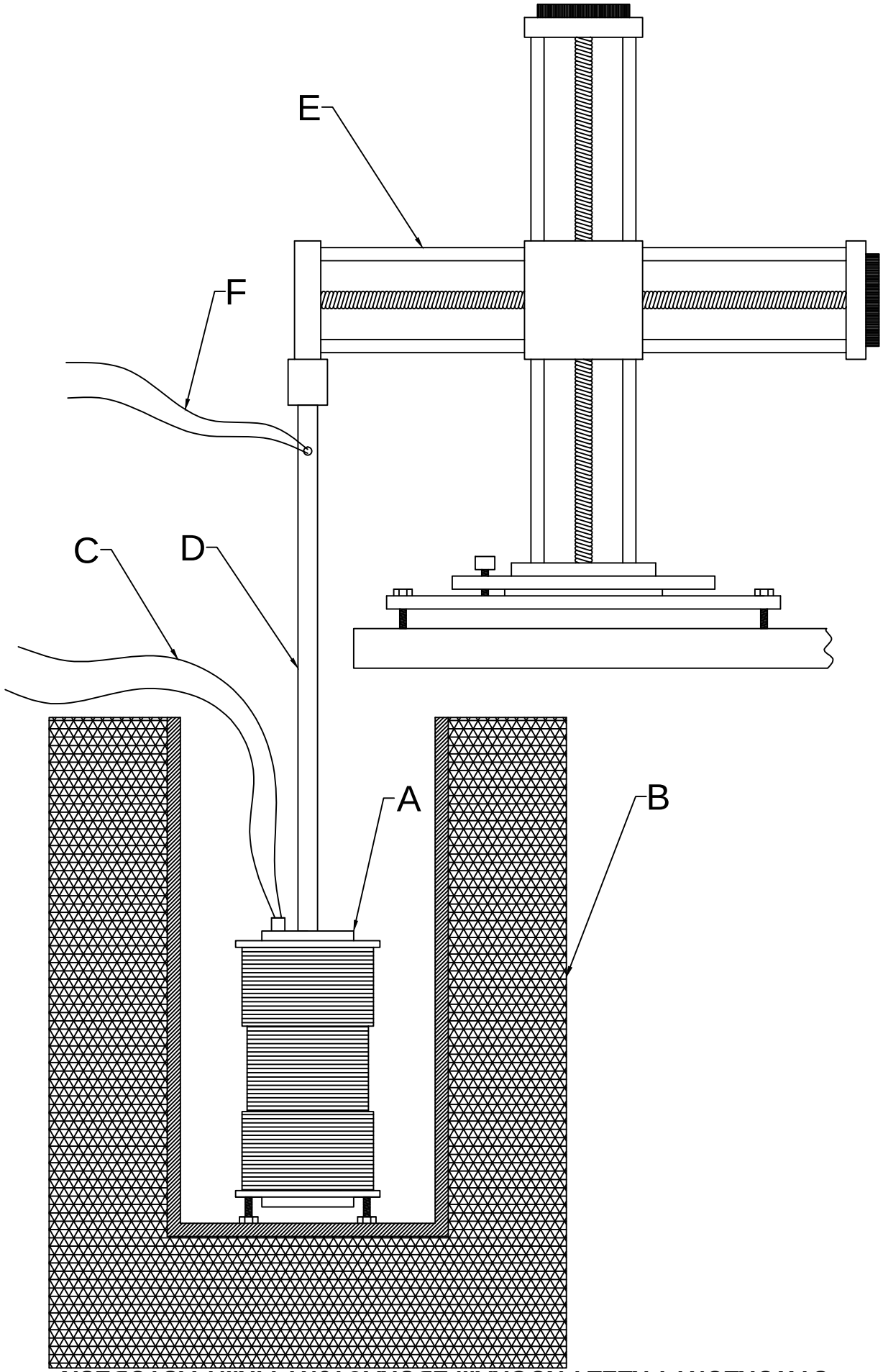

UTWORZONY PRZEZ PROGRAM EDUKACYJNY FIRMY AUTODESK

UTWORZONY PRZEZ PROGRAM EDUKACYJNY FIRMY AUTODESK

UTWORZONY PRZEZ PROGRAM EDUKACYJNY FIRMY AUTODESK

TOSHIBA HALL SENSOR GaAs ION IMPLANTED PLANAR TYPE

THS118

HIGH STABILITY MOTOR CONTROL.
DIGITAL TACHOMETER.
CRANK SHAFT POSITION SENSOR.

- Super Small Package.
- Excellent Temperature Characteristics.
- Wide Operating Temperature Range. (; −55~125°C)
- Excellent Output Voltage Linearity.

Unit in mm

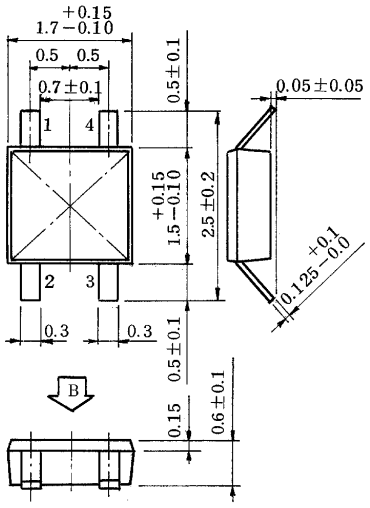

1(+) − 3(−) (INPUT)
2(+) − 4(−) (OUTPUT)

JEDEC	—
EIAJ	—
TOSHIBA	10-2A1A

Weight : 0.0047g

MAXIMUM RATINGS (Ta = 25°C)

CHARACTERISTIC		SYMBOL	RATING	UNIT
Control Current	DC	I_C	10**	mA
	1s		15**	
Power Dissipation		P_D	100**	mW
Operating Temperature Range		T_{opr}	−55~125	°C
Storage Temperature Range		T_{stg}	−55~150	°C

** Mounted on a printed circuit board.

MARKING

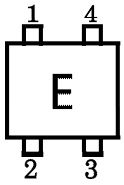

ELECTRICAL CHARACTERISTICS (Ta = 25°C)

CHARACTERISTIC	SYMBOL	TEST CONDITION	MIN.	TYP.	MAX.	UNIT
Internal Resistance (Input)	R_d	I_C=5mA	450	—	900	Ω
Residual Voltage Ratio	V_{HO}/V_H	I_C=5mA, B=0/B=0.1T	—	—	±10	%
Hall Voltage (Note 1)	V_H	I_C=5mA, B=0.1T	55	—	140	mV
Temperature Coefficient (Note 2)	V_{HT}	I_C=5mA, B=0.1T T1=25°C, Ta=125°C	—	—	−0.06	%/°C
Linearity (Note 3)	ΔK_H	I_C=5mA, B1=0.1T, B2=0.5T	—	—	2	%
Specific Sensitivity (Note 4)	K*	I_C=5mA, B=0.1T	—	27	—	$\times 10^{-2}$/T
Internal Resistance (Output)	R_{OUT}	I_C=5mA	580	—	1350	Ω

Note 1 : $V_H = V_{HM} - V_{HO}$ (V_{HM} is meter indication)

Note 2 : $V_{HT} = \frac{1}{V_{H(T1)}} \cdot \frac{V_{H(T2)} - V_{H(T1)}}{T2 - T1} \times 100\ (\%/°C)$

Note 3 : $\Delta K_H = \frac{K_{H(B2)} - K_{H(B1)}}{1/2\{K_{H(B1)} + K_{H(B2)}\}} \times 100(\%)$, $K_H = \frac{V_H}{I_C \cdot B}$

Note 4 : $K^* = V_H/(R_d \times I_C \times B) = K_H/R_d$

V_{HO} : Residual Voltage

K_H : Product Sensitivity

961001EAA2

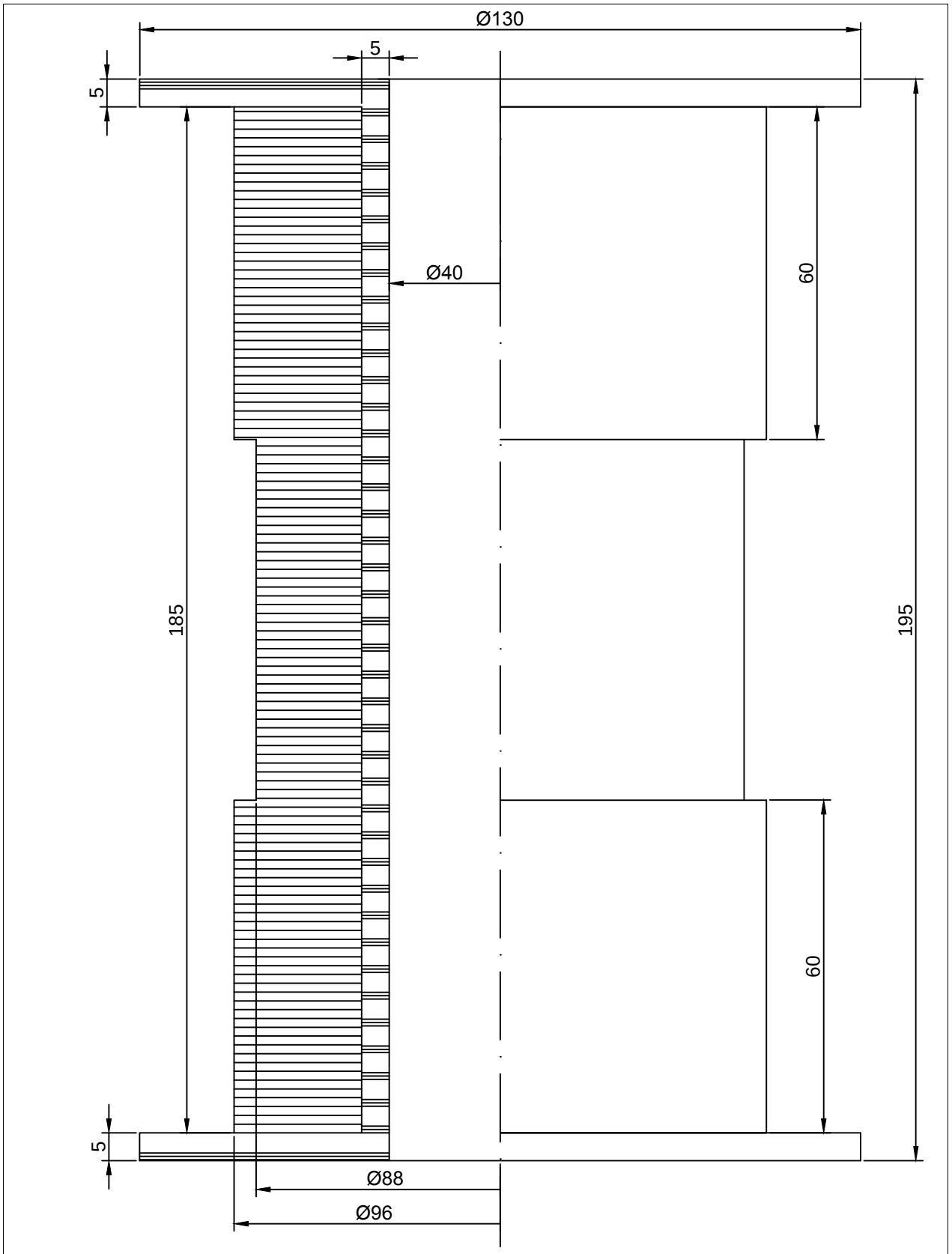

FILE NAME		SHEET	SCALE 1:1
DRAWN Tomków L.	Magnet	DWG NO 8.3	
APPR.			

UTWORZONY PRZEZ PROGRAM EDUKACYJNY FIRMY AUTODESK

UTWORZONY PRZEZ PROGRAM EDUKACYJNY FIRMY AUTODESK

UTWORZONY PRZEZ PROGRAM EDUKACYJNY FIRMY AUTODESK

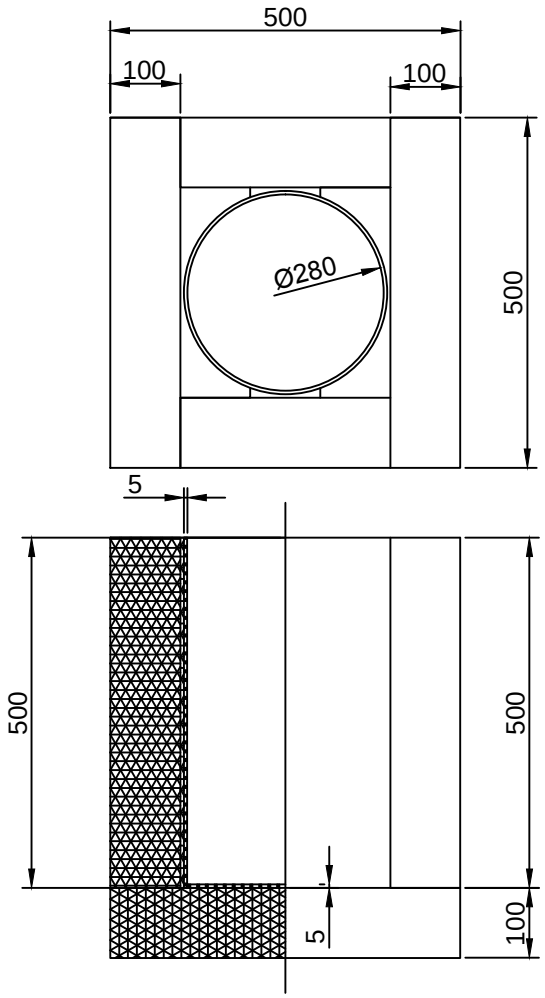

FILE NAME		SHEET	SCALE 1:10
DRAWN Tomków L.	Cryostat	DWG NO 8.4	
APPR.			

UTWORZONY PRZEZ PROGRAM EDUKACYJNY FIRMY AUTODESK

UTWORZONY PRZEZ PROGRAM EDUKACYJNY FIRMY AUTODESK

UTWORZONY PRZEZ PROGRAM EDUKACYJNY FIRMY AUTODESK

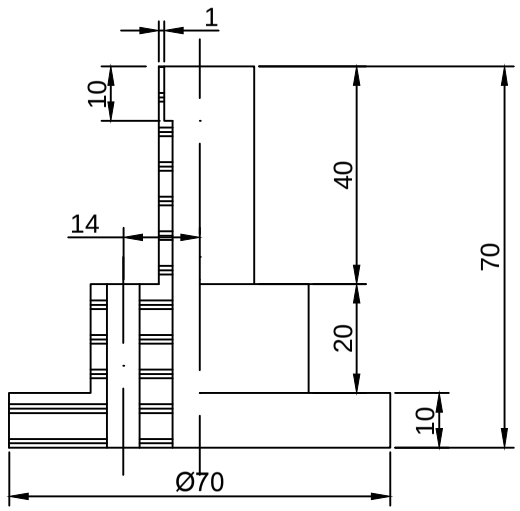

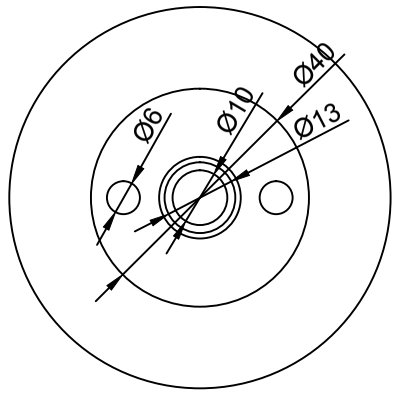

FILE NAME		SHEET	SCALE 1:1
DRAWN Tomków L.	Holder	DWG NO 8.5	
APPR.			

Superconducting Magnetic Shields

Characteristic

Material: Bi1.8Pb0.26Sr2Ca2Cu3O10+x (2223 phase)
Density: > 5.0 g/cm^3
Wall thickness: approx. 1.5 mm

Shielded magnetic flux density (77 K): > 5 mT (typical value 10 mT)
Shielding factor (77 K, amplitude 2 mT, frequency 20 Hz – 10 kHz): > 10^6
Shielding effectiveness (77 K, amplitude 2 mT, frequency 20 Hz – 10 kHz): > 120 dB

Field noise at 1 Hz (cooled at 77 K in zero field): < 50 fT/sqrt(Hz)
Critical temperature: 108 K

Product range – Superconducting Magnetic Shields

Tubes		
Inner diameter	10 mm - 28 mm	
Length	80 mm - 140 mm	
Type	**Inner diameter**	**Length**
CST-10/80	10 mm	80 mm
CST-12/80	12 mm	80 mm
CST-15/80	15 mm	80 mm
CST-18/120	18 mm	120 mm
CST-21/120	21 mm	120 mm
CST-22/120	22 mm	120 mm
CST-24/120	24 mm	120 mm
CST-28/140	28 mm	140 mm

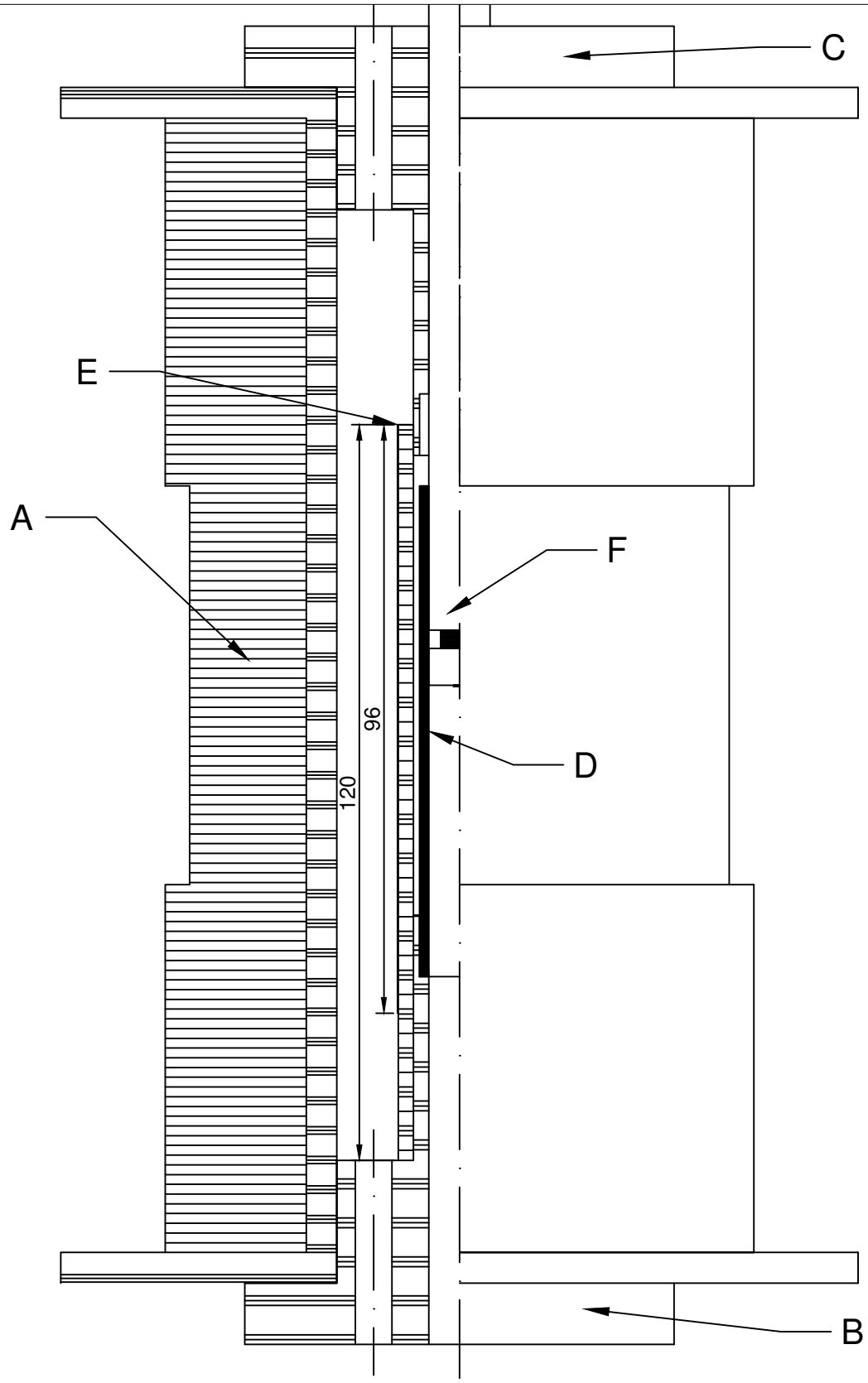

FILE NAME		SHEET	SCALE 1:1
DRAWN Tomków L.	Magnet assembly	DWG NO 8.7	
APPR.			

UTWORZONY PRZEZ PROGRAM EDUKACYJNY FIRMY AUTODESK

UTWORZONY PRZEZ PROGRAM EDUKACYJNY FIRMY AUTODESK

UTWORZONY PRZEZ PROGRAM EDUKACYJNY FIRMY AUTODESK